Flagellar motor tuning
The hybrid motor in *Shewanella oneidensis* MR-1

Dissertation

zur Erlangung des Doktorgrades
der Naturwissenschaften
(Dr. rer. nat.)

dem
Fachbereich Biologie
der Philipps-Universität Marburg
vorgelegt

von

Anja Paulick

aus Hoyerswerda

Marburg (Lahn), 2012

Die Untersuchungen zur vorliegenden Arbeit wurden von Mai 2008 bis März 2012 am Max-Planck-Institut für terrestrische Mikrobiologie unter der Leitung von Dr. Kai M. Thormann durchgeführt.

Vom Fachbereich Biologie der Philipps-Universität Marburg (HKZ: 1180)
als Dissertation angenommen am: 03.04.2012

Erstgutachter: Dr. Kai M. Thormann
Zweitgutachter: Prof. Dr. Martin Thanbichler

Weitere Mitglieder der Prüfungskommission:

Prof. Dr. Klaus Lingelbach

Prof. Dr. Uwe G. Maier

Prof. Dr. Alexander Böhm

Tag der mündlichen Prüfung: 06.09.2012

Die während der Promotion erzielten Ergebnisse sind zum Teil in folgenden Originalpublikationen veröffentlicht:

Paulick A, Koerdt A, Lassak J, Huntley S, Wilms I, Narberhaus F, Thormann KM: **Two different stator systems drive a single polar flagellum in *Shewanella oneidensis* MR-1**. *Mol Microbiol* 2009, **71**:836-850.

Koerdt A[1], Paulick A[1], Mock M, Jost K, Thormann KM: **MotX and MotY are required for flagellar rotation in *Shewanella oneidensis* MR-1**. *J Bacteriol* 2009, **191**:5085-5093.

Thormann KM, Paulick A: **Tuning the flagellar motor**. *Microbiology* 2010, **156**:1275-1283.

Ergebnisse aus in dieser Promotion nicht erwähnten Projekten sind in folgenden Originalpublikationen veröffentlicht:

Bubendorfer S, Held S, Windel N, Paulick A, Klingl A, Thormann KM: **Specificity of motor components in the dual flagellar system of *Shewanella putrefaciens* CN-32.** *Mol Microbiol* 2011.

[1] diese Autoren wirkten gleichberechtigt an der Publikation mit

Ich versichere, dass ich meine Dissertation:

"Flagellar motor tuning

The hybrid motor in *Shewanella oneidensis* MR-1"

selbstständig, ohne unerlaubte Hilfe angefertigt und mich dabei keiner anderen als der von mir ausdrücklich bezeichneten Quellen und Hilfen bedient habe. Die Dissertation wurde in der jetzigen oder einer ähnlichen Form noch bei keiner anderen Hochschule eingereicht und hat noch keinen sonstigen Prüfungszwecken gedient.

Marburg (Lahn), den 03. April 2012

_____

Anja Paulick

"*By the means of Telescopes, there is nothing so far distant but may be represented to our view; and by the help of Microscopes, there is nothing so small as to escape our inquiry; hence there is a new visible World discovered to the understanding.*"

Robert Hooke, 1665

ABSTRACT

Bacteria are exposed to constantly changing environments. An efficient way to navigate towards favourable conditions is flagella-mediated motility. Flagellar rotation is achieved by the bacterial flagellar motor, composed of the rotor and stator complexes which surround the rotor in a ring-like structure. As an exception among the *Shewanella* species, the fresh-water organism *S. oneidensis* MR-1 harbours two different stator complexes, the sodium-ion dependent PomAB and the proton-dependent MotAB, differentially supporting rotation of a single polar flagellum. Both PomAB and MotAB are simultaneously present and required for full speed under low sodium-ion conditions. Although tightly anchored to the cell wall, stators are constantly exchanged even during ongoing rotation. Moreover, sodium-ion and proton-dependent stators can function with the same rotor. This raises the question of how PomAB and MotAB contribute to rotation of a single flagellum and whether PomAB and MotAB coexist in the stator ring of *S. oneidensis* MR-1, forming a hybrid motor.

Here, I report a novel model for the dynamic adaptation of the rotor-stator configuration in response to the environmental sodium ion level in *S. oneidensis* MR-1. Transcriptional fusions to *lucB* revealed that both *pomAB* and *motAB* are concurrently transcribed. By using fluorescence microscopy, functional fusions of mCherry to the B-subunits revealed that in sharp contrast to MotB, a fraction of PomB is polarly positioned independently of the sodium-ion concentration. At low sodium-ion concentration, PomB and MotB appear to coexist in the flagellar motor. However, in the absence of PomAB, MotB is recruited to the flagellated pole independently of the sodium-ion concentration. Interestingly, induced production of PomAB displaces polar MotB from the motor and confines it to the membrane. By quantifying single sfGfp molecules fused to PomB, I could show that the number of PomB in the stator ring is reduced from nine to five complexes when cells were shifted from a high to a low sodium-ion concentration. Thus, the incorporation efficiency of PomAB is directly modified in response to the sodium-ion concentration, whereas the association of MotAB into the stator ring rather depends on the presence of PomAB. Furthermore, two auxiliary proteins, MotX and MotY, were identified and shown to be essential for functionality of both PomAB and MotAB. Localisation studies revealed that, in contrast to *Vibrio* MotXY are not required for recruitment of the stator complexes to the flagellated pole. Taken together, my data support the model of dynamic stator swapping to tune the flagellar motor in response to environmental conditions, e.g. the availability of sodium ions. The concurrent presence of PomB and MotB at low sodium-ion concentration suggests the existence of a hybrid motor in *S. oneidensis*.

Since it remains to be demonstrated whether MotAB stators are functionally incorporated in this hybrid motor, the second aim of this work was to biophysically analyse the contribution of MotAB and PomAB to motor rotation at the single cell level. To this end, a 'bead assay' and a 'tethered cell assay' were established. These set-ups required the delocalisation of the polar filament to a lateral position, the preparation of a highly specific antibody against the modified filament and, for the bead assay the attachment of polystyrene beads to the filament. While the bead assay was limited to short-term measurements, the tethered cell assay was optimised for long-term studies. The optimisation now permits a constant buffer exchange as well as the modulation of the stator complex level by an inducible promoter upstream of *pomAB* and *motAB*. Single cell analysis comparing the wild-type and the PomAB-driven motor revealed a significantly higher rotation speed for the wild-type motor at low sodium-ion concentration. Moreover, induced production of

PomAB in a stator deletion background resurrected rotation speed in a stepwise manner, whereas production of MotAB in a PomAB-driven motor decreased rotation speed stepwise. These results strongly indicate that MotAB is incorporated into the force-generating PomAB-occupied stator ring, slowing down motor rotation. MotAB production in a stator deletion background did not restore rotation. However, swimming assays revealed that MotAB is sufficient to drive flagellar rotation in a subpopulation of cells, strongly suggesting that both stators are able to function together in a single motor. To clearly characterise the role of MotAB and PomAB in the hybrid motor of *S. oneidensis* MR-1 further biophysical studies are required. The genome wide bioinformatic analysis of all sequenced bacterial genomes revealed that dual or multiple stator complexes along with a single flagellar system are surprisingly widespread among bacterial species. Moreover, stator complex homology comparison in *S. oneidensis* MR-1 indicated that MotAB has recently been acquired by lateral gene transfer as a consequence of adaptation to a fresh-water environment. Thus, the flagellar motor might still be in a process of optimisation.

Collectively, I hypothesize that *S. oneidensis* tunes its flagellar motor by exchanging stator complexes and that stator swapping represents a common mechanism applicable to other bacteria to adapt to changing environments.

ZUSAMMENFASSUNG

Bakterien sind in ihren Lebensräumen ständig wechselnden Bedingungen ausgesetzt. Dies erfordert eine aktive und gerichtete Fortbewegung, um das Überleben und die Anpassungsfähigkeit zu sichern. Ein höchst effizienter Weg der Fortbewegung wird durch die Rotation von Flagellen vermittelt. Der Modellorganismus *Shewanella oneidensis* MR-1 stammt – im Gegensatz zu anderen Shewanellen – aus einem Süßwasserhabitat und besitzt eine polare Flagelle, die sowohl von einem natriumabhängigen PomAB- als auch von einem protonenabhängigen MotAB-Statorsystem getrieben werden kann. Zwar wird der Flagellenmotor in *S. oneidensis* in erster Linie von PomAB betrieben, jedoch sind beide Statorsysteme durchgehend präsent und werden für maximale Geschwindigkeit der Flagellenrotation unter natriumlimitierenden Bedingungen benötigt. Für die Erzeugung des Drehmoments, bzw. der Rotation der Flagelle ist der Flagellenmotor – bestehend aus einem rotierendem Element, dem Rotor, und mehreren statischen Elementen, den Statoren – von essentieller Wichtigkeit. Obwohl die Statoren – welche den Rotor als ringähnliche Struktur einfassen – zur Erzeugung des Drehmoments fest in der Zellwand verankert sind, werden dessen Elemente stetig ausgetauscht, was erstaunlicherweise auch während der Rotation des Motors funktioniert. Klar ist bislang nur, dass sowohl Natrium- als auch Protonenabhängige Statoren denselben Motor antreiben können, jedoch wurde noch nie ein Hybridmotor beschrieben für dessen volle Leistung zwei verschiedene, gleichzeitig arbeitende Statorsysteme unabdingbar sind. Das wirft die Frage auf, wie PomAB und MotAB von *S. oneidensis* in einem Flagellenmotorsystem arbeiten.

Während meiner Arbeit konnte ich ein neuartiges Modell für den dynamischen Statoraustausch, als Anpassung an unterschiedliche Salzkonzentrationen, im Flagellenmotor von *S. oneidensis* entwerfen. Eine wichtige Voraussetzung für dieses Modell war eine synchrone und von der Salzkonzentration unabhängige Expression von *pomAB* und *motAB*, deren Nachweis über transkriptionelle Fusionen an *lucB* erbracht wurde. Mit Hilfe von Fluoreszensfusionen der B-Untereinheiten der Statoren an mCherry wurde deutlich, dass eine Fraktion von PomB – im Gegensatz zu MotB – unabhängig von der Natriumkonzentration polar lokalisiert. Bei hohem Salzgehalt wird PomB effizienter rekrutiert und erschwert somit vermutlich den Einbau von MotAB in den Statorring. Dagegen ließ das Lokalisationsmuster unter niedrigen Natriumkonzentrationen auf einen zeitgleichen Einbau von PomAB und MotAB in den Statorring schließen. Interessanterweise wird MotB in Abwesenheit von PomAB unter allen Natriumbedingungen zum flagellierten Pol rekrutiert. Wird jedoch PomAB wieder produziert, wird MotAB aus dem Statorring in die Membran verdrängt und von PomAB ersetzt. Über eine Quantifizierung von sfGfp-PomB Molekülen wurde deutlich, dass sich die Anzahl von mindestens neun in salzhaltiger auf fünf PomAB Komplexe in salzarmer Umgebung reduziert. Diese Ergebnisse unterstützen die These, dass die Inkorporation von PomAB dynamisch und in direkter Antwort auf die Natriumbedingung erfolgt, während die Rekrutierung von MotAB von der Anzahl an inkorporierten PomAB Statoren abhängig ist. Zwei weitere Proteine, MotX und MotY wurden im Laufe dieser Arbeit als essentiell für die Funktionalität, jedoch nicht für die Rekrutierung, von PomAB oder MotAB in den Flagellenmotor beschrieben. Zusammenfassend unterstützen diese Daten das Modell des dynamischen Statoraustausches zur Anpassung des Flagellenmotors an wechselnde Umweltbedingungen. Der zeitgleiche Einbau von PomAB und MotAB in einen funktionellen Statorring lässt auf die Existenz eines Hybridmotors in *S. oneidensis*

schließen. Es bleibt zu zeigen, welche Rolle MotAB in diesem bislang einzigartigen Hybridmotor übernimmt.

Daher sole sich nun der zweite Abschnitt meiner Arbeit mit der biophysikalischen Charakterisierung des Flagellenmotors auf Einzelzellebene und somit mit der Analyse der Beteiligung von MotAB und PomAB an der Flagellenrotation beschäftigen. Dafür wurden zwei Assays etabliert, zum einen der "bead assay" und zum anderen der "tethered cell assay". Die Vorrausetzungen dafür waren, eine lateral lokalisierte Flagelle und ein Antikörper gegen natives Flagellin, um sowohl die Anheftung der "beads" an die Flagelle, als auch die Anheftung der Flagelle an eine Oberfläche zu gewährleisten. Während der "Bead Assay" auf Kurzzeitmessungen beschränkt war, konnte der "tethered cell assay" funktional etabliert werden. Letzterer erlaubt nun einen konstanten Pufferwechsel und eine Modulierung des Statorproteinlevels. Erste Ergebnisse zeigten, dass der Motor des Wildtyps bei geringen Natriumkonzentrationen signifikant schneller rotiert, als der rein natriumabhängige Motor. Desweiteren konnte über die kontrollierte Produktion von PomAB ein schrittweiser Anstieg der Rotationsgeschwindigkeit beobachtet werden. Die Produktion von MotAB hingegen senkte die Geschwindigkeit eines PomAB-getriebenen Motors schrittweise ab. In anderen Arbeiten konnte bereits zuvor gezeigt werden, dass MotAB-getriebene Motoren geringere Rotationsgeschwindigkeiten erreichen, als PomAB-getriebene. Diese Ergebnisse deuten auf einen Einbau von MotAB hin, was in der Folge zu einem Abbremsen des PomAB getriebenen Motors führt. Die alleinige Produktion von MotAB konnte die Rotation des Zellkörpers nicht wiederherstellen. Jedoch können Zellen, welche nur MotAB besitzen, schwimmen, was impliziert dass MotAB prinzipiell funktional ist. Statorhomolgievergleiche deuten darauf hin, dass MotAB erst vor kurzem – vermutlich über lateralen Gentransfer in Zusammenhang mit der Anpassung an niedrige Salzbedingungen im Oneida See – in *S. oneidensis* gelangte. Die Aufnahme eines protonenabhängigen Stators erleichtert eventuell die Rotation der Flagelle im natriumarmen Süßwasserhabitat. Eine bioinformatischen Analyse aller sequenzierten bakteriellen Genome zeigte, dass multiple Statorsets bei Organismen mit nur einem Flagellensystem häufiger vorkommen, als bisher angenommen. Der dynamische Statoraustausch, mit dem *S. oneidensis* vermutlich seinen Flagellenmotor adaptiert, könnte auch in anderen Organismen eine Strategie zur Anpassung an schnell wechselnde Umweltbedingungen darstellen. *S. oneidensis* besitzt einen Hybridmotor, der sich vermutlich noch immer in einem Prozess der Optimierung befindet. Die spezifische Charakterisierung von MotAB und dessen Beitrag zur Rotation in einem dual getriebenen Statorring ist notwendig, um die Existenz eines funktionalen Hybridmotors auf biophysikalischer Ebene zu beweisen.

CONTENT

1 INTRODUCTION

In 1678 Antoni van Leeuwenhoek developed the first single-lense microscope and examined bacteria isolated from a puddle. He was fascinated by their different types of motion and described them as *little living animalcules*: "[…] *there were many very little living animalcules, very prettily a-moving. The biggest sort had a very strong and swift motion, and shot through the water like a pike does through the water* [..] " [1]. Van Leeuwenhoek could not see anything which allows these *little animalcules* to move but he was convinced that they possessed some type of paws which had to be extremely small: " […] *I can make out no paws, though from their structure and the motion of their body I am persuaded that they too are furnished with paws withal: and if their paws be proportioned to their body, like those of the bigger creatures* […] *a million of their paws together make up but the thickness of a hair of my beard; while these paws, besides their organs for motion, must also be furnished with vessel whereby nourishment must pass through them.*"

More than 350 years later, we know that the structure Antoni van Leeuwenhoek proposed for those fast swimming *little animalcules* is the bacterial flagellum. For many bacteria a flagellar structure allows various ways of movement to constantly and rapidly respond to environmental changes. It promotes swimming and swarming motility in diverse species, such as *Escherichia*, *Rhodobacter, Shewanella* and *Vibrio* species. In contrast, *Myxococcus* and *Neisseria* twitch and glide by using a different structure, type IV pili, and Mycoplasma species glide over surfaces employing so-called 'leg-protein'. Unlike swimming animals using muscle power-driven structures, swimming motility in bacteria is achieved by rotation of a long helical filament, the flagellum, propelling the cell towards optimal environments [2]. By employing this propeller bacteria can reach speed of up to 500 body lengths per second. In comparison, the cheetah and the Tiger Beetle (fastest animal on earth) reach up to 20 and 171 body lengths per second, respectively [1].

1.1 Architecture of the bacterial flagellum

The bacterial flagellum is a rotary motor as well as a protein export/assembly machinery. More than 20 different structural proteins and about another 30 proteins are required for regulation and assembly, respectively (see Table 1); [3]. From a structural perspective, protein production and assembly must be accurately coordinated to ensure a proper function of this multiprotein complex [4]. Due to its complexity, size and localisation in the membrane, an in-depth structural model of the bacterial flagellum remains to be elucidated. However, by combining X-ray structures, site-directed mutagenesis, freeze-fracturing electron microscopy, and cryo-electron microscopy a rather detailed model has evolved (Figure 1 A); [5-8]. Although there are some variations in the complex structure of the basal body, the overall structural characteristics appear to be similar among different species (Figure 1 B).

[1] taken from: http://www.pbrc.hawaii.edu/~petra/animal_olympians.html

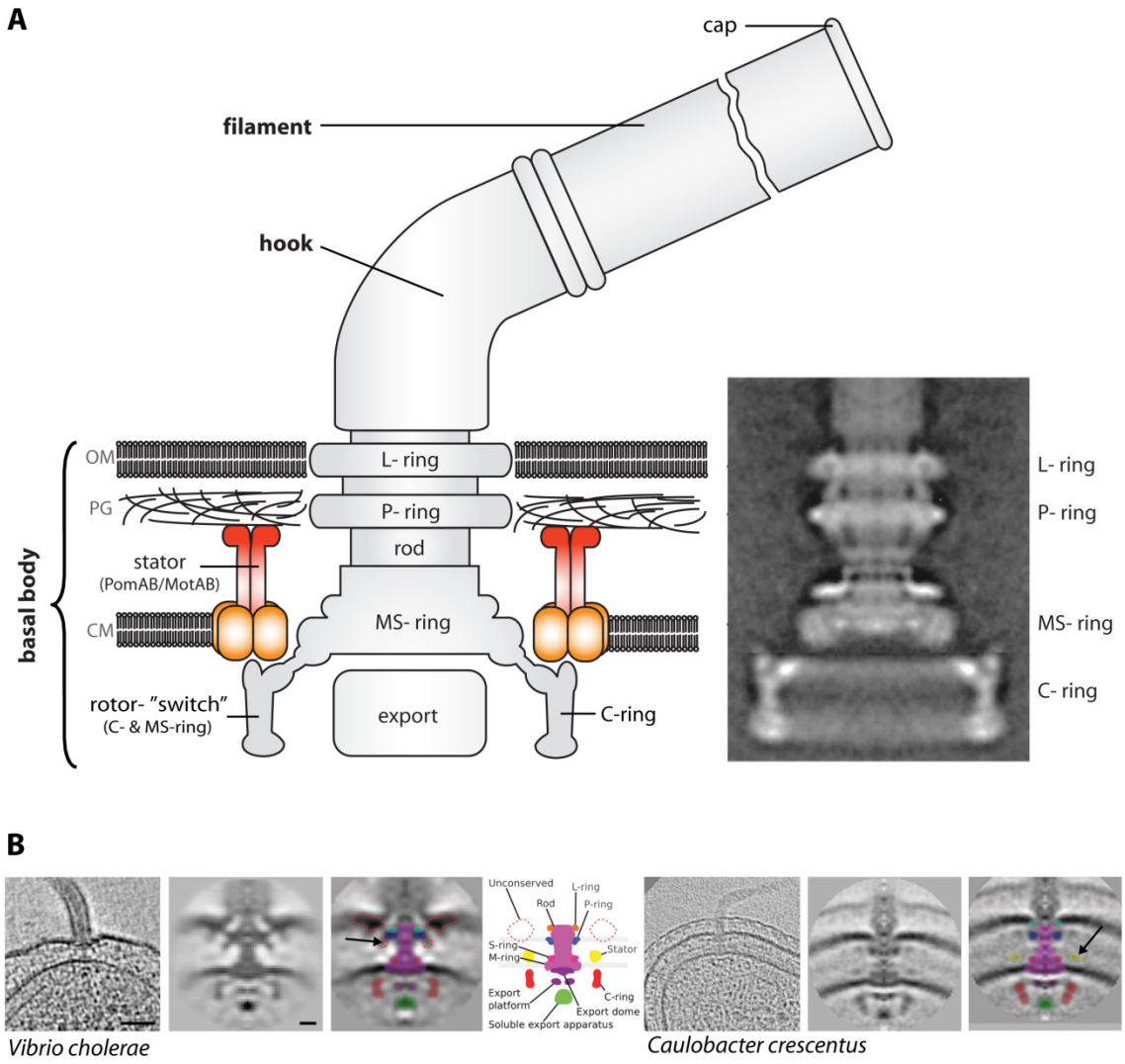

Figure 1: Main components of the bacterial flagellum. A) left: Displayed is a schematic sideview of the three major structures of the bacterial flagellum: filament, hook, and basal body. Flagellin subunits assemble with the help of the cap structure and form the filament. The hook connects the filament with the basal body and functions as a torque transmitting unit. The basal body is composed of ring-like structures (C-, MS-, P-, and L-ring), the rod and the motor. Stator and rotor are forming the motor. The stator complexes are anchored to the peptidoglycan layer and surround the MS-ring. MS-ring and C-ring function as rotor and binding of chemotaxis proteins induces a switch in direction of rotation. The export apparatus translocates late flagellar proteins, e.g. flagellin subunits. **Right:** An averaged reconstructed cryo-EM image of isolated basal bodies of *Salmonella*, nicely illustrating the ring-like structure. The EM-image was taken from [2]. OM, outer membrane; PG, peptidoglycan; CM, cytoplasmic membrane. **B)** Subtomograms of the flagellar motor reconstructed from electron cryotomograms of whole cells of *Vibrio cholerae* and *Caulobacter crescentus*. Left column: central slice trough subtomogram; middle column: axial slice through averaged reconstructed subtomogram; right column: conserved components as depicted in the cartoon. Note that in *V. cholerae* at the outside of the P-ring an additional ring-structure, the T-ring, is visible (annotated as unconserved region, black arrow). In *Caulobacter crescentus* the stator subunits surrounding the MS-ring are visible (highlighted by a black arrow). Images were adapted from [9]. Scale bar central slice, 50 nm and axial slice subtomogram, 10 nm.

Table 1: Main components of the *E. coli* flagella involved in assembly and functionality[a]. Modified after [2,10]

Gene product	Function or motor component	Cellular location	Structural components	Operon class
FlhC FlhD	master transcription activator complex for class II genes	cytoplasmic		I
FliF	MS-ring	cytoplasmic membrane	basal body	II
FliM FliN FliG	C-ring also called "switch" complex	peripheral	basal body	II
FlhA FlhB	export apparatus integral membrane proteins, interact with FliH-J	center of MS-ring	basal body	II
FliO FliP FliQ FliR	export apparatus integral membrane proteins, type three secretion	center of MS-ring	basal body	II
FliH FliI FliJ	export apparatus cytoplasmic proteins, delivery and unfolding of secretion proteins	cytoplasm	basal body	II
FlgB FlgC FlgF FlgG	proximal rod distal rod	periplasmic space	basal body	II
FlgI	P-ring	periplasmic space	basal body	II
FlgH	L-ring	outer membrane	basal body	II
FlgE FliK	hook hook length mediator	cell exterior	hook	II
FlgK FlgL	hook-filament junction, at hook hook-filament junction at filament	cell exterior	hook	III
FliA FlgM	sigma factor for class III operons anti-sigma factor, initiates transcription of class III genes	cytoplasm		II III
FliD	pentameric filament cap	cell exterior	filament	III
FliC	filament (flagellin)	cell exterior	filament	III
MotA/PomA[b]	stator subunit, exerts torque against "switch"	cytoplasmic membrane	basal body	III
MotB/PomB[b]	stator subunit, anchored to peptidoglycan layer, converts protons or sodium ions to energy	periplasmic space	basal body	III
MotX[b] MotY[b]	T-ring, surrounding L- and P-ring stabilisation stator complex	periplasmic space	basal body	late genes
FlgT[b]	H-ring, surrounding L- and P-ring stabilisation flagellar and stator ?	periplasmic space	basal body	late genes

[a] includes proteins involved in gene regulation but not in signal processing, chronologically ordered
[b] proteins are not present in *E. coli*, but found for example in *Vibrio* species [11,12].

Structurally, the bacterial flagellar motor consists of three major parts: the filament, the hook, and the basal body (for a detailed overview of major proteins see Table 1). The basal body is about 45 nm in diameter and embedded in the cell envelope. It is composed of ring-like structures (C-ring, MS-ring, P-ring and L-ring) and contains the motor. The motor is composed of a rotating component, the rotor (C-ring and MS-ring) and static components, the stator complexes (PomAB/MotAB). Hook and filament extend to the ouside of the cell. Their assembly is mediated by export of the corresponding proteins through an export apparatus, which is embedded in the central pore of the flagellar motor [13]. The hook connects the basal body to the filament and functions as a universal joint to transmit motor torque to the filament. The filament itself is about 20 nm in diameter, consists of thousands of flagellin (FliC) molecules and functions as a propeller [2,10]. Torque generation of this sophisticated multiprotein complex is driven by the motor fuelled by transmembrane ion gradients, protons and sodium ions [14-16].

Although the overall morphological features are similar, different movement strategies to actively navigate towards favourable environments have evolved. The knowledge of locomotion has long been driven by the understanding of rotational switching in *E. coli*. Environmental signals are processed and generate tactic behaviour through induced switching of the direction of motor rotation resulting in a randomly biased change of swimming direction. In peritrichous flagellated bacteria like *E. coli*, *Salmonella typhimurium* or *Bacillus subtilis* switching from counter clockwise (CCW) to clockwise (CW) converts smooth swimming (run) to tumbling [2]. Other bacteria, such as *Shewanella oneidensis* or *Vibrio alginolyticus*, have a single flagellum and thus, lack the tumbling mode. Here, switching from CCW to CW causes a run and reverse mode. In *V. alginolyticus* this two-stage mode was recently reported to be expanded to three stages, including a flick, which induces a fast cell reorientation [17]. In contrast, the single lateral flagellum of *Rhodobacter sphaeroides* and the flagella in *Sinorhizobium meliloti* employ unidirectional rotation, alternating between stop and go and changing speed, respectively [18,19]. Thus, although the flagellar motor has been studied for decades, the exact mechanism for switching as well as for torque generation are still not fully understood.

1.1.1 Regulation and assembly

Flagellar gene expression is temporally coordinated and coupled to the assembly state of the flagellum. Gene expression in *E. coli* and *Salmonella typhimurium* is arranged in a regulatory cascade of three classes [20-22]. Class I genes encode a σ^{70} factor (FlhDC), a master transcription activator complex essential for the initiation of class II gene transcription. Class II gene products comprise the hook-basal body complex, the σ^{28} factor (FliA), and the anti-σ^{28} factor FlgM. Class III promoters are negatively regulated by the anti-σ^{28} factor FlgM, which is released by the export apparatus, once it is assembled. Class III gene products are: filament, junction proteins, filament cap, motor proteins and components of the chemotaxis system [23]. Thus, functional assembly of early and middle gene products, starting with the MS-ring structure, determines whether late flagellar genes are transcribed.

In *Pseudomanas aeruginosa*, *Aeromonas hydrophila* and *Vibrio cholerae* late genes are regulated by the σ^{28} factor, however, the regulatory cascade is expanded to four tiers [24,25]; (Figure 2). Classes II and III genes are σ^{54}-dependent, whereas class IV genes are σ^{28}-dependent. At the top of the hierarchy is a σ^{54} factor (FlrA in *Vibrio*) which activates class II dependent promoters. Class II

genes encode a two-component-regulatory system (in *Vibrio* FlrBC), whose regulator (FlrC) activates transcription of hook basal body-encoding genes. Moreover, class II promoters in *Vibrio* also encode the σ^{28} factor (FliA), which activates transcription of class IV genes upon secretion of the anti σ^{28} factor [26,27]. Sequence homology comparison indicates that this four-tiered regulatory circuit also applies for flagellar transcription in *Shewanellae* species.

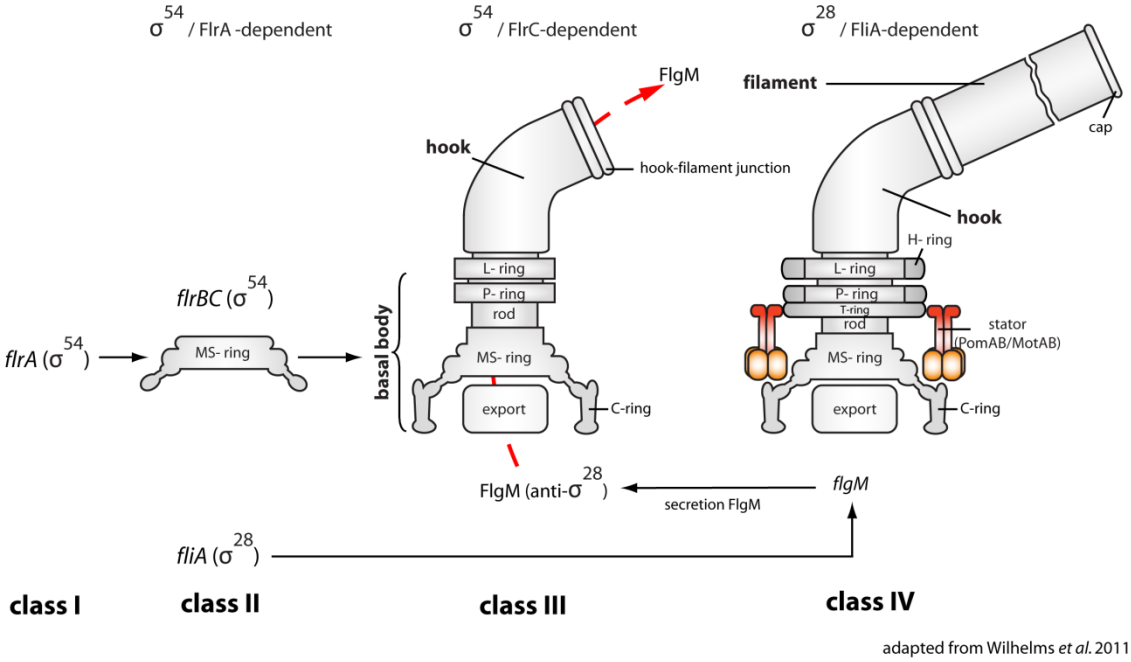

Figure 2: Regulation of assembly of the bacterial flagellum of *V. cholerae*. In *V. cholerae* the regulatory cascade is expanded to four tiers. Class II and III are σ^{54}-dependent, whereas late genes in class IV are σ^{28}-dependent. FlrA activates transcription of class II genes, which encode for FliF, a two-component regulatory system FlrBC and FliA (σ^{28} factor). FlrC activates transcription of the hook basal body-complex. FliA activates the transcription of FlgM, which itself negatively regulates σ^{28} and therefore blocks transcription of late flagellar genes. Once the export machinery is assembled, FlgM is exported and transcription of late genes, e.g. genes encoding for filament and stator complexes, is activated. Sequence homology comparisons suggest that this four-tiered circuit also applies *Shewanella* species. The figure was designed after the four-tiered circuit presented in Wilhelms *et al.* 2011 [24,28].

Main proteins important for the assembly and the structure of the bacterial flagellar motor are listed in Table 1 in chronological order regarding their assembly. The first structure to be assembled is the basal body with the protruding central rod. Assembly of the basal body is initiated by the formation of the MS-ring in the inner membrane, comprising 26 copies of FliF. Next, the C-ring, or the "switch" -complex termed after its function, attaches to the MS-ring. Together, C-ring and MS-ring constitute the rotor. Once those structures are formed the export apparatus is assembled within the central pore of the MS-ring. By using a secretion mechanism, which is part of a type III secretion system family (T3SS) the export apparatus translocates all proteins, except for those forming the P- and L-ring, across the cytoplasmic membrane. Secreted by the export apparatus, the rod structure, composed of FlgB, FlgC, FlgF and FlgG, congregates in the periplasmic space. P- and L-ring made of FlgI and FlgH, respectively, are transported by a Sec secretion system into the periplasm and assemble around the rod structure [10,29]. The hook, composed of FlgE, polymerises. Reaching a critical length of about 55 nm, the substrate specificity of the export apparatus is switched from

hook or rod proteins to filament subunits [30,31]. As a result the anti-σ^{28} factor FlgM is exported and the transcription of late flagellar proteins can start. The next structure formed externally is a pentameric filament cap (FliD) [32]. Afterwards, flagellin monomers are transported through the central shaft and the central core before being incorporated at the distal end of the filament by the assistance of the filament cap [32,33]. Typically, the filament is between 5-10 μm in length and 20 nm in width, and may contain more than 10,000 copies of flagellin monomers.

1.1.2 Propeller and universal joint

The propelling structure, the filament, is connected to the motor by a universal joint, called the hook. Forming a tubular structure, the filament is constructed of 11 strands of protofilaments consisting of a single protein, flagellin [34]. The filament is a polymorphic structure, undergoing a transformation from left-handed into right-handed helical forms induced by pH or torsion [35]. In swimming mode (CCW rotation) the filament is in a left-handed helix, switching to the right-handed curvature when swimming is interrupted and cells tumble (CW rotation) [36-39]. In contrast to the filament, the hook switches continuosly between the left- and the right-handed helical form during rotation [2].

1.1.3 Basal Body

A general morphological feature of the basal body is its ring-like structure. According to their localisation in Gram-negatives, they are referred to as the C-ring (**c**ytoplasmic), the M-ring (cytoplasmic **m**embrane), the S-ring (**s**upramembranous), the P-ring (**p**eptidoglycan) and the L-ring (**l**ipopolysaccharide) [40]. The M- and S-ring function as a unit and are composed of FliF proteins only and therefore are denoted MS-ring [41,42].

From a functional perspective, the basal body contains, besides the flagellar motor, the rod, the export apparatus, the L- and the P-ring. The bacterial flagellar motor, composed of rotor and stator complexes is responsible for torque generation and modulation of swimming performance upon tactic stimuli. The rotor is consisting of the C- and MS-ring and four A- and two B-subunits form one stator complex. The L-ring and the P-ring are thought to act as bushings, supporting the transmission of torque generated by the motor via rod and hook to the filament [2].

FliF is assumed to selfassemble and to form the MS-ring in a 26-fold symmetry within the cytoplasmic membrane [43,44]. FliM and FliN, constituting the C-ring, are responsible for rotation and for switching of motor direction to rotate either CW or CCW [45]. The C-ring is thought to have a 34-fold symmetry, *in situ*. However, Cryo EM tomography studies for phylogenetically diverse species demonstrated a variation of the C-ring symmetry [9]. FliN tetramers interact with FliM in a 34-fold symmetry [2]. The exact arrangement of the subunits and the molecular mechanism for switching is still widely discussed, but it is thought that two subpopulations of FliM exist to match the 26-fold symmetry of the MS-ring. About 26 out of 34 FliM molecules might be bound to the C-terminal domain of FliG and about 8 molecules might be bound in a different conformation to the middle region of FliG (Figure 3 C); [46-49]. FliG participates in forming both,

the C-ring and the MS-ring and has an interface for electrostatic interactions with the A subunit of the stator complexes [50,51].

Isolation of a complete basal body, also including the stator has not been successful so far. The number of stator units in the stator ring depends on the bacterial species. As initially observed in electron micrographs of freeze-fractured *E. coli* cells, at least 11 stator units surround the MS-ring (Figure 5 B); [5]. Recently, it has been shown that the torque-generating units are highly dynamic, which might explain the difficulties in visualisation.

1.1.4 Torque-generating units

The torque-generating units, the stator complexes, are composed of two different subunits and are commonly referred to as PomA and PomB, for the sodium ion-driven motor, e.g. in *Vibrio* species, and as MotA and MotB, for the proton-driven motor, e.g. in *E. coli.* [52,53]. Currently, there are no detailed atomic structures of the stator complexes available. However, site-directed mutagenesis and cross-linking studies identified stoichiometry, topology, and function-specific regions (Figure 3) [52,54,55]. The A-subunit (MotA/PomA) of a stator complex comprises four transmembrane domains and one large cytoplasmic domain between the second and third transmembrane region [56,57]. This cytoplasmic loop contains two conserved charged residues important for electrostatic interactions with conserved residues in FliG of the rotor (Figure 3 B); [58-60]. The B-subunits (MotB/PomB) anchor the stator to the cell wall via a C-terminal PG-binding motive [61]. As deducted from disulfide-crosslinking studies one stator complex, consisting of four A- and two B-subunits, forms two ion channels with a function specific Asp32 residue in MotB [52-54,62].

In *Vibrio* species, two auxiliary proteins, MotX and MotY, are involved in functional PomAB-motor assembly for the sodium ion-driven single polar flagellum [63-65]. These proteins form an additional ring structure, the T-ring, visible in electron micrographs of isolated basal body complexes [11]. MotX interacts with MotY and PomB whereas MotY binds to the PG-layer by a C-terminal PG-binding motif [66]. In *V. alginolyticus* and *V. parahaemolyticus* MotXY are required for recruitment of PomAB into the motor and they are proposed to play a role in stabilisation of the stator [11]. An ortholog to MotY (LafY) is involved in proton-dependent flagellar rotation of the lateral system in *V. parahaemolyticus*, thus, MotX and MotY are no peculiarity for sodium ion-dependent motors [67].

The bacterial flagellar motor is driving flagellar rotation and is fuelled by ion-gradients, sodium ions and protons. Equipped with a chemotaxis-navigated motility system, bacteria gain the ability to actively leave unfavourable environments and to move towards better conditions. Modulation of motor activity, e.g. rotational switching, and generation of torque are mechanisms driven by this highly sophisticated nanomachine. Although studied extensively, the exact mechanisms are still not fully understood. The next chapter focuses on recent findings in the molecular processes in this nanorotor.

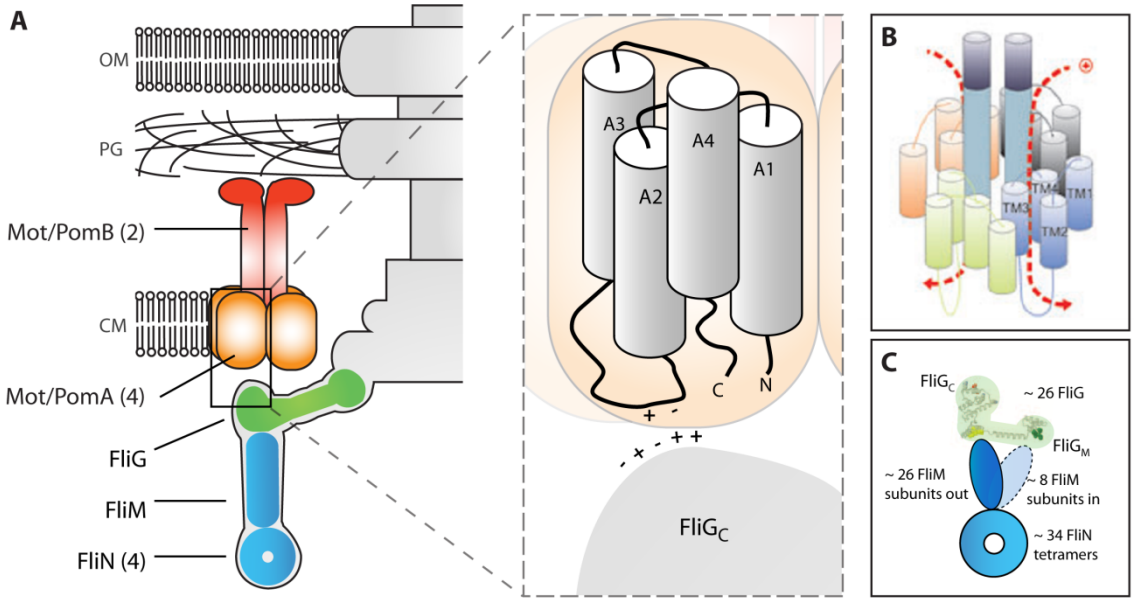

Figure 3: The bacterial flagellar motor. A) Displayed is a side view of the flagellar motor with the switch complex composed of FliG/FliM/FliN and the stator complexes PomAB and MotAB, each consisting of four A- and two B-subunits. **Close up dashed rectangle:** One A-subunit has four transmembrane domains (A1 to A4). The cytoplasmic loop between A2 and A3 has conserved charged residues thought to interact electrostatically with the conserved charged residues of the C-terminal domain of FliG. **B)** Topology of the membrane segments of one stator complex (A_4B_2) based on cross-linking studies as proposed by Kim *et al.* [68]. The four A-subunits and the corresponding transmembrane domains are displayed in blue, green, red and black. Individual transmembrane domains of the two B-subunits are in the middle of the complex and shown in cyan, the C-terminal peptidoglycan-binding domain is coloured in dark blue. One stator complex forms two ion-channels. The dashed line in red suggests the path of the driving ion through one channel. **C)** Enlarged view of the composition of the C-ring. It is assumed that FliM interacts with a FliN tetramer. Both proteins are thought to have a 34-fold symmetry. FliM is pictured in two orientations. First, about eight subunits interact with the middle domain of FliG (green). Second, about 26 FliN subunits interact with a hydrophobic patch in the C-terminal domain of FliG (yellow). The cartoon showing the membrane topology (B) taken from [69]; (C) modified after [46].

1.2 Physiology of the bacterial flagellar motor

Contrary to the propagation of helical waves, as suggested by its denotation (lat.: *flagellum* – whip) rotation of individual flagellar motors was first visualised by Silverman and Simon in the 1970s who tethered filaments to a coverslip and observed the rotation of the cell body [70]. At the same time, Larsen and co-workers discovered that motility is not coupled to ATP, but is rather depending on an ion-gradient [71]. Hence, those studies defined motor rotation or torque as the output of the bacterial flagellar motor and the ion-gradients as the input.

1.2.1 Output and Input of the bacterial flagellar motor

Propelling of the flagellar filament is propagated by the rotation of the flagellar motor. Motor performance can be described by physical parameters of rotation/swimming speed and torque. Under low Reynolds numbers torque can be determined by multiplying the angular velocity of the motor with the viscous drag (e.g. the load on the flagellar filament). In a motor-specific range at a

given torque, rotation speed could be varied by changing the drag, e.g. by viscosity, by attaching beads to the filament or by applying external torque [72].

Techniques to measure torque and rotation speed of the flagellar motor have advanced during the last decades (Figure 4 A). To date, they can be modified and monitored by i) microscopy of swimming cells at different viscosities [73,74]; ii) tethered cell assays [70,75,76]; iii) bead assays with different sizes of polystyrene beads [77,78]; and iv) electrorotation of tethered cells, where external torque is applied to the cell body [79-81]. Video microscopy of swimming cells is a simple approach to compare cell populations regarding their flagellar performance under low load (Figure 4 B), however, it does not allow to exchange the buffer and to monitor differences in rotation speed at the single cell level. By using the tethered cell assay or the bead assay, rotation speed can be analysed at the single cell level while the buffer is transiently exchanged. In a tethered cell assay, cells are attached to the surface by their flagellar filament and the cell body itself serves as a marker for rotation. Due to the size of the cell body (high load), cells will only rotate at low speeds (Figure 4 B). Using the bead assay allows changing the load on the filament by varying the bead size.

OUTPUT

When functional stator complexes are produced in a stator deletion mutant, motor rotation speed can be resurrected in a step-wise manner (Figure 4 C); [76,82]. Early experiments have been carried out with tethered cell assays, in which the cell body was spinning at 10 Hz. By using this setup, the cell body has a larger drag coefficient than the filament. Thus, rotating motors work under unphysiological high load and; consequently; cell bodies rotate at low speed [76]. In resurrection experiments with tethered cells or with 1 μm polystyrene beads attached to the filament, motor speed is proportional to the number of incorporated stator units. The step-wise increments in speed demonstrate the association of functional stator complexes into the stator ring. However, resurrected motors labelled with smaller beads (0.3 μm) have diminished steps of speed increments and a plateau of maximal speed is reached [78]. Interestingly, resurrection experiments under zero load, by attaching a 60 nm gold bead to the hook to filament-loss mutants, revealed a sudden single step to the maximal value of rotation speed [83]. These data indicate that under low/zero load rotation speed reaches a maximal value independent of the number of incorporated stator units. Thus, under conditions of low load the rotation rate is the limiting factor after which the motor cannot be speeded up anymore. In contrast, under conditions of high load individually engaged stator complexes increase rotation speed in a step-wise fashion.

INPUT

The flagellar motor can be fuelled by the proton-motive force (pmf) or the sodium-motive force (smf) through the stator complexes across the cell membrane. Generally, sodium ion-driven motors rotate faster than proton-driven ones. Speed measurements, under low load, revealed that the sodium ion-dependent motor of *V. alginolyticus* spins up to 1700 Hz [84], whereas the proton-driven motor of *E. coli* achieves a maximum of 300 Hz (Figure 4 B) [79]. Direct measurement of the proton stoichiometry by voltage clamp techniques estimated that about 1200 ions are required for one revolution of the motor [85]. As mentioned above, rotation measurements under low load indicated that ion movement is the major rate-limiting factor for rotation. Therefore, more rapid rotation of the sodium-ion dependent motor is explained by the presence of higher sodium-ion gradients [72,84,86].

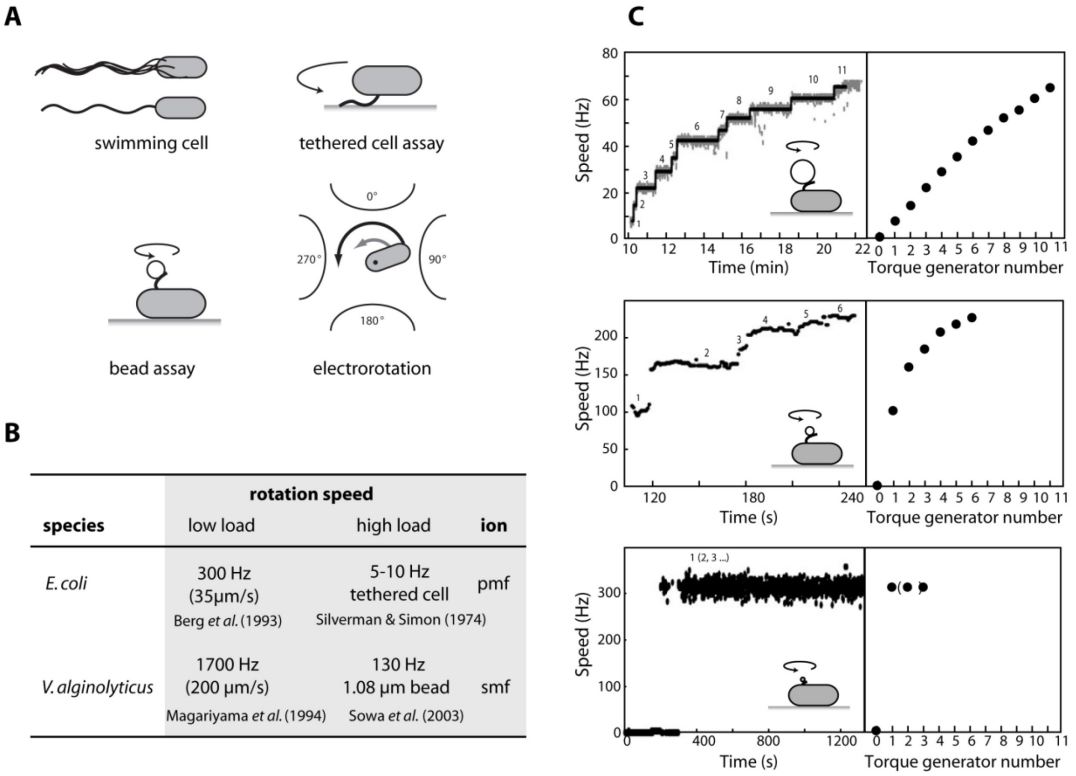

species	rotation speed: low load	rotation speed: high load	ion
E. coli	300 Hz (35µm/s) Berg *et al.* (1993)	5-10 Hz tethered cell Silverman & Simon (1974)	pmf
V. alginolyticus	1700 Hz (200 µm/s) Magariyama *et al.* (1994)	130 Hz 1.08 µm bead Sowa *et al.* (2003)	smf

Figure 4: Output of the flagellar motor. A) Schematic overview of techniques to measure flagellar motor performance. **Upper left,** swimming speed can be determined by video microscopy (flagellar filament equals low load). **Upper right,** in a tethered cell assay, the cell is attached by the flagellar filament and rotation of the cell body is measured (cell body equals high load). **Bottom left,** in a bead assay cells are attached to the surface and rotation speed of the filament is measured, by a polystyrene bead attached to the filament. The advantage of the bead assay is that the load is variable due to the size of the polystyrene bead. **Bottom right,** external torque is applied to a tethered cell by generating a megahertz rotating electric field with microelectrodes [80]. **B)** Displayed are the observed rotation speeds/ swimming speeds (in brackets) for the proton-driven and sodium-ion driven flagellar motor of *E. coli* and *V. alginolyticus*, respectively. **C)** Resurrection experiments for a proton-dependent motor under different loads. **Upper panel**: 1 µm bead attached to the filament; middle panel: 0.3 µm bead attached to the filament and lower panel: 60 nm gold bead attached to the hook. Motors labelled with 1 µm beads show 11 steps in speed (high load equally to the load of a cell body in a tethered cell assay), motors labelled with 0.3 µm beads show six steps (low load). Motors labelled with 60 nm gold beads display a sudden jump to the maximal speed of 300 Hz. A) and C) modified after Sowa *et al.* [72].

1.2.2 Flexible rotor-stator interactions in the bacterial flagellar motor

Torque generation and modulation of motor activity, e.g. by switching direction of rotation, enables bacteria to actively navigate towards favourable conditions. The best studied mechanism for directional switching is the response to chemoeffectors in *E. coli*. Changes of chemoeffector levels are detected by chemoreceptors and signals are processed and transferred via a complex pathway to the response regulator CheY [87]. Phosphorylated CheY molecules (CheY-P) interact with FliM and FliN of the switch complex and induce a switch in the direction of rotation from CCW to CW, as a consequence cells tumble or reverse [88-90]. Rotational switching is caused by a reorientation of the C-ring through CheY-P in a cooperative manner. Thus, it is thought that the stator-rotor interface is reorientated and therefore the direction of torque generation is reversed [91-93].

Torque is thought to be generated by electrostatic interactions between the cytoplasmic loop of the stator A subunits and the C-terminal domain of FliG in the rotor. However, the exact mechanism

for generating torque in bacterial flagellar motors is still unknown. The favoured model for the proton-driven flagellar motor of *E. coli* is that protonation of the conserved Asp32 residue in MotB coordinates conformational changes in MotA. Subsequently, two charged residues in the cytoplasmic loop of the A-subunit, which are assumed to interact electrostatically with five charged residues in the C-terminal domain of FliG, are shifted, by that mediating motion in FliG and therefore create torque (Figure 3 A); [52,61,94,95]. It is assumed that this interaction between stator and rotor causes the rotor to move a step of approximately 14°°.This implies that the motor undergoes approximately 26 steps per revolution, which is consistent with the estimated number of FliG proteins [96].

Mutational studies in *E. coli* identified seven charged residues in the cytoplasmic loop of MotA and the C-terminal region of FliG that are involved in electrostatic interactions [95]. Interestingly, neither reversing the charge of one nor neutralising the charge of two residues completely abolished rotation, indicating rather robust interactions. However, mutations reversing the charge of both protein interfaces can compensate each other. These findings indicate an electrostatic interaction between the conserved charged residues in the cytoplasmic loop of MotA and the C-terminal domain of FliG [97,98].

Comparative studies using *Vibrio* stator and/or rotor components in an *E. coli* background, strongly indicated that PomA and FliG interact in a similar manner to MotA and FliG [99,100]. The conserved Asp24 in PomB of *V. alginolyticus* is equivalent to Asp32 in MotB of *E. coli*. However, recent studies strongly indicated that ion conductivity in PomAB and the electrostatic interaction with FliG is more robust in *Vibrio* species. Both PomA and PomB are less sensitive to mutations in their conserved charged residues and it is proposed that auxiliary proteins, such as MotXY, might enhance this robustness and with that motor functionality [12,59,101,102]. Taken together, FliG can functionally interact with foreign stators. The interaction between rotor and stator is rather flexible and the main mechanism to create torque is similar for proton- and sodium ion-driven motors. This suggests that one motor is able to rotate simultaneously with stators depending on different coupling-ions, although so far this has not been shown to exist in natural systems. Moreover, the component of the stator complex which directly determines the characteristics of the motor is not known to date.

1.2.3 Dynamic rotor-stator interactions in the bacterial flagellar motor

A single stator in a tethered cell can generate torque to rotate the whole cell body. Therefore, it must be tightly anchored to the cell wall. This strong linkage is achieved by a putative C-terminal PG-binding domain in the periplasmic part of the B-subunits [103]. Ion-channel activity of the stator complexes is coupled to incorporation into the stator ring [55,75]. The current model for stator activation postulates that a "plug" in the periplasmic region of the B-subunit opens the ion channel upon association into the stator ring. This activation is thought to be caused by a conformational change within the periplasmic region of the B-subunit when anchored to the PG-layer [104,105].

In contrast to what may be expected, the stator complexes are not permanently incorporated into the stator ring, but rather in a process of dynamic turnover. It has been reported that inactive stator A_4B_2 precomplexes are freely diffusing in the membrane before getting recruited into the stator ring (Figure 5 A); [103,106]. The dynamic exchange with membrane-embedded precomplexes, even in a

functioning motor, was described in early experiments with tethered *E. coli* cells. Here, transient speed changes in wild-type motors were observed, indicating dissociation and reassociation of stator complexes [76,107]. Moreover, as already described above motor rotation speed can be resurrected in a step-wise manner by production of stator units in a stator deletion mutant [76,78,82]. Taken together, these studies indicate that torque is generated by independent stator units and that even a single stator unit is sufficient to drive flagellar rotation. In addition, the variability in rotation speed indicates that stator units can enter and leave the stator ring (Figure 5 C).

The first direct evidence that single stator units associate and dissociate from the rotating motor was obtained by FRAP and FLIP experiments using fluorescently labelled MotB subunits in *E. coli* [104]. Thereby, a constant exchange of 11 stator units in the stator ring was demonstrated. This number is in accordance with resurrection experiments and earlier EM micrographs (Figure 5 B); [5,104,108]. Individual stator units are rapidly exchanged in a rotating motor within 30 s, indicating that the stator ring is in a surprisingly high constant turnover. Whether or not this is coincidence in this highly sophisticated nano-machinery remains unclear, however, it might allow replacement of mechanically damaged stators or it might be a mechanism to tune the flagellar motor according to environmental conditions.

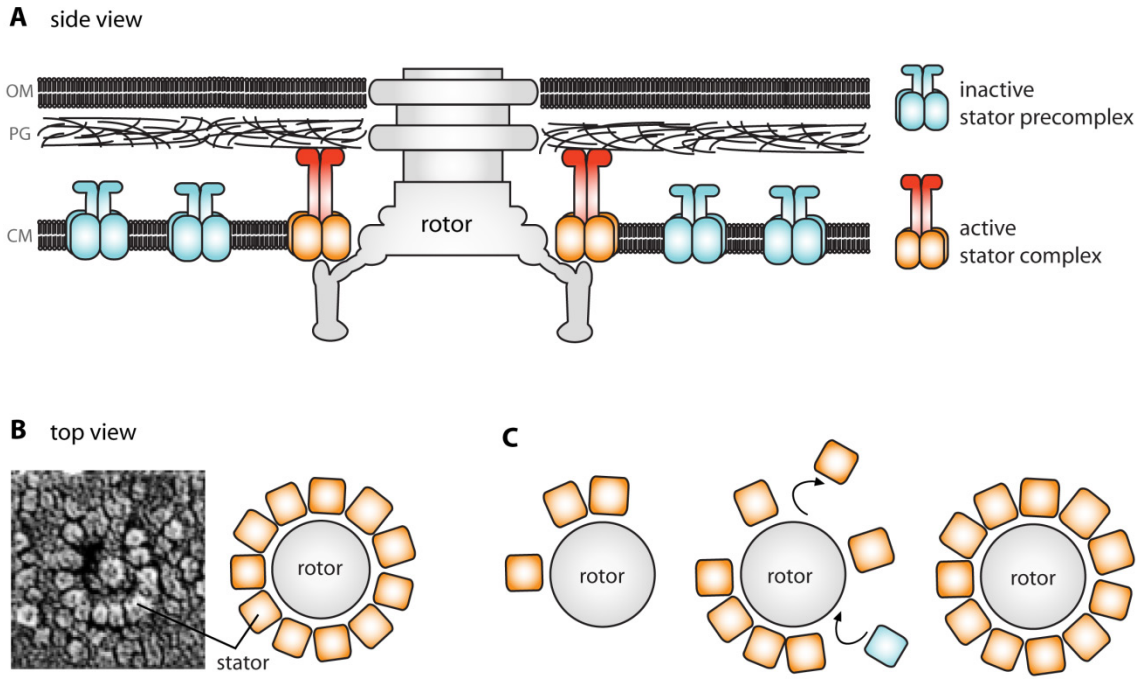

Figure 5: Dynamic rotor-stator interactions. A) Side view of the flagellar motor showing inactive stator precomplexes (blue) diffusing in the membrane. Activated stator complexes are anchored via their C-terminal PG-binding domain to the cell wall (red). **B) Top view** of the bacterial flagellar motor; left: a freeze-fracture EM picture with stator particles arranged in a circle, EM picture taken from Khan *et al.* [5]; right: cartoon of the arrangement of the stator complexes. **C)** Cartoon showing that individual stator complexes are able to rotate the flagellar motor. Stator complexes are highly dynamic and are constantly exchanged. Red: active stator complex, blue: inactive stator complex

Recently, Fukuoka and colleagues suggested how stator assembly in a sodium-ion dependent motor might be regulated. They provided evidence that incorporation of the PomAB-driven stator complexes in the polar flagellum of *V. alginolyticus* depends on the presence and concentration of sodium ions [15,109]. By fluorescence tagging of PomA and PomB subunits they demonstrated that the polar localisation of PomAB was lost in the absence of sodium chloride, but was rapidly restored upon addition of the same. Furthermore, blocking the sodium-ion transport, collapsing the sodium-ion gradient or substituting the critical PomB-Asp24 residue to Asn resulted in delocalisation of PomAB stator complexes, indicating that sodium-ion flux as well as binding of the sodium ion in PomB is essential for functional assembly into the flagellar motor. Thus, the rotor-stator interactions are highly dynamic and directly linked to the sodium chloride concentration in the environment.

The turnover described for stator units in the stator ring was the first evidence for a dynamic rotor-stator interaction. However, as further investigations revealed, even rotating parts in a functioning motor undergo a dynamic turnover. By using fluorescent fusions to the rotor proteins FliG, FliM and FliN, Fukuoka and colleagues demonstrated that FliM and FliN are exchanged, whereas FliG is not [110]. Accordingly, FliM turnover and stoichiometry in a functioning flagellar motor of *E. coli* was analysed by TIRF microscopy and coupled with FRAP and FLIP analysis by Delalez and colleagues [111]. In this system, approximately 30 FliM-YPet molecules were detected in two discrete subpopulations, one, representing about two third of all FliM molecules, undergoing turnover and the other tightly associated with the C-ring. This ratio is in agreement with a structural model of the C-ring, which suggests that ~ 26 out of ~ 34 FliM molecules are bound to the C-terminal domain of FliG and ~ 8 molecules in a different conformation are bound to the middle region of FliG (Figure 3 C); [46]. Thus, the recent findings on the bacterial flagellar motor inspire a novel view on the assembly process of this sophisticated nanomachine, proposing that protein turnover and the dynamic exchange of subunits in response to environmental changes are important mechanisms to modify flagellar motor performance.

In this work, I expanded the model using the flagellar motor of *S. oneidensis* MR-1 as model system.

1.3 *Shewanella oneidensis* MR-1

1.3.1 The genus *Shewanella*

The first *Shewanella* species was isolated as *Achromobacter putrefaciens* in 1931 as one of the microorganisms responsible for butter putrefaction [112]. In 1941 the taxon was renamed to *Pseudomonas* [113] and after further reclassifications in the 60ies and 70ies, e.g. to *Alteromonas* [114], finally reclassified in 1985 on the basis of 5S rRNA into a new genus within the order of *Alteromonadales* to *Shewanella* [115]. Currently about 40 species (19 fully sequenced), isolated from different habitats, are assigned to the genus *Shewanella* (Figure 6); [116]. *Shewanella* species (www.shewanella.org) are Gram-negative, rod-shaped, γ-proteobacteria with 2-3 μm length and 0.4-0-7 μm diameter [117].

Shewanellae compose a physiological and ecological diverse group of facultative anaerobic bacteria, which are widely distributed in sedimentary and aquatic environments including marine and fresh-

water habitats (Table 2). Remarkable capacities of this genus are their respiratory diversity and their ability to grow under low temperatures, which allows these species to thrive in diverse ecological niches. Members of the genus *Shewanella* have been isolated from a range of salt concentrations, temperatures, barometric pressures, in symbiosis and syntrophy with other organisms and even as pathogens [116]. The respiratory diversity allows Shewanellae to use a wide range of terminal electron acceptors including toxic elements and insoluble metals [118]. The discovery of the capability of *S. oneidensis* MR-1 to reduce manganese oxides under anaerobic conditions started a new era for the genus *Shewanella* in 1988 [119]. Numerous studies identified for *Shewanella* spp. an impressive number of alternative electron acceptors for respiration in the absence of oxygen [117,119]. More than 20 organic and anorganic substrates, including a number of toxic elements and insoluble metals, including uranium [U(VI)] [120], chromium [Cr(VI)] [121], iodate [122], technetium [123], neptunium [124], plutonium [125], selenite [126], tellurite [126] and vanadate [127] can be respired by *Shewanella* [116]. This extraordinary respiratory capacity presents opportunities for converting toxic soluble compounds into insoluble non-toxic compounds in polluted groundwater and makes them interesting candidates as tools for the process of bioremediation.

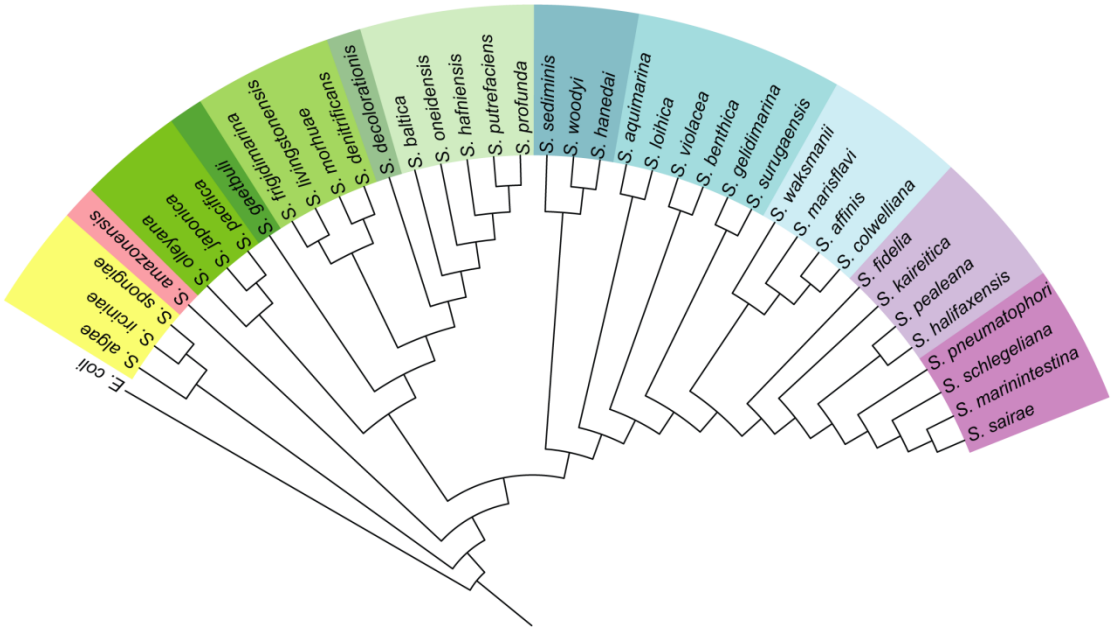

Figure 6: Phylogenetic analysis of the genus *Shewanella* adapted from Hau *et al.* 2006 [116]. Phylogenetic comparison within the genus *Shewanella* shows clusters of some groups that were isolated from similar habitats. Different colours highlight different groups of *Shewanella* (see also Table 2). Coloured in purple forming a monophyletic group for example are isolates from fish intestinals (*S. pneumatophori, S. schlegeliana, S. marinintestina,* and *S. sairae*). Phylogenetic relationships were analysed based on 16S rRNA sequences, trimmed to ~1200 bp to facilitate comparison between species with incomplete sequences. The alignment was performed using ClustalW and the phylogenetic tree was calculated using the neighbour-joining algorithm after 1000 bootstraps using PAUP. *E. coli* MG1655 was used as outgroup.

Flagella-mediated motility is versatile within this environmentally relevant group of bacteria. A recently in our lab performed phylogenetic analysis of the 16 fully sequenced *Shewanella* isolates revealed that most of the *Shewanella* species, e.g. *S. amazonensis; S. sp.* MR-4 and MR-7 and *S. baltica*,

harbour at least one flagellar system along with one stator complex, which is homologous to the sodium ion-dependent PomAB system in *Vibrio* species (Table 2); [3,116,128]. Some *Shewanella* isolates, e.g. *S. putrefaciens* CN-32 and *S. piezotolerans* WP3 posses a second flagellar system with homologies to the lateral flagellar system of *Vibrio* species. These complete flagellar systems also include a second set of stator complexes [129,130]. As an exception among the *Shewanella* species, *S. oneidensis* MR-1 which was isolated from a fresh-water habitat, possesses two distinct stator complexes but only a single polar flagellum.

Table 2: Putative stator and flagellar systems and habitats of sequenced *Shewanella* species.

strain	number of putative		Gene ID (coupling ion*)	isolation site	reference
	flagellar systems	stator system			
S. amazonensis	1	1	Sama2432/2433 (smf)	Amapa River, Brazil sediments	[131]
S. baltica OS155	2	2	Sbal1360/1361 (smf)	Baltic Sea marine habitat, 90 m depth	[132]
S. baltica OS185	1	1	Shew1851346/1347 (smf)	Baltic Sea marine habitat, 120 m depth	[132]
S. denitrificans OS217	2	2	Sden2568/2567 (smf) Sden3632/3631 (pmf)	Baltic Sea marine habitat, 120 m depth	[133]
S. frigidimarina NCIMB 400	1	1	Sfri2787/2786 (smf)	Coast of Aberdeen, UK marine, North-Sea	[134]
S. loihica PV-4	1	1	Shew2768/67 (smf)	Hawaiian Sea mount, US iron-rich mat, hyrothermal vent	[135]
S. oneidensis MR-1	1	2	SO_1529/1530 (smf) SO_4287/4286 (pmf)	Lake Oneida; US sediments, fresh-water	[136]
S. pealeana ATCC70034	2	2	Spea2987/2988 (smf) Spea0056/0057 (pmf)	Woods Hole Harbour, US squid nidamental gland	[137]
S. piezotolerans WP3	2	2	Swp5126/5127 (smf) Swp3615/3616 (pmf)	West Pacific site sediment, 1,914 m depth	[138]
S. putrefaciens CN-32	2	2	Sputcn32_1279/1278 (smf) Sputcn32_3447/3448 (pmf)	Albuquerque; US subsurface, shale sandstone	[139]
S. sediminis HAW-EB3	2	2	Ssed3326/3325 (smf) Ssed0050/0049 (pmf)	Halifax Harbour, CAN sediment, 215 m depth	[140]
S. sp. ANA-3	1	1	Shewana32898/2897 (smf)	Woods Hole, US brackish-water, arsenic threatened wooden pier	[141]
S. sp. MR-4	1	1	Shewmr42728/2727 (smf)	Black Sea marine, 16°C, 5 m depth	[142]
S. sp. MR-7	1	1	Shewmr72800/2801 (smf)	Black Sea marine, high NO_3, 60 m depth	[142]
S. sp. W3-18-1	2	2	Sputw31812827/2828 (smf) Sputw31810491/0492 (pmf)	Pacific Ocean, US marine sediment	[143]
S. woodyi	1	1	1177/1178 (smf)	Strait of Gibraltar detritus, 370 m	[144]

* based on homology comparison; smf, sodium-motive force; pmf, proton-motive force

1.3.2 Motility of *S. oneidensis* MR-1

S. oneidensis MR-1, isolated from the fresh-water habitat Lake Oneida, is environmentally and biotechnically important due to its ability to use a wide range of alternative electron acceptors. Its genome consists of a 4.9 Mbp circular chromosome and a 1.6 Mbp Megaplasmid, with an average GC content of ~ 43% and 5,066 encoded open reading frames [136].

The Gram-negative organism exhibits optimal growth at sodium chloride concentrations between 100 mM and 300 mM. Natural sodium chloride concentration in fresh-water environments reach a maximum of 35 mM, thus, the optimal growth concentration for *S. oneidensis* is rather high [145]. To be able to swim towards redox-active surfaces or to form biofilm communities, *S. oneidensis* MR-1 requires flagella-mediated motility [146,147]. Motility towards anaerobic electron acceptors is therefore directed by a chemotactic response [142,146]. Little is known about the chemotaxis system in *S. oneidensis*, however, a highly conserved chemotaxis cluster has been identified recently. Genomic analysis revealed that two uninterrupted *cheA* gene loci, annotated as *cheA-1* and *cheA-3* (SO_2121 and SO_3207, respectively) and one interrupted *cheA-2* gene locus are located in this chemotaxis cluster. The CheA-3 protein which is conserved among all sequenced *Shewanella* species is essential for chemotactic response towards anaerobic electron acceptors, but not for aerotaxis [148]. Although, CheA-1 is conserved in a sub-set of *Shewanella* it does not play a role for chemotactic response to redox-active surfaces or in aerotaxis [148].

Genome sequence analysis revealed that *S. oneidensis* MR-1 harbours one flagellar cluster, including single orthologous to FliF, an early protein and the basic component of the MS-ring, and a single orthologous to FliG, FliM and FliN, switch complex proteins important for flagellar rotation. However, genes encoding for two putative stator complexes were found in the genome of *S. oneidensis* MR-1. One of the stator complex (SO_1529/SO_1530) shares homologies with the sodium ion-dependent system in *Vibrio* species and was therefore annotated as *pomAB*. The second system (SO_4287/SO_4286), annotated as *motAB*, exhibits homologies to proton-driven stator complexes in the lateral flagella system of *Vibrio* species [149]. Previous characterisation performed in my diploma thesis accredits MotAB to be proton-dependent and PomAB to be sodium ion-dependent. Furthermore PomAB has been shown to be the dominant stator complex [150]. As shown by the constructed functional fluorescent protein fusions to the B-subunits, PomAB and MotAB localise polarly. Interestingly, swimming speed measurements revealed that full speed at low sodium-ion concentration requires both PomAB and MotAB, suggesting that MotAB and PomAB are simultaneously active in the single flagellar motor under low sodium-ion conditions. Supportively, according to single cell analysis with short-lived Gfp both *pomAB* and *motAB* are concurrently transcribed [128].

Although, those earlier studies indicate that PomAB and MotAB simultaneously contribute to motility in *S. oneidensis*, the exact mechanism remains to be elucidated.

1.4 Scope

The bacterial flagellar motor has become a model system for assembly, function, dynamics and adaptation of a multiprotein nanomachine. Chemical energy of an ion gradient is converted into mechanical energy of filament rotation and a remarkable sensory system allows the rapid response to changing conditions. Structure and physiology of the bacterial flagellar motor has been well studied, however, recent advances in fluorescent labelling methods and microscopic approaches start to expand our understanding of the mechanics of and the dynamics within this nanomachine. It has recently been shown that subunits from the static and rotating part can be exchanged while the flagellar motor continues to operate, suggesting that static and rotating units might be exchanged in response respect to different environmental conditions.

The textbook model organism *E. coli* has a single stator system along with a single flagellar system. Interestingly, the number of stator systems can exceed the number of flagellar system, as described for *Bacillus* species or *S. oneidensis* MR-1, the model organism studied in this work. *S. oneidensis* MR-1 harbours two different stator systems, one proton- and one sodium ion-dependent, along with a single flagellar system. Both, PomAB and MotAB contribute to motility, and swimming speed measurements propose that they are both incorporated into the same stator ring at low sodium-ion concentration. The process of the incorporation of the stator complexes into the flagellar motor is very limited. Here, I determine how dual stator systems might function and propose a novel model on how flagellar function might be modulated.

Specifically the following questions were addressed:

1) **What dynamic underlies the stator exchange of PomAB and MotAB in the single flagellar motor of *S. oneidensis* MR-1 at different sodium-ion concentrations?** To address this question, protein and transcription levels of the stators were determined. Furthermore, the incorporation of the stator complexes into the stator ring at different sodium-ion concentrations was monitored by fluorescent protein fusions to the B-subunits. Quantification of single molecules was carried out to reveal whether both stator complexes are simultaneously incorporated, or whether they form distinct stator rings, occupied by either PomAB or MotAB.

2) **Does the composition of the stator ring influence the performance of the polar flagellum?** To this end the contribution of PomAB and MotAB to rotation speed and their biophysical properties was required to be determined. In order to monitor rotation speed at the single cell level a bead assay and a tethered cell assay had to be established for the polarly flagellated species.

2 RESULTS

2.1 Two different stator complexes for one polar flagellum

The first chapter will focus on the characterisation of PomAB and MotAB in *S. oneidensis* MR-1. The in this work conducted phylogenetic analyses propose that PomAB is a natural stator complex of *S. oneidensis*, whereas MotAB has likely been acquired by lateral gene transfer. The localisation dynamic of PomB-mCherry and MotB-mCherry at different sodium-ion concentrations was analysed and it was found that at low sodium-ion concentration MotB-mCherry and PomB-mCherry localise at the flagellated pole in more than 70 % of the cell. Additionally, the localisation of MotB-mCherry is dependent on the presence and abundance of PomAB. Furthermore, a functional N-terminal fusion of Gfp to PomB was constructed, which was then used to analyse the number of PomB incorporated into the stator ring at different sodium-ion concentration. The obtained data provide evidence for the existence of a hybrid motor in *S. oneidensis* MR-1 which concurrently uses proton and sodium ions under low sodium-ion conditions.

2.1.1 MotAB is most likely acquired by lateral gene transfer

Homology comparisons of PomAB and MotAB subunits of *S. oneidensis* MR-1 at the amino acid level resulted in two major clusters (Figure 7, extract of the comparison for the B-subunits).

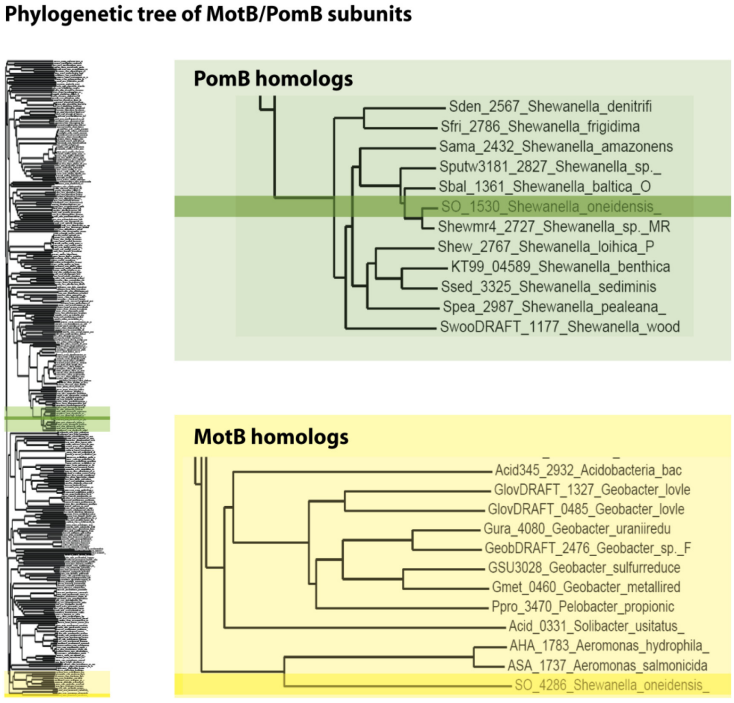

Figure 7: MotAB is most likely acquired by lateral gene transfer. Extract of the homology comparison of MotB (SO_4286) and PomB (SO_1530) protein sequences by separate BLAST analyses against the NCBI non-redundant database with an expect value cutoff of 1E-10. Homologs to PomB and MotB are highlighted in green and yellow, respectively. PomB homologous cluster with all *Shewanella* isolates sequenced so far. In contrast, MotB homologs are not clustering with other *Shewanella* species. The highest similarity was found for the B subunits in *Aeromonas* species. Bioinformatic analysis was performed by Stuart Huntley (Department of Eco-physiology, MPI Marburg).

Orthologs of PomB were found in all sequenced *Shewanella* species, in contrast, the MotB subunits of *S. oneidensis* MR-1 are not related to other *Shewanella* stators, instead the highest similarity for MotB was found for stator subunits of *Aeromonas* species. Furthermore, in comparison to the GC content of the overall genome in *S. oneidenis* MR-1 (45.88 %), a gene region comprising *motA* (39.04 %) and *motB* (36.32 %) exhibit a significantly lower GC content [136]. Thus, the MotAB stator system appears to be of foreign origin, indicating that the MotAB stator complex has been recently acquired by lateral gene transfer driven by motility adaptation to a low sodium environment.

2.1.2 PomAB and MotAB contribute to motility

In order to determine how PomAB and MotAB contribute to motility of *S. oneidensis,* swimming ability on soft-agar plates and under the microscope was tested for stator deletion mutants.

A comparison of the contribution to motility on soft agar-plates of PomAB and MotAB stator complexes is displayed in Figure 8. On soft agar plates, aΔ *pomAB* mutant was drastically impaired in swimming ability and a Δ*motAB* mutant had a slightly increased swimming diameter compared to the wild type. As a negative control the swimming behaviour of the non-motile mutant, which was lacking the flagellar filament (SO_3236-3238, Δ*flag*), and a double mutant (Δ*pomAB*/*motAB*) was determined. Both strains remained non-motile under all conditions tested. All mutants lacking the stator complexes PomAB or MotAB were flagellated like wild-type cells, as observed by flagella staining (data not shown).

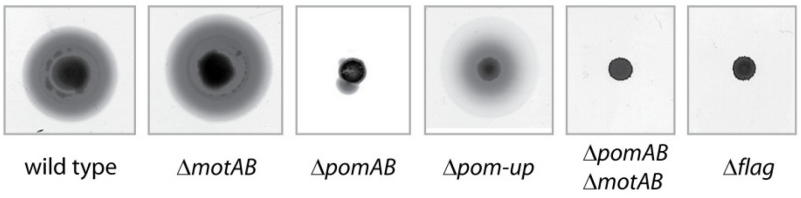

Figure 8: Motility of *S. oneidensis* MR-1 stator deletion mutants on soft agar plates. Exponentially growing cells of wild type, Δ *motAB* and Δ*pomAB* were spotted on LB soft agar plates (0.2 % agar). Cells of the double deletion strain, Δ*pomAB*/Δ*motAB*, and the negative control, lacking the flagellar filament,Δ *flag*, were non-motile. Wild type and Δ *motAB* showed similar swimming diameters, Δn *pomAB* flares of elevated motility evolved after prolonged incubation. Reinoculation of Δ*pomAB* cells generated genetically non-fixed and genetically fixed subpopulations of upmotile mutants. A genetically fixed mutant is further referred to as Δ*pomAB up*.

Interestingly, after prolonged incubation of Δ*pomAB* mutants on soft agar plates flares of swimming cells evolved from the inoculation center. PomAB mutants extracted from these flares retained their motility on soft agar plates. Note that it was also possible to enrich Δ*motAB* or wild-type strains for elevated motility. Microscopic observations showed that the enrichment primarily increased the number of motile cells for wild type, Δ*motAB*, and Δ*pomAB*. In enriched Δ*motAB* and wild-type cultures the percentage of motile cells was slightly increased from ~ 60 % of non-enriched to 70 % in enriched cultures, the percentage in Δ*pomAB* cultures shifted from ~2 % to 15 %. In order to visualize the single flagellar motor in *S. oneidensis* cells, the switch complex protein FliN was fused to sfGfp. Microscopic analysis revealed that 95 % of either enriched or non-

enriched cultures possessed a basal body. Furthermore, filament staining showed that 50 to 60 % of cells for wild type, Δ*motAB* and Δ*pomAB* were flagellated. Thus, enrichment did not increase the number of cells harbouring a flagellar filament or a basal body. Enrichments of Δ*pomAB* cells of flares of elevated motility revealed two different types of cells: a genetically non-fixed subpopulation and a genetically fixed one. The phenotypes were defined as genetically fixed, when the upmotility was retained after repeated passaging in planktonic cultures. Sequencing *flrABC*, *fliFG*, *fliMN*, *motXY* and *motAB* genes of the genetically fixed mutants indentified a substitution in MotB, residue 56, from serine to proline. To verify that the substitution, which occurred in the periplasmic region of MotB, did not change the ion specifity of the MotAB stator complexes, inhibitor studies with phenamil, amiloride and the protonophor carbonylcyanide m-chlorophenylhydrazone (CCCP) were performed. Phenamil, an amiloride analogue, has been shown to specifically and efficiently block sodium ion-dependent flagellar motors [151,152]. Motility of Δ*pomAB upmotile* and Δ*pomAB* mutants was not influenced by amiloride and phenamil. In contrast, CCCP inhibited swimming, indicating that motility in Δ*pomAB upmotile* and Δ*pomAB* depends on the proton-dependent MotAB stator complex. Growth was not significantly altered in the Δ*pomAB upmotile* strain compared to wild-type and other stator deletion strains.

In summary, both MotAB and PomAB are able to drive flagellar rotation. MotAB has likely been acquired by lateral gene transfer, whereas PomAB has orthologs within all other *Shewanella* species. PomAB is the dominant stator complex in *S. oneidensis* MR-1. However, MotAB is able to rotate the filament, but is less efficient on soft agar plates. Enrichment of cells with elevated motility on soft agar plates increased the number of motile cells, but not the number of cells harbouring a basal body or a flagellar filament. The substitution in MotB residue 56 from serine to proline might have increased motility by stabilising MotAB-rotor interaction.

2.1.3 *pomAB* and *motAB* are concurrently transcribed

Translational promoter fusions of *pomAB* and *motAB* to a short-lived *gfp* (Gfp-ASV) demonstrated that both stators are expressed simultaneously and that there are no subpopulations of cells expressing only one stator system [150]. In order to determine whether stator selection is dependent on the sodium-ion concentration, a transcriptional fusion of *motAB* and *pomAB* promoters to *lucB* was used [128]. Promoter activity was then measured by luciferase activity [RLU] in cultures grown for 8 h in LM supplemented with the corresponding sodium-ion concentration (Figure 9 A). Both promoters were active at all concentrations tested. The *mot* promoter exhibited a peak in activity at 2 mM, thereafter its activity decreased. Activity of the *pom* promoter had a first peak at 2 mM and a second one at 100 mM. Notably, according to the reporter activities, the activity of the *pom* promoter was about 50 fold lower than the *mot* transcription rate. However, changes of the expression rate of *pom* and *mot* in dependence of the sodium-ion concentrations occured at a maximum of two-fold.

To further determine whether the protein level is regulated by the environmental sodium-ion concentration, an immunoblot assay was performed, using cultures grown for 8 h in LM supplemented with the corresponding sodium-ion concentration (Figure 9 B). The PomAB level remains relatively constant, with a slight decrease in the protein amount at 0 mM sodium chloride, whereas the MotAB level is constant at all sodium-ion concentrations.

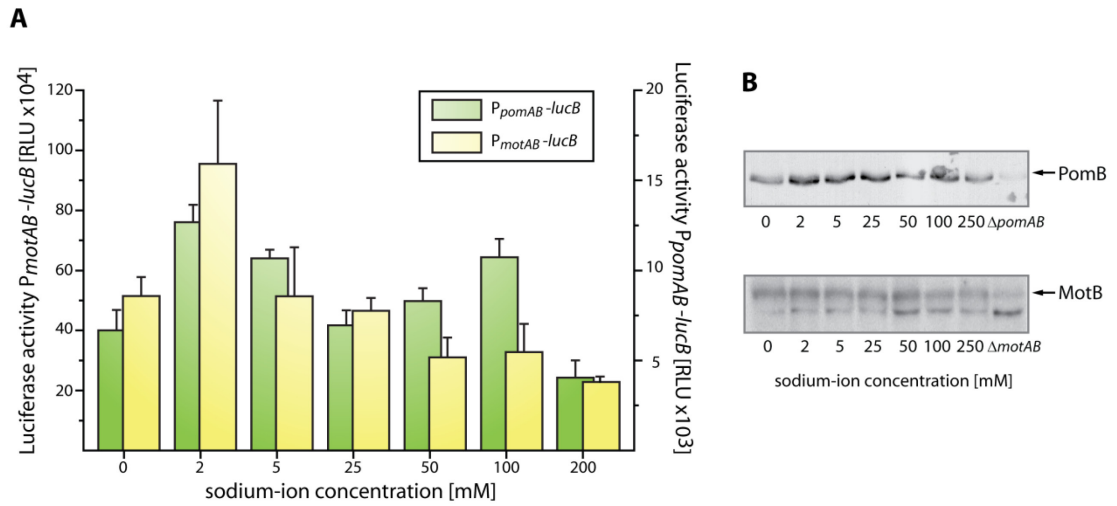

Figure 9: *pomAB* and *motAB* are concurrently transcribed. A) Luciferase activity of *pomAB* and *motAB* transcriptional fusions to *lucB*. RLU, relative light unit. A slight increase of luciferase activity was observed at 2 mM and 100 mM for *motAB* and *pomAB*, respectively. *pomAB* and *motAB* are concurrently transcribed. **B)** Wild type lysates for 0, 2, 5, 25, 50, 100, and 250 mM were analysed by immunoblotting with anti-PomB and anti-MotB antiserum. Δ*pomAB* and Δ*motAB* served as a control. The level of the MotB protein was unaffected by the sodium-ion concentration, the PomB level was slightly decreased at 0 mM sodium chloride.

Taken together, the promoter fusions to *lucB* and to the short lived Gfp indicate that both stators are concurrently transcribed independently of the sodium-ion concentration. Additionally, I showed that the protein levels of PomAB and MotAB are only weekly dependent of the sodium-ion concentration. This suggests that stator selection is regulated in a different manner.

2.1.4 PomAB and MotAB have a dynamic localisation pattern

Recent work showed that the stator ring in *E. coli* is composed of about eleven stator complexes which are constantly exchanged with a membrane embedded pool of ~ 300 stator precomplexes [104,108]. Fluorescence microscopy using PomB-mCherry and MotB-mCherry fusion proteins in *S. oneidensis* MR-1 revealed a polar localisation for PomB and MotB. Size and integrity of the stator fusions to mCherry were verified by immunoblot analysis (Figure 10 C). Functionality of the fluorescent fusions was validated by soft agar motility assays and microscopic swimming analysis. By co-staining the flagellar filament with Alexa Fluor® 488 Succinidimyl Esters (Invitrogen™, Germany) with PomB-mCherry and MotB-mCherry in a *pomAB* deletion background, I confirmed that MotB- and PomB-mCherry colocalise with the flagellar filament (Figure 10 D). This localisation pattern is a strong indication that PomB- and MotB-mCherry are incorporated into the stator ring system [103]. Furthermore, it was verified by Andrea Koerdt that PomA and MotB-mCherry, and MotA and PomB-mCherry do not form a functional stator hybrid in *S. oneidensis* (appendix, Figure 34).

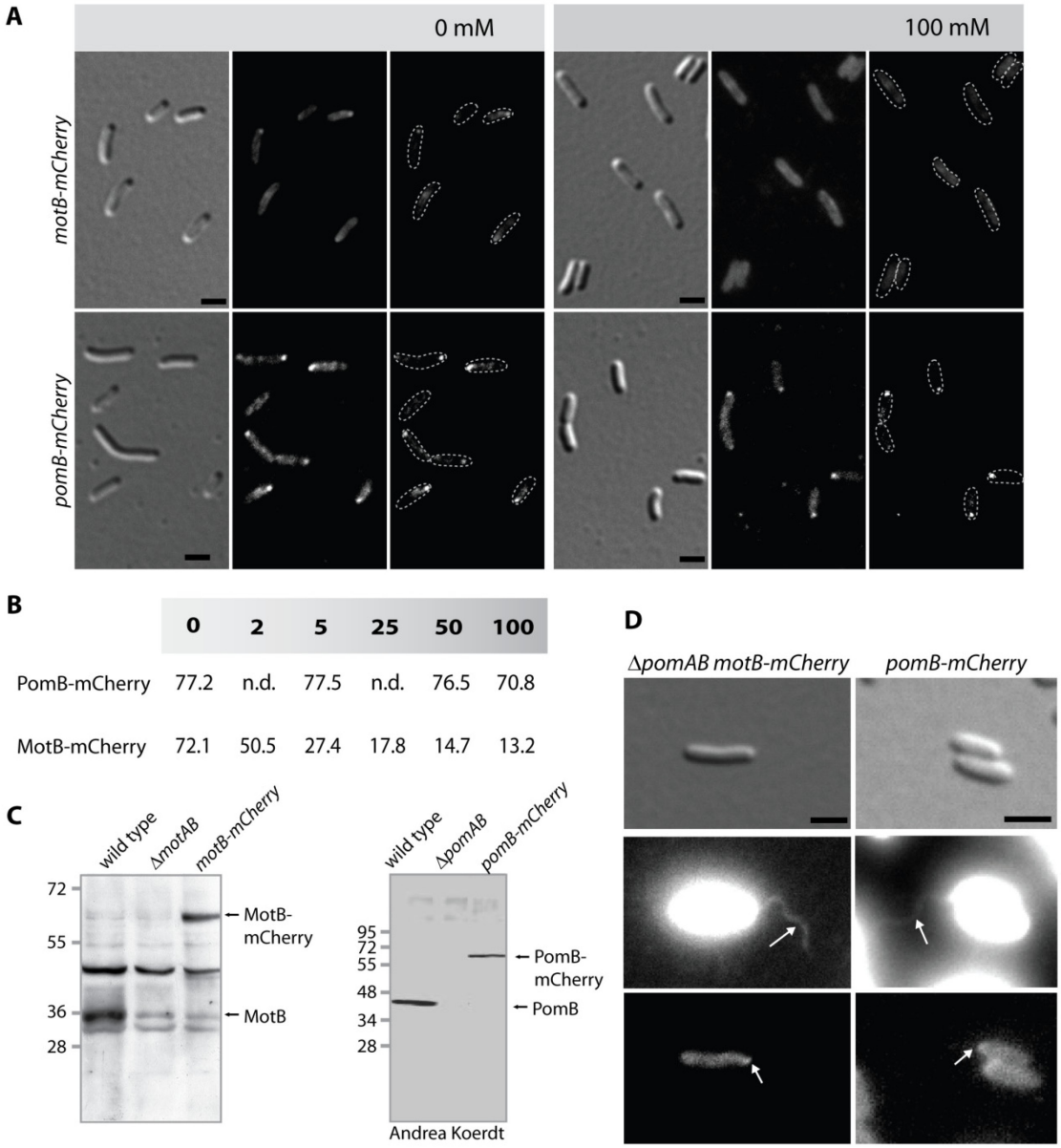

Figure 10: Dynamic localisation pattern of PomB- and MotB-mCherry. A) Polar localisation of MotB- and PomB-mCherry at 0 mM (three panels on the left) and 100 mM sodium chloride (three panels on the right). DIC and fluorescence micrographs of *S. oneidensis* cells harbouring *motB-mCherry* and *pomB-mCherry* are displayed in the upper and lower panel, respectively. Cells were grown in LM with the appropriate sodium-ion concentration for 8 h. **B)** Percentage of polar localisation of MotB- and PomB-mCherry (for n = 500), grown for 8 h in LM with the indicated sodium chloride concentration. PomB-mCherry localises polarly in all sodium chloride concentrations, polar localisation of MotB-mCherry decreases with increasing sodium chloride concentration. Analysis was performed in collaboration with Andrea Koerdt. **C)** Stability of MotB-mCherry (57 kDa) and PomB-mCherry (61 kDa) was confirmed by immunoblot analysis, using anti-MotB and anti-PomB antiserum, respectively. As a control, wild type and Δ *motAB* or wild type and Δ*pomAB* were used. **D)** Displayed are DIC and fluorescence micrographs for the colocalisation of flagellar filaments and MotB-mCherry (left panel) or PomB-mCherry (right panel). Filaments were stained with Alexa Fluor® 488 Succinidimyl Esters (Invitrogen™). The scale bar represents 2 µm.

To further investigate how the stator composition in *S. oneidensis* MR-1 might be regulated, the localisation pattern of MotB-mCherry and PomB-mCherry was examined at 0 mM and 100 mM sodium chloride (Figure 10). To this end cultures were grown in LM containing the appropriate sodium-ion concentration for 8 h. The quantification of polar localisation in 500 cells at different

sodium-ion concentration revealed that a fraction of PomB-mCherry localises polarly in more than 70 % of the cells independent of the sodium-ion concentration. In contrast, the localisation of MotB-mCherry to the flagellated pole was strongly depending on the sodium-ion concentration. In media containing 0 mM sodium chloride more than 70 % of the cells exhibited one polar focus, however, by increasing sodium-ion concentration polar localisation of MotB-mCherry decreased. At a concentration of 100 mM sodium chloride MotB-mCherry was predominantly delocalised to the cell membrane and only a subpopulation of < 13 % showed a polar localisation pattern (data summarised in Figure 10 B).

In *Vibrio alginolyticus* functional incorporation of PomAB is dependent on the sodium-ion concentration. Resuspending in buffer containing 0 mM sodium chloride rapidly decreased the polar localisation from 80 % to 5 % [109]. To further characterise the localisation dynamics of the stator complexes in *S. oneidensis* MR-1, the temporal dynamics of MotB-mCherry and PomB-mCherry upon buffer change from high to low sodium-ion concentration was elucidated. Cells harbouring either MotB-mCherry or PomB-mCherry were grown in LM supplemented with 100 mM sodium chloride overnight and then resuspended in LM containing 100 mM potassium chloride. Figure 11 shows a timelapse for the resulting localisation dynamics of MotB- and PomB-mCherry. PomB-mCherry was found to localise polarly during all time points. In accordance with the drop in fluorescence intensity evaluated by Andrea Koerdt for PomB-mCherry in *S. oneidensis* MR-1 at different sodium-ion concentration [128], the fluorescence intensity of PomB-mCherry slightly decreases over time. Conversely, in 0 mM sodium chloride the percentage of cells with polarly localised MotB-mCherry increased over time, suggesting elevated incorporation efficiency for MotAB. First polar foci for MotB-mCherry were observed between 45 and 90 min.

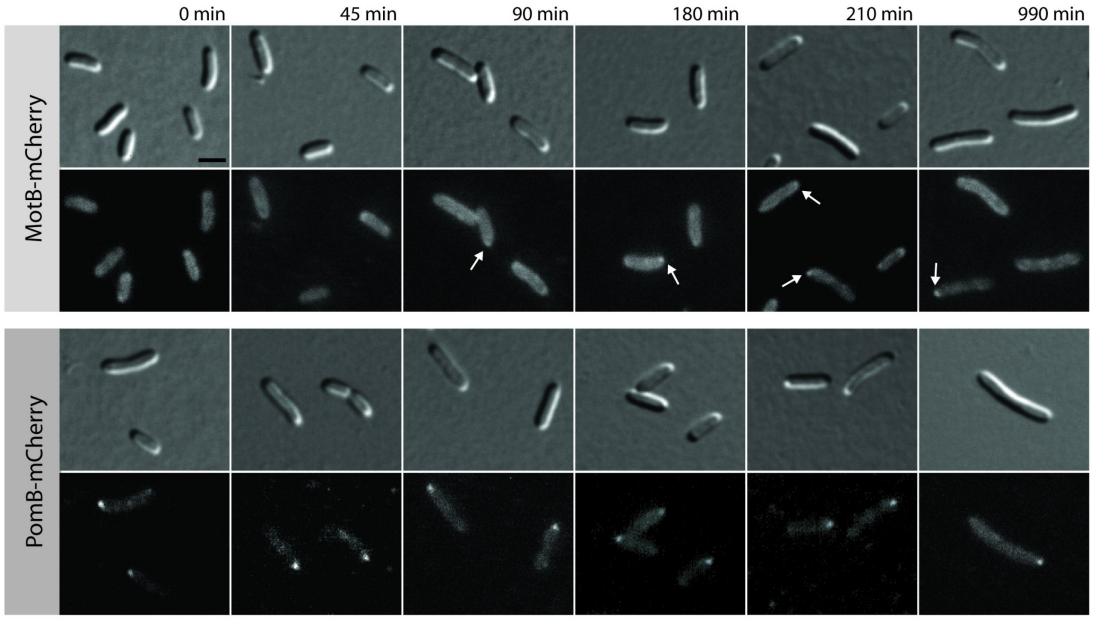

Figure 11: Time-lapse fluorescence microscopy of MotB-mCherry and PomB-mCherry after resuspension in 0 mM sodium chloride. Displayed are DIC and fluorescence micrographs with the localisation patterns of MotB-mCherry (upper panel) and PomB-mCherry (lower panel). Cells were grown overnight in LM 100 mM sodium chloride, washed and resuspended in LM with 100 mM potassium chloride. Time elapsed after resuspension in sodium-ion free medium as indicated above the figures. Scale bar equals 2 μm.

Taken together, these experiments indicate that at least a subpopulation of PomB-mCherry is incorporated into the stator ring independent of the sodium-ion concentration, whereas MotB-mCherry incorporation is strongly dependent on sodium-ion concentration, indicating that PomB-mCherry and MotB-mCherry have a different dynamic localisation pattern. At high sodium-ion concentration two subpopulations of cells may exist, that either have PomAB or MotAB incorporated into the stator ring. Polar localisation of PomB- and MotB-mCherry in 77% and 72% of the cells at low sodium-ion concentration, respectively, suggests that both stators are co-localising to the flagellated pole and are simultaneously incorporated into the same stator ring system.

2.1.5 Stoichiometry of sfGfp-PomB is sodium-ion dependent

To address the question whether the number of PomAB stators in the stator ring system drops dynamically with decreasing sodium-ion concentration, the stoichiometry of PomAB stator proteins should be determined at different sodium-ion concentrations.

In order to do so I used a fluorescence microscopy set-up, built in the Molecular Motors Group in the Physics Department of the University of Oxford by Dr. Nicolas Delalez, Dr. Bradley Steel and Dr. Richard Berry, which allows the determination of the number of single Gfp molecules by photobleaching. Due to laser restrictions, this approach required a functional fusion of Gfp to PomA/PomB.

CONSTRUCTION OF A FUNCTIONAL POMB-GFP FUSION

Intensive efforts have been made in the past to generate a functional fusion of any fluorophor to the stator complexes. Here, the B-subunit rather than the A-subunit has been choosen for two reasons: (1) one stator complex is formed out of four A- and two B-subunits, which doubles the number of fluorophores fused to a single stator complex. (2) So far, no functional fusions to the A-subunit were generated, whereas fusions to B-subunits have been demonstrated to be at least partially functional [103,104]. The B-subunits of the stator complexes have a N-terminal cytoplasmic region, one transmembrane domain and a C-terminal periplasmic region. The N-terminal cytoplasmic region of *S. oneidensis* MR-1 PomB is 16 amino acid in length, followed by a transmembrane region (aa 17-37) and a long periplasmic region (aa 38-308) with a putative PG-binding domain (Figure 12 A). Since the C-terminus of PomB is located in the periplasm where Gfp is not functional if transported unfolded an N-terminal Gfp-PomB fusion needed to be constructed.

Recently, Gfp was functionally fused to MotB in *E. coli*, and the number of incorporated stator complexes was determined. Thus, a similar cloning strategy was applied. To this end, 500bp upstream of PomB, including the first 16 cytoplasmic residues, were fused to *gfp,* the N-terminal 16 amino acids were repeated followed by a 500bp fragment of *motB* [104]. I constructed several N-terminal fusions of Gfp to PomB and MotB in *S. oneidensis* MR-1 (see appendix, Table 15). Thereby, different variants of fluorophores were used (Gfp-mut3, Gfp-mut2, sfGfp, mAzami and mOrange), the cytoplasmic region was either repeated or the length of residues was varied; or different linker sizes downstream of Gfp were introduced (three, six, nine, twelve amino acids). The fusions were

tested for polar localisation under the fluorescence microscope and for swimming motility on soft agar plates (see appendix, Table 15).

The repetition of the 16 cytoplasmic amino acids and the introduction of an additional linker $(GGS)_4$ generated a functional N-terminal fusion of Gfp to PomB (Figure 12 B). It is worth noting, that PomB and MotB of *S. oneidensis* MR-1 have a shorter cytoplasmic region than MotB of *E. coli* (Figure 12 A). Introducing a long linker might have increased the flexibility of sfGfp, allowing the stator to be incorporated. To confirm the functionality of the resulting sfGfp-PomB fusion in *S. oneidensis* MR-1, I performed localisation studies and verified motility on soft agar plates (Figure 12 C, D). Size and integrity of the fusion protein was verified by immunoblot analysis (not shown). Although motility was decreased, sfGfp-PomB was stable and polar foci of the sfGfp-PomB were detected in 50% of the cells. This fusion was used to identify the number of sfGfp-PomB incorporated into the stator ring at different sodium-ion concentrations in *S. oneidensis* MR-1.

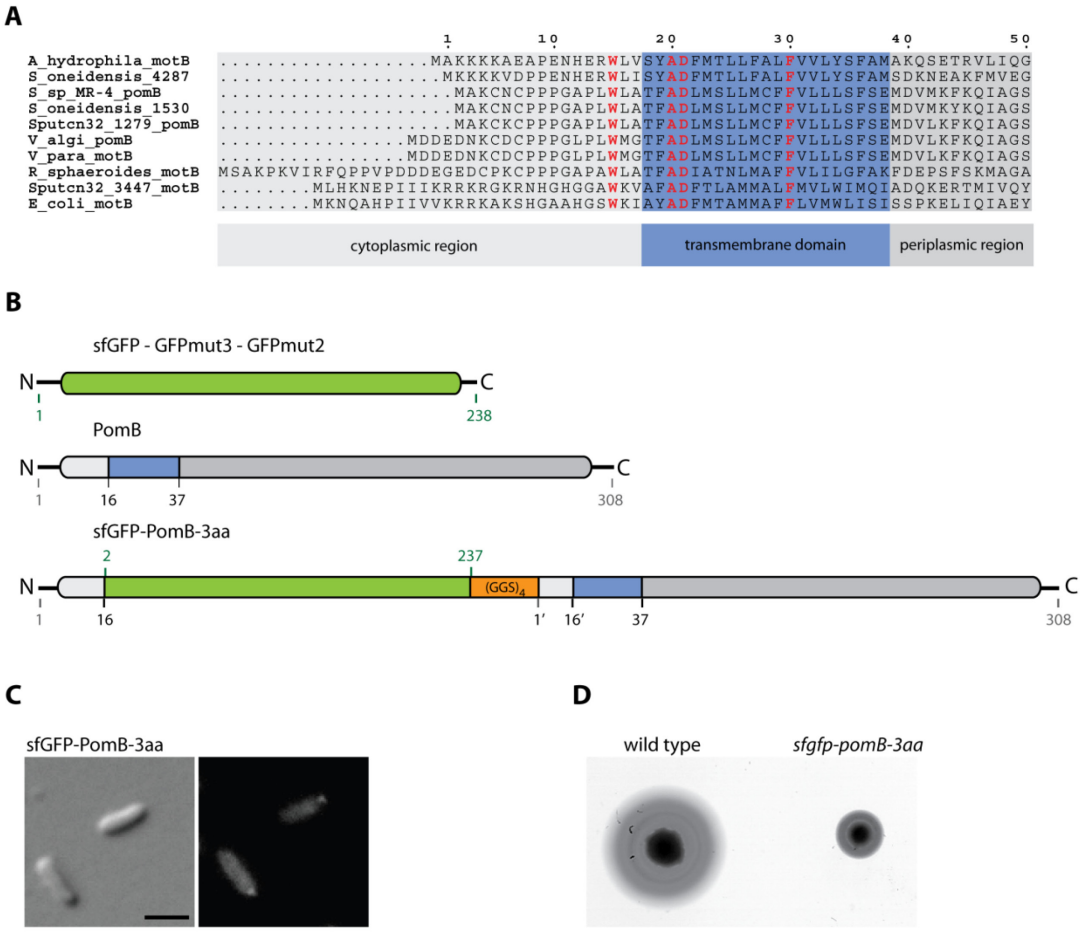

Figure 12: Construction of a functional Gfp fusion. A) sequence alignment of stator B-subunits from different organisms by ClustalW, using the BLOSSUM matrix. Light grey, cytoplasmic region; blue, transmembrane domain; dark grey, first aa of the periplasmic region. Identical aa are shown in red. B) schematic representation of sfGfp, PomB of *S. oneidensis* MR-1 and the constructed fusion protein sfGfp-PomB-3aa. C) DIC and fluorescent micrograph of sfGfp-PomB-3aa, scale bar represents 2 µm. D) Functionality was verified on soft agar motility plates.

SODIUM-ION DEPENDENCE OF THE SFGFP-POMB STOICHIOMETRY

Up to eleven stator complexes are incorporated into the stator ring of *E. coli*. My localisation data for *S. oneidensis* suggest that both PomAB and MotAB are incorporated simultaneously at low sodium-ion concentration. Thus, the number of PomAB stator complexes should be decreased compared to higher sodium-ion concentrations. In order to analyse whether the stoichiometry of PomAB is dependent on the sodium-ion concentration, the number of single sfGfp molecules was determined by fluorescence photobleaching in collaboration with the Physics Department in the University of Oxford.

To analyse the stoichiometry of PomAB stator complexes, the *sfgfp-pomB* strain was subcultured in LM, supplemented with the appropriate sodium-ion concentration, grown to exponential phase (oD_{600} of 0.6) and resuspended in 4M buffer containing 0 mM, 5 mM, and 200 mM sodium chloride. Time-lapse microscopy image series were taken on a 4M agar pad, supplemented with the appropriate sodium-ion concentration, for a period of 500 frames (until the foci were bleached completely) at an exposure time of 50 ms and a laser power of 2.5 mW (473 nm DPSS laser). The fluorescence image series were recorded and analysed according to Leake *et al.* [104]. Figure 13 A shows an overview of extracted frames for sfGfp-PomB spots over the period of photobleaching at different sodium-ion concentrations. As mentioned before, this method allows to visualise and to determine single sfGfp. Due to the fact that *S. oneidensis* MR-1 has a single polar flagellum, only polar spots were considered to be incorporated into the stator ring system. As expected, photobleaching of sfGfp-PomB foci at high sodium-ion concentration occurs over a longer time period than bleaching at low sodium-ion concentration. This is in accordance with earlier fluorescence intensity quantifications for PomB-mCherry foci at high and low sodium-ion concentrations [153].

To quantifiy the number of sfGfp-PomB molecules, time-lapse microscopy image series were analysed using a MATLAB code written by Dr. Bradley Steel. It has been shown that single Gfp molecules photobleach in a single step [104]. Based on this algorithm, the number of single photobleached sfGfp molecules in the stator ring was determined. Fluorescence spots were detected and the loss in intensity over time was used to calculate the number of steps, equalling the number of sfGfp molecules. The dominant peak in the power spectrum of the pairwise difference distribution function was used to extract the brightness of a single Gfp and hence the number of Gfp molecules originally present in the polar spot. Quantification of 45, 34 and 58 cells for 200 mM, 5 mM and 0 mM revealed a median number of Gfp molecules of 18.7, 15.3 and 11.3, respectively. Considering that one stator complex is composed of two B-subunits, 9.4, 7.7 and 5.6 stators are considered to be incorporated into the stator ring at 200 mM, 5 mM and 0 mM sodium chloride, respectively (Figure 13 B). An independent t-test at the 0.01 level revealed that these numbers are significantly different. Additionally, the distribution of the number of stator complexes was plotted as a histogram Figure 13 C. A Gaussian fit revealed 4.8 ± 0.2 and 7.3 ± 0.1 stators for 0 mM and 5 mM, respectively. The distribution of stators in 200mM sodium chloride suggests two subpopulations, one having 6.8 ± 0.2 and the other having up to 11.7 ± 0.6 PomAB stator complexes incorporated. Notably, at low sodium-ion concentration more foci were detected moving quickly in the membrane. Rough analysis suggests that these complexes represent units of up to four sfGfp molecules.

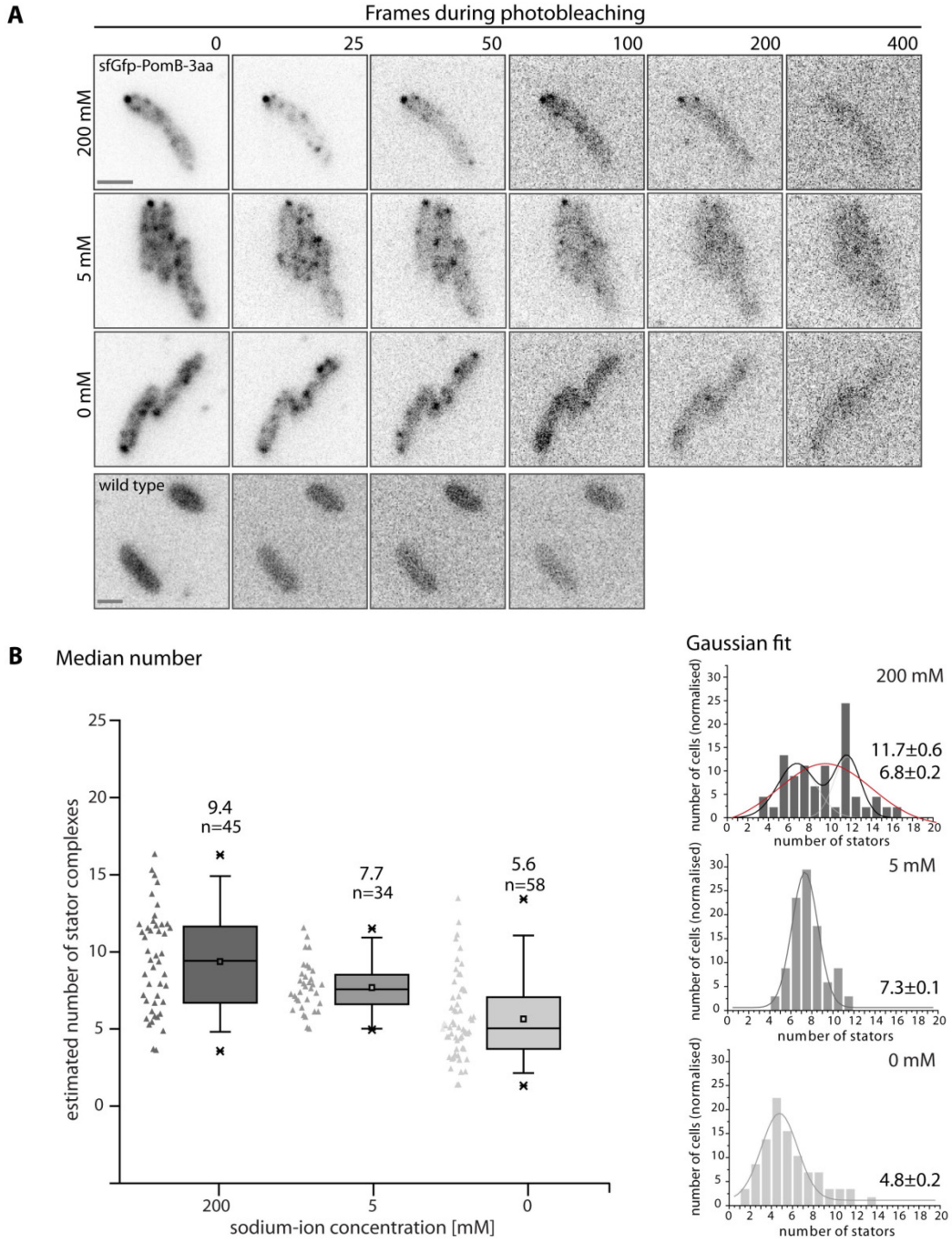

Figure 13: Stoichiometry of sfGfp-PomB molecules at different sodium-ion concentrations. A) Photobleaching of sfGfp-PomB. Displayed are fluorescence micrographs during photobleaching at the indicated timepoints (frames) of *sfgfp-pomB-3aa* in 4M supplemented with 200 mM, 5 mM and 0 mM sodium chloride. Micrographs were modified in Photoshop, using the 'Autocontrast' and 'Autolevel' application. Wild-type cells as a control did not exhibit fluorescent foci. Scale bar, 1 µm. **B) Quantification of single sfGfp-PomB molecules. Left Median:** The number of single sfGfp-PomB molecules was determined by analysis of the respective movies (500 frames, each exposed for 50 ms, 473 nm DPSS laser, laser power 2.5 mW) using a MATLAB code (written by Dr. Bradley Steel, University of Oxford, according to Leake *et al.* [104]). The estimated number is graphically compared in a box-whisker-plot, with the corresponding data distribution shown as '▲' on the left. The box and the included line represent the middle 50 % and the median of the data, respectively. The average is shown as '□', and the whiskers denote the data range of the 5 th and 95th percentile. Minimum and maximum are represented by 'x'. Polar foci of 45, 34 and 58 cells for 200 mM, 5 mM and 0 mM sodium chloride were analysed, revealing a median number of 9.4, 7.7 and 5.6 stators, respectively. **Right Gaussian fit:** The distributions were plotted in a histogram, individually normalised to the total number of cells analysed for 200 mM, 5 mM and 0 mM sodium chloride (bin size 1). Gaussian fits were applied to obtain the number of stator complexes (grey fitting curves, and red fitting curve for 200 mM). Notably, the distribution at 200 mM suggests the existence of two subpopulations, with 6.8 ± 0.2 and 11.7 ± 0.6 PomAB stators (black fitting curve). Fluorescence movies were taken and analysed in collaboration with the Physics Department at the University of Oxford.

Taken together, these data support the idea that PomAB is always present in the stator ring, but its affinity decreases with decreasing sodium-ion concentrations. Thus, the lower abundance of PomB in the stator ring might increase the probability of MotB binding, as more vacant positions in the ring occur. If this is the case, more sfGfp-MotB molecules should be present at low sodium-ion concentrations. To further analyse this, e.g. to determine if the number of sfGfp-PomB increases when no MotAB is present, a Δ*motAB pomB::sfgfp-pomB* strain will be constructed. Furthermore the sfGfp-MotB dynamic needs to be analysed. How both stators colocalise at different sodium-ion concentrations could be investigated by using different fluorophores on MotB and PomB.

2.1.6 Localisation of MotAB depends on the presence of PomAB

Several lines of evidence imply that the abundance and presence of PomAB influences the incorporation of MotAB into the stator ring system. I hypothesized that PomAB localises more efficiently to the flagellated pole at high sodium-ion concentration, excluding the MotAB stator from being incorporated into the stator ring system. To clarify whether the presence of PomAB excludes the MotAB stator complex from being incorporated into the stator ring system, a Δ*pomAB motB::motB-mCherry* strain with a plasmid-encoded arabinose-inducible copy of *pomAB* was constructed [153]. As predicted, in the absence of PomAB, MotB-mCherry was localising to the flagellated pole in more than 75% of the cells independent of the sodium-ion concentration (Figure 14). Upon induction of *pomAB* expression by L-arabinose (0.08%), the polar localisation of MotB-mCherry decreased and predominantly occured in the cell-membrane. In the uninduced control MotB-mCherry was not displaced over time (data not shown). Displacement of MotB-mCherry appears to occur more rapidly under high sodium-ion conditions. To verify this, further determination regarding the stoichiometry of MotB is necessary. Additionally, overexpression of *pomAB* decreased the polar localisation of MotB-mCherry at low sodium-ion concentrations from 69.9% to 26.4% [153] indicating that a higher level of PomAB inhibits MotAB incorporation. The protein level of PomB upon induction was followed by immunoblot analysis (Figure 14 B), the level of MotB protein did not change upon expression of *pomAB* (data not shown). Induction of *pomAB* expression also complemented motility to wild-type level, as verified on soft agar plates. Expression of *motAB* in a Δ*motAB pomB::pomB-mCherry* strain was not analysed. However, my fluorescence data do not suggest that the percentage of cells with polarly localised PomB-mCherry in this background decreases, instead the amount of incorporated PomB-mCherry stators might drop. Accordingly, stoichiometry analysis regarding the amount of PomAB incorporated will be interesting.

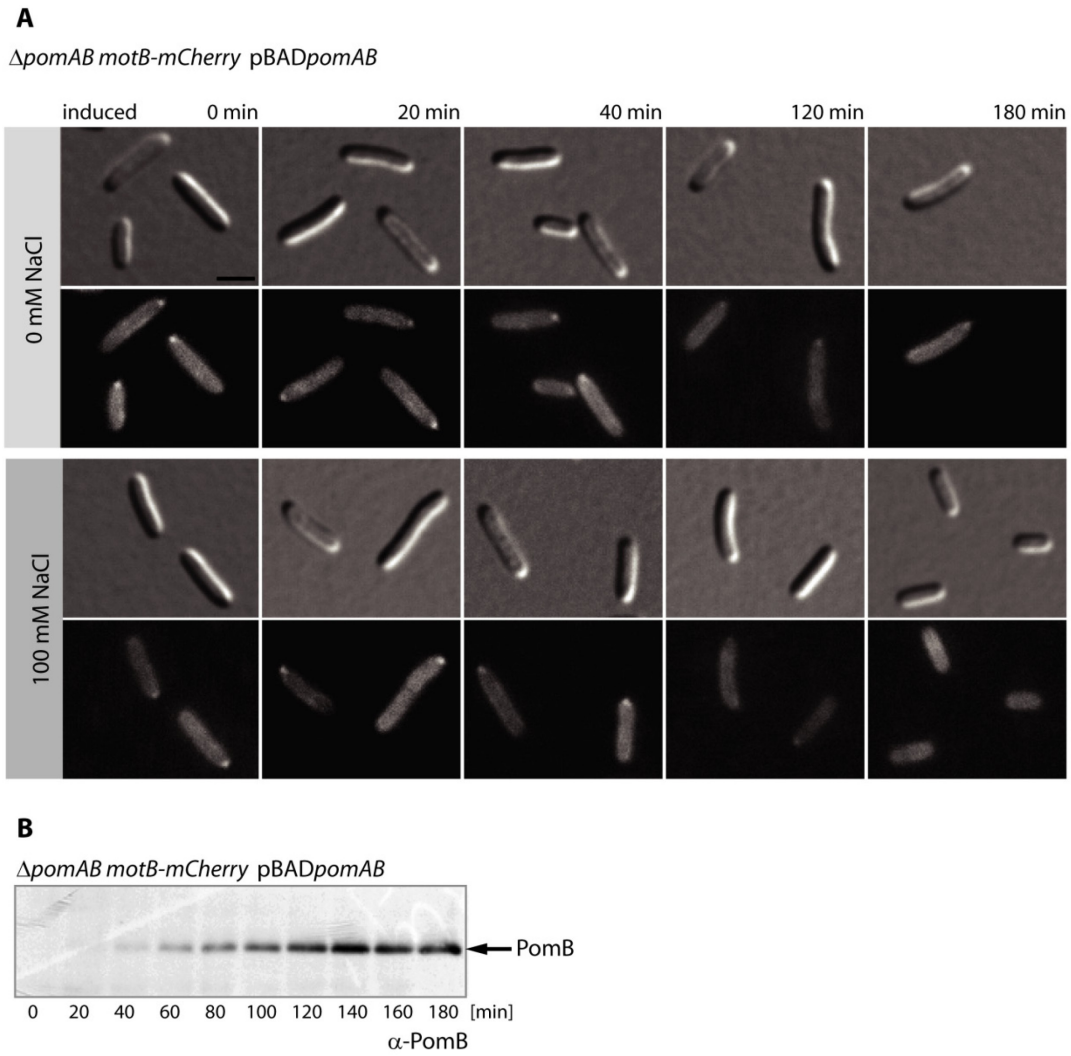

Figure 14: Presence of PomAB influences localisation of MotB-mCherry. A) Shown are DIC and fluorescence micrographs of cells harbouring MotB-mCherry and an inducible copy of *pomAB* under control of a P_{ara}-promoter in a *pomAB* deletion background. Cultures were grown overnight in LM 100 mM, washed and resuspended in LM with the indicated sodium chloride concentration (0 mM and 100 mM, upper and lower panel, respectively). Images were taken prior induction (non-induced) and after induction with 0.08 % arabinose of *pomAB* expression to the indicated timepoints. **B)** Protein levels of PomAB were followed by immunoblot analysis with an anti-PomB antiserum in 20 min intervals. Scale bar size equals 2 µm.

Taken together, a fraction of PomB-mCherry localises to the flagellated pole at all sodium-ion conditions. The number of polarly localised PomB-sfGfp molecules decreases with decreasing concentrations. In contrast, polar localisation of MotB-mCherry increases under low sodium-ion conditions, suggesting the incorporation of both, PomAB and MotAB in the stator ring system. Furthermore, my data indicate that the presence and abundance of PomAB influences the localisation of MotB-mCherry. Hence, a single flagellar motor along with two different stator complexes, both simultaneously incorporated into the stator ring system at low sodium-ion concentrations represents a novel mechanism of the flagellar motor to rapidly adapt to environmental changes.

2.2 Two auxiliary proteins MotX and MotY

For *Vibrio* species it has been shown that two auxiliary proteins, MotX and MotY, are important for the acquisition of PomAB stator complexes to the flagellar motor [11,154,155]. Orthologs of *motX* (SO_3936) and *motY* (SO_2754) have been annotated for *S. oneidensis* MR-1 and the sequence of *motY* was corrected for an annotated frame shift, which would result in a truncated protein [156]. MotX has been predicted to have a molecular mass of 23.2 kDa and to contain three Sel1 domains, which are thought to take part in protein-protein interactions [157,158]. In contrast, MotY is predicted to have a putative PG-binding domain at the C-terminus and a molecular mass of 33.0 kDa.

2.2.1 MotX and MotY are important for PomAB and MotAB function

In order to investigate a potential role of MotX and MotY for motility in the flagellar motor of *S. oneidensis* MR-1, corresponding deletion mutants were tested for motility (Figure 15 A). None of the mutants was motile either on soft agar plates or in liquid media supplemented with different concentrations of sodium chloride. Southern Blot analysis confirmed that no further copy of *motX* and *motY* remained in the genome (Figure 15 B). In collaboration with Andrea Koerdt it was shown by filament staining that the loss of motility was not caused by a defect in flagellar assembly. Moreover, polar positioning of stable functional C-terminal fusions of MotX and MotY to mCherry was confirmed to be located at the flagellated pole by filament staining with Alexa Fluor® 488 Succinidimyl Esters (Invitrogen™, Germany); (Figure 15 C). MotX- and MotY-mCherry localised polarly independently of the presence of PomAB and MotAB. However, polar positioning of MotX-mCherry depends on the presence of MotY, while MotY-mCherry localises to the flagellated pole in the absence of MotX. Notably, polar foci of MotX- and MotY-mCherry did not rely on the sodium chloride concentration [156].

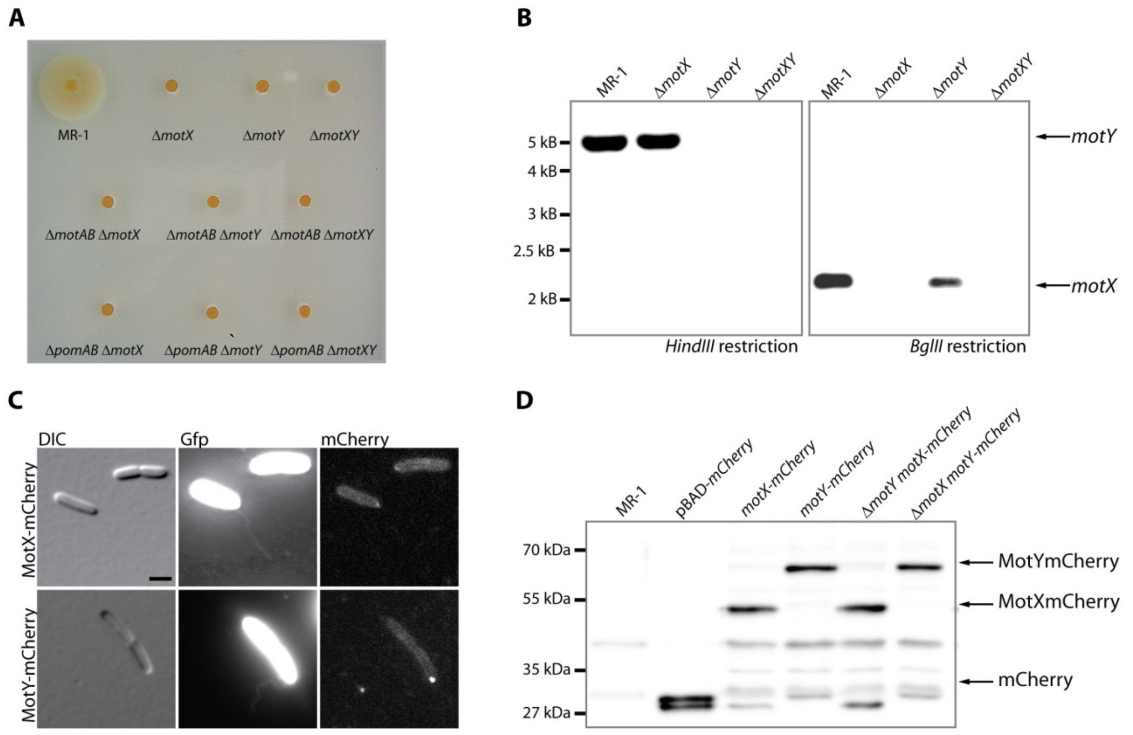

Figure 15: MotXY are crucial for motility in *S. oneidensis* MR-1. A) Motility assay on soft agar plates for deletion strains in MotX and/or MotY in wild-type and stator deletion backgrounds of PomAB and MotAB. The absence of either MotX and/or MotY inhibited swimming motility. **B)** Southern Blot analysis confirmed that MotX and MotY do not have additional copies in the genome. **Left:** Chromosomal DNA of wild type, Δ*motX*, Δ*motY* and Δ*motXY* was restricted with *HindIII*. A specific probe against *motY* revealed a single band at 4.8 kbp for wild type and Δ*motX*. **Right:** Accordingly, restriction with *BglII* and a probe against *motX* showed a specific band at 2.1 kbp for wild type and Δ*motY*. **C)** Colocalisation of the stained flagellar filament with MotX- and MotY-mCherry. Displayed are DIC and fluorescent micrographs of strains harbouring C-terminal mCherry fusions to MotX and MotY, upper and lower panel respectively. The filament was stained using Alexa Fluor® 488 Succinidimyl Esters (Invitrogen™, Germany), second panel. Scale bar equals 2 µm. **D)** Size and integrity of MotX- and MotY-mCherry was verified by immunoblot analysis using anti-dsRed antibody (Clontech). MotX- and MotY-mCherry are stably produced independently of the presence of MotY and MotX, respectively. Wild type and pBAD-mCherry were used as negative and positive control.

2.2.2 MotX and MotY are not essential for localisation of PomB and MotB

To further investigate whether MotX and MotY are crucial for stator recruitment and whether they are responsible for stator selection at low and high sodium-ion concentrations, the localisation pattern of PomB-mCherry and MotB-mCherry was analysed in a Δ*motX*, a Δ*motY* and a Δ*motXY* strain during this work. To this end, *pomB-mCherry* and *motB-mCherry* were chromosomally intgegrated in the corresponding deletion strains by double homologous recombination at the native locus of *pomB* and *motB*, respectively [156]. Cells were grown overnight in LM and resuspended in LM supplemented with the appropriate sodium chloride concentration for 8 hours. Only minor influence was observed on PomB- and MotB-mCherry localisation in the absence of MotX and/or MotY (Figure 16). PomB-mCherrry localised independently of the sodium-ion concentration in wild type as well as in deletion strains of Δ*motX,* Δ*motY* and Δ*motXY* in more than 70% of the cells to the flagellated pole (Figure 16). The localisation of MotB-mCherry shifted from 13 % in wild-type cells to 24 % in Δ*motXY* mutants at 100 mM sodium chloride. In the absence of sodium chloride MotB-mCherry localised to the flagellated pole in more than 50 % in

wild-type or Δ*motXY* cells. In addition, MotB-mCherry localisation in a Δ*pomAB* strain was not affected by the presence or absence of MotX and/or MotY.

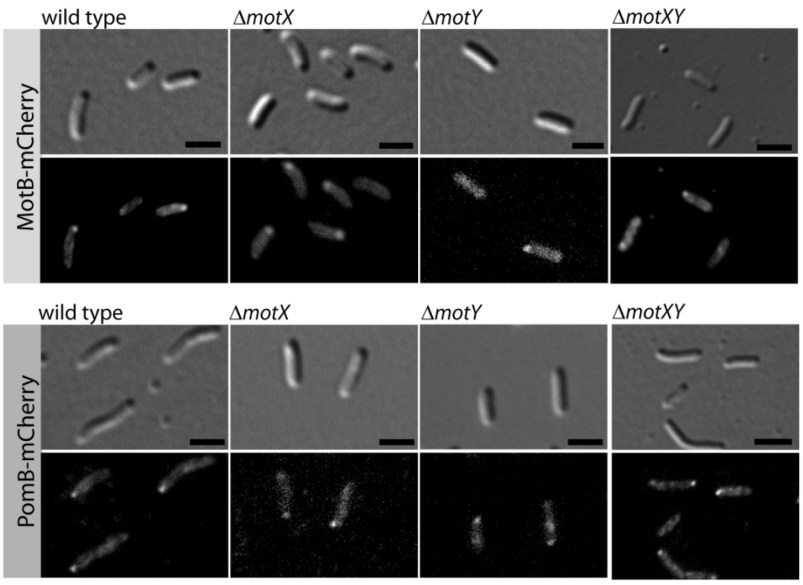

polar localisation in %

	0 mM	100 mM
wild type	49.3	13.2
Δ*motXY*	48.8	23.5

polar localisation in %

	0 mM	100 mM
wild type	73.7	70.8
Δ*motXY*	67.2	69.9

Figure 16: MotX and MotY are not required for recruitment of PomB- and MotB-mCherry. Displayed are DIC and fluorescence micrographs of MotB-mCherry and PomB-mCherry localisation in wild-type, *ΔmotX*, *ΔmotX* and *ΔmotXY* deletion strains. Fluorescent micrographs for polar localisation of MotB-mCherry and PomB-mCherry were taken at 0 mM and 100 mM sodium chloride, respectively. 250 cells harbouring MotB- and PomB-mCherry (upper and lower panel, respectively) were quantified with respect to polar localisation at 0 mM and 100 mM sodium chloride as summarised on the right side. Scale bar, 2 μm.

Thus, MotX and MotY are not required for polar localisation of PomB-mCherry or MotB-mCherry. However, they are important for function of MotAB and PomAB, as demonstrated by motility assays. These results suggest that MotX and MotY may play a role in stabilising or aligning the stator complexes, rather than for stator recruitment or selection, as thought for *V. alginolyticus* [11,154].

2.3 Biophysical characterisation of the bacterial flagellar motor

As described *S. oneidensis* MR-1 might use dual stators to form a dynamic hybrid motor which is concurrently using sodium-ions and protons to rapidly adapt the flagellar motor to changing environmental conditions. In order to test this hypothesis it is essential to get deeper insights into the flagellar motor performance at the single cell level. There are different approaches to study the performance of single flagellar motors in lateral flagellated species. Two of them, the *bead assay*, and the *tethered cell assay* were established for *S. oneidensis* in this work. In a *tethered cell assay*, cells are tethered by their filament and the rotation rate of the cell body is monitored and quantified by video microscopy [70]. In the so called *bead assay* a small polystyrene bead (µm size range) is attached to the flagellar filament as a marker for rotation [78]. A microscopy approach, called Back Focal Plane Interferometry (BFPI), allows easy measurement of the rotation rate of the polystyrene bead. Two methods for measuring rotation speed at the single cell level were established for the first time for polarly flagellated species. Applying these methods strongly indicated that MotAB is incorporated into the rotating PomAB-driven motor of *S. oneidensis* MR-1.

2.3.1 The *S. oneidensis* MR-1 bead assay

The bead assay is well established for single stator motors of the lateral flagellar systems in *E. coli* and *Rhodobacter sphaeroides*. [18,78]. However, so far there is no set up for a polarly flagellated species that allows a constant exchange of buffer conditions, as it is necessary for studying the dynamics in response to changing sodium chloride concentrations in the dual stator system for *S. oneidensis*. Thus, the aim of this part of the project was to establish a bead assay for *S. oneidensis* MR-1 that allows first insights into *S. oneidensis* wild-type flagellar motor performance.

PREREQUISITES FOR A FUNCTIONAL BEAD ASSAY

In a bead assay beads of sub-micron size are attached to truncated flagellar filaments. The bead assay for the polarly flagellated species *S. oneidensis* MR-1 was performed similarly to the one in *R. sphaeroides* and was developed in collaboration with Dr. Mostyn Brown and Dr. Bradley Steel in the Molecular Motors group of the Biophysics and Biochemistry Department at the University of Oxford (see for protocol Material and Methods). Carboxyl-modified polystyrene beads were crosslinked with goat anti-rabbit IgG and attached to flagellar filaments coated with polyclonal anti-filament antibodies of immobilised cells in a *tunnel slide* (Figure 17). Trajectories of the rotating bead were taken by BFPI in an optical trap and analysed by a LabView code developed by the Molecular Motors Group in the Physics Department of the University of Oxford.

Reliable data of the flagellar motor revolution frequency requires conditions in which:

A) the bead is attached to the truncated flagellar filament;
B) the filament with the attached bead rotates freely;
C) the cell body is tightly immobilised on a proper microscopic surface; and
finally a combination of B) and C): a freely rotating bead upon tightly immobilised cells.

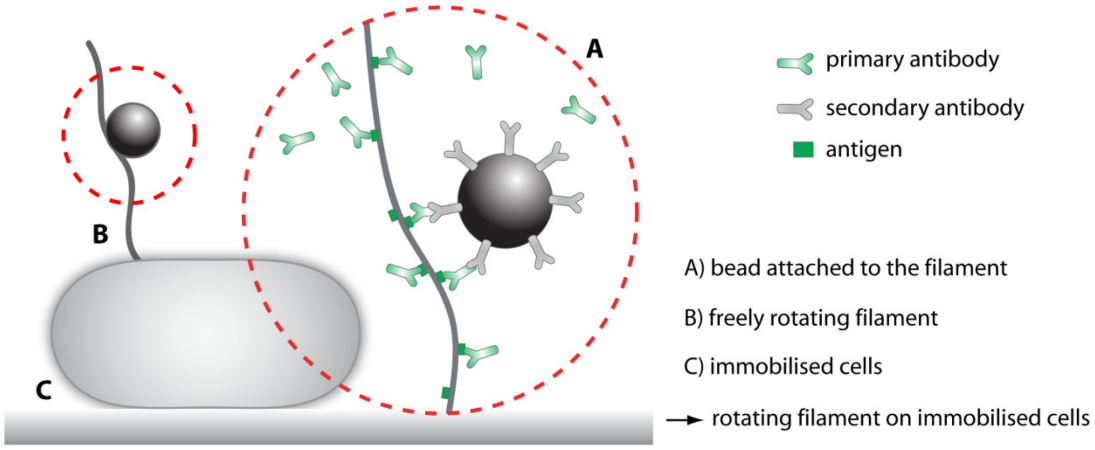

Figure 17: *S. oneidensis* MR-1 bead assay. In this approach the flagellar filament is treated with polyclonal antibodies raised against the whole modified filament. Secondary antibody-coated polystyrene beads will bind covalently to the flagellar filament (**A**; red circle). The coupled polystyrene bead will then be used for measuring the rotation rate by BFPI. The latter requires a free rotating filament **(B)**, and cells need to be tightly immobilised on the coverslip surface **(C)**. In order to get reliable data, a combination of (B) and (C): a freely rotating bead covalently bound to the filament upon tightly immobilised cells is mandatory. Method adapted from Pilizota *et al.* [18].

(A) Bead attachment to the flagellar filament

In order to attach a bead to the flagellar filament of *S. oneidensis* MR-1 a highly specific antibody had to be generated. The filament consists of thousands of flagellin subunits. *In silico* analysis revealed that *S. oneidensis* MR-1 harbours three putative flagellin subunits, SO_3236, SO_3237 and SO_3238, annotated as *flaG, flaB* and *flaA*, respectively [159]. Deletion of all three genes resulted in a non-flagellated phenotype [128]. Further studies revealed that the gene products of SO_3237 and SO_3238 are the main components of the flagellar filament in *S. oneidensis* MR-1. FlaB is the major flagellin subunit and deletion mutants exhibit short flagellar stubs and decreased swimming ability [160]. Additionally, deletion of FlaA does not affect motility.

Sequence alignment and the structure of FlaB and FlaA, built on the full length flagellar filament atomic model of *Salmonella typhimurium* by using the SWISS-MODEL workspace, revealed a drastic difference in the structure of the flagellin monomers in *S. oneidensis* MR-1 (Figure 35); [38,161-164]. FlaA and FlaB are composed of 272 and 273 aa and have a molecular mass of 28.5 and 28.7 kDa, respectively. The flagellin subunits of *S. typhimurium* (494 aa and 51.5 kDa) have been described to contain four domains, D0, D1, D2 and D3 (Figure 18 A) [38]. A direct structural comparison between FlaB and *S. typhimurium* full length flagellin is shown in Figure 18 A. While the inner domains D0 and D1 show no significant structural changes, the D2 domain is shortened and the D3 domain is missing in *S. oneidensis* MR-1. Although deletions within the D3 domain in *E. coli* led to spontaneous binding of polystyrene beads to the filament (FliC^{sticky}), *S. oneidensis* MR-1 does not produce *sticky* filaments [165]. However, preliminary data, including a band shift of the expected size of 29 to 36 kDa for flagellin subunits, strongly indicate that the filament in *S. oneidensis* is modified (Figure 18 A). Thus, in order to raise a suitable antibody for the bead assay the native modified flagellar filament is required. *S. oneidensis* MR-1 has been described to have two different types of pili, one encoded by *pilM-Q* and the second by the mannose sensitive hemagglutinin cluster (*mshA*) [147]. Deletion of the pili clusters did not interfere with its swimming ability (Figure 18 C)

and by using the *pilM-Q* deletion mutant, flagellar filaments were readily obtained (Figure 18 D). As expected, the filament mutant was not able to swim and did not have any filaments. Specificity of the raised anti-filament-IgG against the isolated native flagellar filaments was verified by immunostain and Western Blot analyses (Figure 19). The antibody was shown to be highly specific and that it exclusively recognizes the flagellar filament of *S. oneidensis* MR-1.

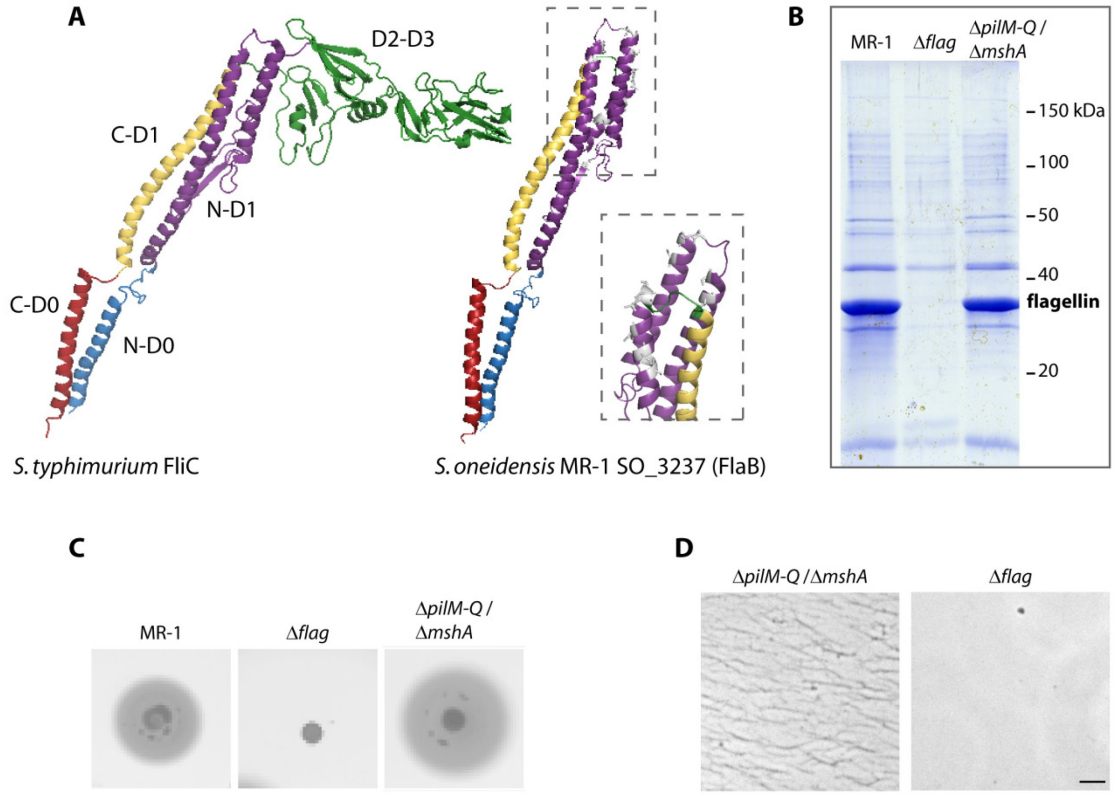

Figure 18: Isolation of the flagellar filament of *S. oneidensis* MR-1. Displayed in A) is a structural comparison of FliC in *S. typhimurium* and the major flagellin FlaB in *S. oneidensis* MR-1. The chain is coloured according to the corresponding flagellin domains: N-D0 and C-D0, blue and red; N-D1 and C-D1, purple and yellow; D2 and D3 domains, green. In *S. oneidensis* MR-1 most of the D2 and the complete D3 domains are missing. Putative modified amino acids are marked in grey in the close up, dashed box. See for a sequence alignment Supplementary figure Figure 35. B) SDS PAGE revealed a band at ~36 kDa for flagellin in the wild type and the *ΔpilM-Q/ΔmshA* mutant, indicating a modification of the flagellin in *S. oneidensis* MR-1 as the predicted size was expected to be 29 kDa. The filament mutant *Δflag* served as a control. C) Motility on soft agar was not altered for the *ΔpilM-Q/ΔmshA* mutant. DIC micrographs of purified flagellar filaments are shown in D). The scale bar corresponds to 1 µm.

To attach beads to the filament carboxy-modified polystyrene beads were treated with EDAC (1-**E**thyl-3-(3-**d**imethyl**a**minopropyl) **c**arbodiimide hydrochloride, Invitrogen, Germany) to crosslink the secondary goat anti-rabbit IgG to the surface. The swimming ability of *S. oneidensis* MR-1 cells in a *tunnel slide* decreases in HEPES, PBS or the *E. coli* motility buffer. Therefore, buffer conditions had to be optimised and a buffer derived from 4M containing HEPES and lactate was used to ensure an excess of a soluble electron donor.

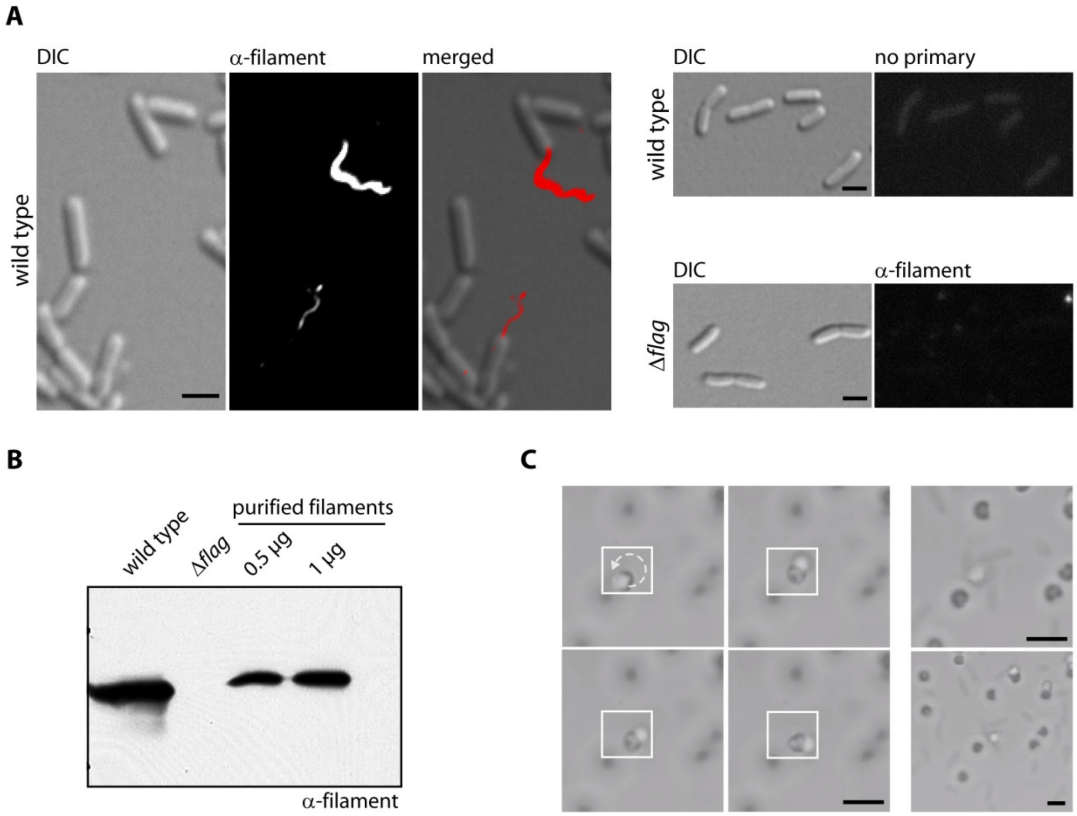

Figure 19: Attachment of a bead to the filament of *S. oneidensis* MR-1. A) Immunostain analysis of the flagellar filament. The specifity of the generated antibody was determined by localisation of the flagellar filament. As a control, wild type cells were either incubated with the secondary antibody (upper right) or the flagellar filament deletion mutant *Δflag* (lower right) was used. The antibody is highly specific to the flagellar filament of *S. oneidensis* MR-1. **B)** Wil- type cell lysates and purified filaments were analysed by immunoblotting with the anti-filament antiserum. *Δflag,* as a control, did not exhibit a dominant band at the expected size of 36 kDa. **C)** Beads attached to the flagellar filament. Goat-anti-rabbit crosslinked polystyrene beads, wild-type cells and the generated anti-filament antiserum were incubated. Left panel: two spinning beads attached to one filament, Right panel: different Z-plane, showing the same cell with the attached bead. Spinning beads are white, darker beads are attached to the coverslip and hence in a different Z-plane. The arrow depicts the direction of bead rotation (CCW). The scale bar represents 2 µm.

Finally, incubation of the cells with primary IgG against the flagellar filament and the crosslinked goat-anti rabbit IgG beads resulted in free swimming cells pushing or pulling a bead (Figure 19 C). Thus, attaching beads to the flagellar filament of *S. oneidensis* MR-1 was successfully accomplished.

(B) Freely rotating flagella filament

Besides having beads successfully attached to the filament, a freely rotating flagellum is necessary to obtain reliable rotation speed data from the bead assay. In contrast to *E. coli*, *S. oneidensis* MR-1 has a single polar filament. A polar filament of cells that are attached by their length to a coverslip is in close proximity to the coverslip surface and, thus, does not freely rotate due to limited space. In order to get a free rotating filament in a polarly flagellated species, two different approaches were pursued.

One approach was to lift up the flagellated pole to increase the space for flagellar rotation by using a bead covered surface. For this purpose polystyrene beads immobilised on a coverslip were coupled with an antibody against the cell surface, obtained from an antiserum raised against the cell

surface of *S. oneidensis* MR-1. To avoid cell lysis and contamination with inner membrane or cytoplasmic substances, cells were fixed by paraformaldehyde treatment and injected as a whole. The antiserum, as tested by immunostaining, was specific. By using fluorescently tagged wild-type cells, it was verified that the cells are bound to the beads (data not shown). However, filaments were not rotating on cells treated that way. Thus, uplifting cells by coupling the cell surface to an immobilised bead did not lead to a freely rotating filament.

A parallel approach aimed at delocalising of the flagellar filament. For *V. cholera*, *V. alginolyticus*, *Pseudomonas aeruginosa* and *P. putida* it was demonstrated that two proteins, FlhF and FlhG, are important for flagella positioning and flagella number. [166-172]. In these species, lack of the GTPase FlhF resulted in a lateral displacement of the polar flagella and a reduced number of flagella, while overexpression of FlhF lead to an increased number of polar flagella. FlhG has been shown to negatively regulate the number of polar flagella in *V. alginolyticus,* overexpression causes a reduction in the number of polar flagella, whereas the lack of FlhG increases the number of polar flagella [168]. FlhF and FlhG have been described to be a unique factor in polarly flagellated bacteria. Potential orthologs to FlhF and FlhG are encoded by SO_3212 and SO_3211, respectively. To identify the role of FlhF and FlhG for flagella placement in *S. oneidensis* MR-1, deletion mutants in the corresponding genes, *ΔflhF*, *ΔflhG* and *ΔflhFG* were generated, and filaments were stained [173]. Additionally, to clearly localise the flagellar motor in these mutants deletions were introduced into a FliN-Gfp background. The colocalisation of FliN-Gfp and the flagellar filament was verified by immunostaining (data not shown). Similarly to *Vibrio* and *Pseudomonas*, the lack of FlhF resulted in displacement and reduction of the flagella number, while deletion in *flhG* increased the polar flagella number. Flagellation of the double deletion mutant was lateral polytrichous (Figure 20 A and Table 3). Additionally, swimming ability tested on soft agar plates was drastically reduced in all mutants compared to that of wild-type cells. To summarise, FlhF was shown to be important for the localisation of the single polar filament in *S. oneidensis* MR-1. A single delocalised filament and, with that, a suitable mutant for the bead assay was observed in the *ΔflhF* strain.

Table 3: Phenotypic characterisation of *ΔflhF*, *ΔflhG* and *ΔflhFG* strains. Phenotypic characterisation was carried out together with Nathalie Heß during her Bachelor thesis [174].

Genotype	Flagellation[a]	Flagellated cells[b] [%]	Swimming ability[c]
wild type	polar, monotrich	95	+++++
ΔflhF	lateral, monotrich	2.5	++
ΔflhF up	lateral, monotrich	10	+++
ΔflhG	polar, polytrich	94	+
ΔflhFG	lateral, polytrich	99	+

[a] Described are the flagellation types after filament staining of *ΔflhF* and/or *ΔflhG*. "*up*" mutants were enriched from *ΔflhF* flares of elevated motility on soft gar plates. polar monotrich, one single flagellum placed polarly; lateral monotrich, one single flagellum placed lateral; polar polytrich, a bundle of filaments placed polarly; lateral polytrich, bundles of filaments placed lateral

[b] the percentage of flagellated cells was analysed by localising the flagellar motor in a *fliN-gfp* strain.

[c] Swimming ability was observed on soft agar plates and by microscopic analysis.

To increase the number of cells with a delocalised flagellar filament, mutants with enhanced swimming ability were enriched by restreaking colony material from the edges of the swimming zones on soft agar plates (*ΔflhF up*). As observed under the microscope, the number of swimming cells in *ΔflhF up* was increased. Filament staining after Ryu and colocalisation with FliN-Gfp revealed that about 10% of the cells were flagellated and exhibited a flagellar motor. The single flagellar filament was not preferentially placed polarly (Table 3 and Figure 20 A). The observation of swimming cells in addition to recent studies lead to the assumption that once a flagellum is assembled in a *S. oneidensis* MR-1 *ΔflhF up* mutant strain, the flagellar motor is functional [168-170].

To measure flagellar motor performance of different stator ring compositions, *in frame* deletions of *pomAB* and *motAB* were generated in a *ΔflhF up* background. Motility of stator deletion mutants, in the wild-type and in the *ΔflhF up* background were compared (Figure 20 B). The swimming diameter of *ΔflhF* on soft agar plates was decreased compared to that of wild-type cells. Accordingly, similar observations were made for different stator deletion mutants in *ΔflhF*. A deletion of *motAB*, resulting in an exclusively PomAB-driven motor, slightly decreased the swimming diameter on soft agar plates. The lack of *pomAB*, resulting in a MotAB-driven motor, drastically decreased swimming ability in this assay. However, microscopic analysis of *ΔflhF up /ΔpomAB* cells revealed that a motile population of cells that was swimming independently of the sodium-ion concentration, demonstrating a functional flagellar motor. Enrichment of cells with elevated motility was unsuccessful for *ΔflhF up ΔpomAB* mutants to date. A population of swimming *ΔflhF up ΔpomAB* cells could always be detected, however, the amount of cells was drastically decreased compared to the wild type due to the deletion in *flhF*. As described in chapter 2.1.2, a substitution in MotB in *ΔpomAB up* was found to increase the number of swimming cells. In future experiments this substitution will be introduced in *ΔflhF up ΔpomAB* to potentially increase the number of swimming cells.

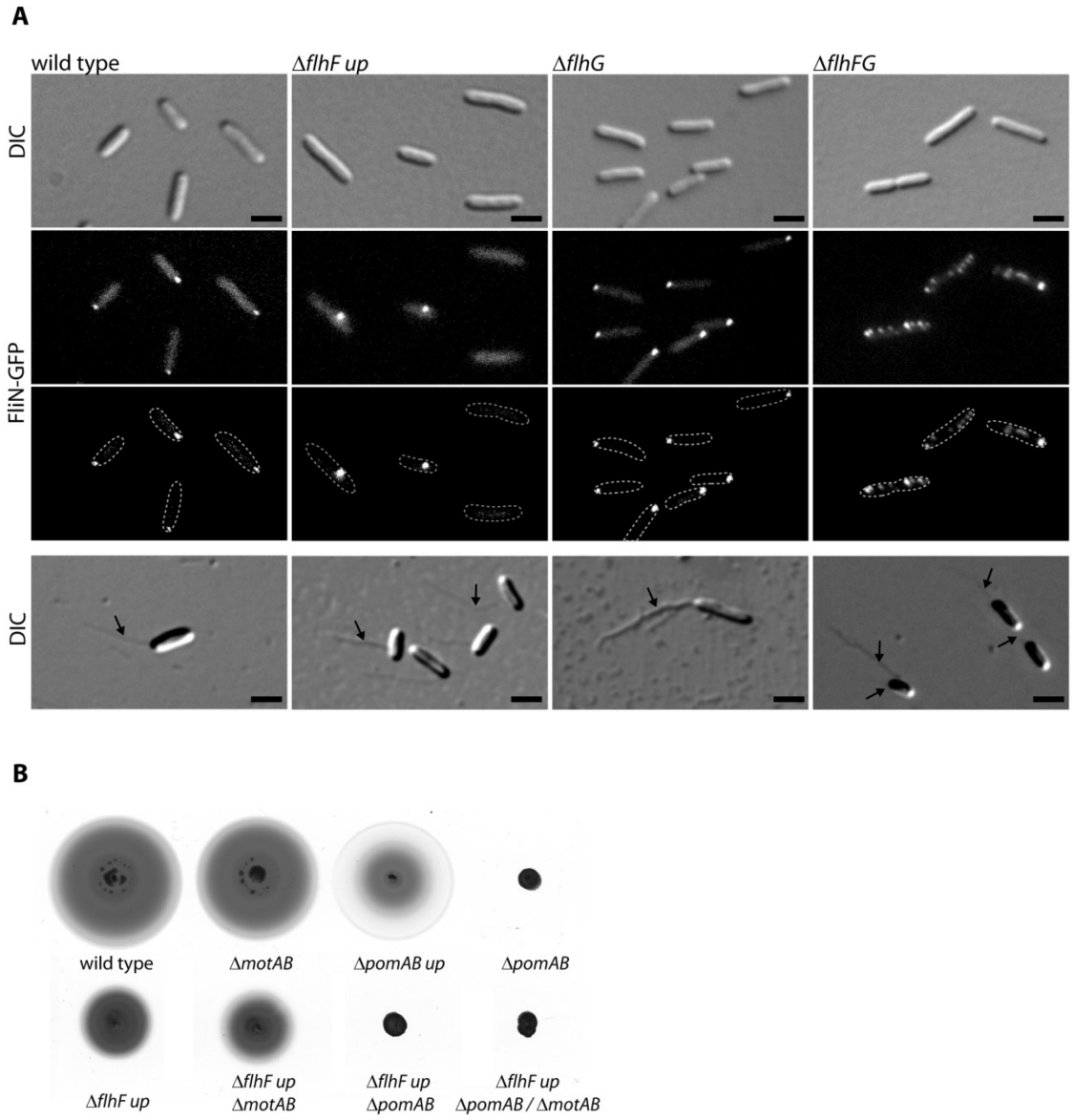

Figure 20: Establishing a freely rotating filament by deleting *flhF*. A) Displayed are DIC and fluorescent micrographs of wild-type, *ΔflhF up*, *ΔflhG*, and *ΔflhFG* cells. Cells with elevated motility in *ΔflhF* were enriched: the corresponding strain is annotated as *ΔflhF up*. Upper panels, visualisation of the localisation of the flagellar motor by FliN-Gfp. Lower panel, flagellar number and placement are visualized by filament staining. The scale bar equals 2 µm. **B)** Comparison of the motility of stator deletion mutants in *S. oneidensis* MR-1 wild-type and *ΔflhF up* background.

Taken together, by deleting *flhF* and enriching motile cells about 10% of the cells possessed a single delocalised rotating flagellar filament. Thus, two requirements for establishing the bead assay for *S. oneidensis* MR-1 were fulfilled.

(C) TIGHTLY IMMOBILISED CELL BODY

In order to obtain reliable data from the bead assay, cells are required to be immobilised to the coverslip surface. As described for *E. coli* and *R. sphaeroides*, poly-L-Lysine was successfully used for

coating of the coverslips [18,78]. In contrast, several approaches showed that *S. oneidenis* MR-1 did not adhere tightly enough to this surface. Therefore, I tested different conditions as summarised in Table 4.

Table 4: Conditions tested to immobilise *S. oneidensis* MR-1.

Condition	Short description - reference	Immobilised cells[a]
Poly-L-Lysine hydrobromide (chain length: > 30 kDa)	positively charged aa polymer enhances electrostatic interaction between negatively charged cell membrane and culture surface	(+)
Poly-L-Lysine hydrochloride (chain length: 1-5 kDa)	Sigma-Aldrich	(+)
Gelatin	used for immobilising cells on agar pads in microscopy	n.d
Agarose	technical limitation due to height in tunnel slide	n.d
Schott Nexterion slides:		
AL	crosslinked aldehyde groups, reacts with primary amines - covalent binding	(+)
E	epoxysilane: binds amine, thiol and hydroxyl groups	(+)
H	alternative for nitrocellulose, linked with NHS-Ester, binds covalently to amine goups	(+)
P	reactive NHS-ester, amine, thiol and hydroxyl groups	(+)
Rain-X® coating	Simple method to obtain hydrophobic surfaces [175]	++
Silanization	generates hydrophobic surfaces	+
Polystyrene coating	coverslips coated by Rainer Kurre at the University of Münster	
Plastic surface	plastic slide from ROCHE (Germany) inappropriate for use as coverslips, poor imaging when used lower surface in tunnel slid	++

[a] Immobilisation of cells was observed microscopically. n.d. non-derived; (+), about 10-20 % of the cells were immobilised, non-suitable for bead assay, as cells either detached quickly or lost their viability; +, cells detached; ++, about 10-20 % of the cells were immobilised

In summary, immobilisation of *S. oneidensis* MR-1 cells was successfully established on hydrophobic surfaces by using Rain-X® coated coverslips or plastic slides. Since cells are required to be attached to the coverslip, and glass slides are required for optimal imaging, Rain-X® coated coverslips were used for further studies.

(D) ROTATING FILAMENT ON IMMOBILISED CELLS

In the final step, delocalised freely rotating filaments with attached beads were combined with immobilised cells in a *tunnel slide* measure the flagellar rotation frequency by BFPI. In a *tunnel slide*, a tunnel of 100 μm height is formed by sealing the edges with sticky tape (see Material and Methods, Figure 33). The advantage of a tunnel slide is the ability to easily and efficiently wash the surface, to change buffers, e.g. to have floating cells or to have a variability in buffer conditions.

ΔflhF up cells cultured in LM were immobilised on Rain-X®-coated coverslips, incubated with the primary anti-filament antibody and supplemented with 1.1 μm polystyrene beads crosslinked with the secondary goat anti-rabbit antibody. Rotating beads were observed under the microscope. Cells with rotating beads were active for a period of several minutes (~5 min). Most of the cells either stopped or detached and swam away pulling or pushing a bead. These findings indicate that the stop of bead rotation is not caused by irreversible attachment of the beads to the surface, but rather due to the physiology of the flagellar motor in *S. oneidensis* MR-1. The organism is well known for its ability to form biofilms, and surface attachment is one of the major stages in biofilm formation. It is conceivable that after surface attachment the flagellar motor slows down and even stops. This interesting fact will be analysed in further experiments.

Although the bead assay as described here is unsuitable for long-term studies of the flagellar motor in *S. oneidensis* MR-1, it is sufficient to get first insights into the properties of the *S. oneidensis* flagellar motor, a polarly flagellated species. By applying Back Focal Plane Interferometry (BFPI) I was able to measure the rotation speed of the filament in *ΔflhF up* mutants as described in the next chapter.

FLAGELLAR ROTATION SPEED ANALYSIS IN *S. ONEIDENSIS* MR-1 BY USING THE BEAD ASSAY

In the following, the performance of the *S. oneidensis* MR-1 wild-type flagellar motor (*ΔflhF up*) was determined by applying the previously established bead assay. To this end, rotation speed of an attached 1.1 μm polystyrene bead[2] was analysed for 30 s. Cells were grown in LB medium to an optical density OD_{600} of 0.6 and washed in 4M buffer supplemented with 200 mM sodium chloride. Immobilisation of cells was carried out in a tunnel slide on a Rain-X®-coated coverslip (detailed protocol see Material and Methods). Trajectories of the rotating bead were taken by BFPI in an optical trap and analysed by applying a LabView code. Optical devices were constructed and the software was written in the Molecular Motors Group of the Physics Department in the University of Oxford.

The first insights into-wild type flagellar motor performance of *S. oneidensis* MR-1 by BFPI in an optical trap are summarised in Figure 21. First, the direction of rotation, either clockwise (CW) or counter-clockwise (CCW), viewed from the distal end of the filament was determined. The convention for clockwise (CW) and counter-clockwise (CCW) is schematically shown in Figure 21 A, a positive rotation is classified to be CCW and a negative rotation CW rotation. A trajectory of 1 s and 10,000 data points for the analysed 1.1 μm rotating bead is displayed in Figure 21 B. Trajectories depend on the size of the flagellar stub, the bead size and how steadily the filament is rotating (given that the beads are well aligned in the trap). The obtained speed data were 200 point median filtered, which gives a resolution of 20 ms. Only approximately circular trajectories were taken into account for further analysis. Angle-time and rotation speed-time traces for a 1.1 μm bead, recorded for 30 s are shown in Figure 21 C. The observed cell was switching between CW

[2] Note that rotation of a 1.1 μm polystyrene bead reflects rotation under high load.

and CCW rotation bias, shown in light grey and dark grey, respectively. A stop (highlighted in white) was observed between 20 and 23.5 s. The flagellar stub of the analysed *ΔflhF up* cell was rotating at about 16.0 ± 8.9 Hz in CCW and 17.5 ± 5.5 Hz in CW direction, and motion was assessed by averaging speeds greater than 1 Hz to exclude stop periods ('±' depicts standard deviation).

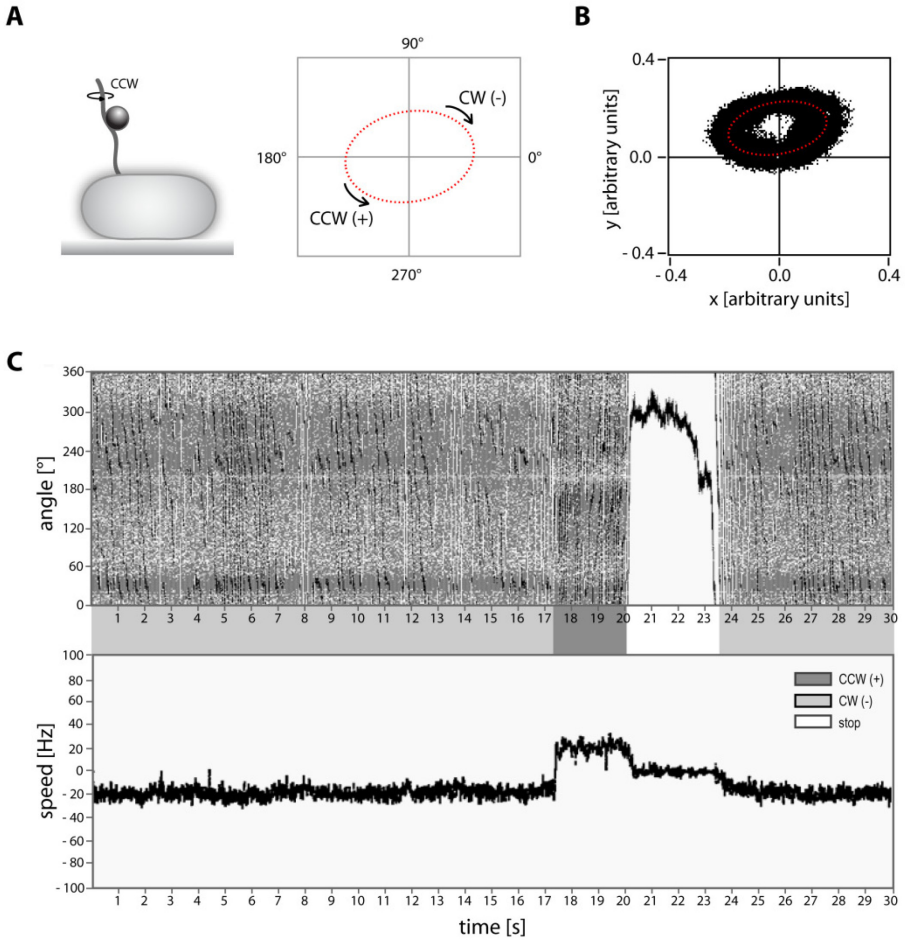

Figure 21: Trajectory, angle-time, and speed-time trace for the *S. oneidensis* MR-1 bead assay. A) Schematic presentation of the bead assay (right) and a simplified trajectory of a rotating bead, illustrating clockwise (CW) and counter-clockwise (CCW). CW has a negative and CCW a positive convention. **B)** Trajectory for the analysed cell, shown is a measurement of 1 s with 10,000 data points in x-y direction as arbitrary units. **C)** Angle-time and speed-time trace for the analysed motor performance in *S. oneidensis* MR-1 with a 1.1 µm polystyrene bead, upper and lower graph respectively. Marked in dark grey CCW bias, in light grey CW bias, the white area is comparable with a stop of rotation. The averaged rotation speed of the analysed *S. oneidensis* MR-1 filament was 16.0 ± 8.9 Hz for CCW and 17.5 ± 5.5 Hz for CW direction (with averaged rotation speed data greater than 1 Hz to exclude stopping periods).

Additional speed-time traces for six different *ΔflhF up* cells are shown in Figure 22. A general feature of the *S. oneidensis* MR-1 wild-type motor is that it switches between CW and CCW direction. The averaged angular velocity was between 13.7 Hz and 18.5 Hz for CCW and 7.4 and 17.5 Hz for CW rotation. In comparsion, the flagellar motor of *E. coli* reaches between 5-10 Hz under high load for CW and CCW direction [70]. The speed-time traces of the last two *ΔflhF up* cells illustrate, as observed earlier, that the flagellar motor slows down or stops during the recording period. Notably, in the same slide also tethered cells were observed.

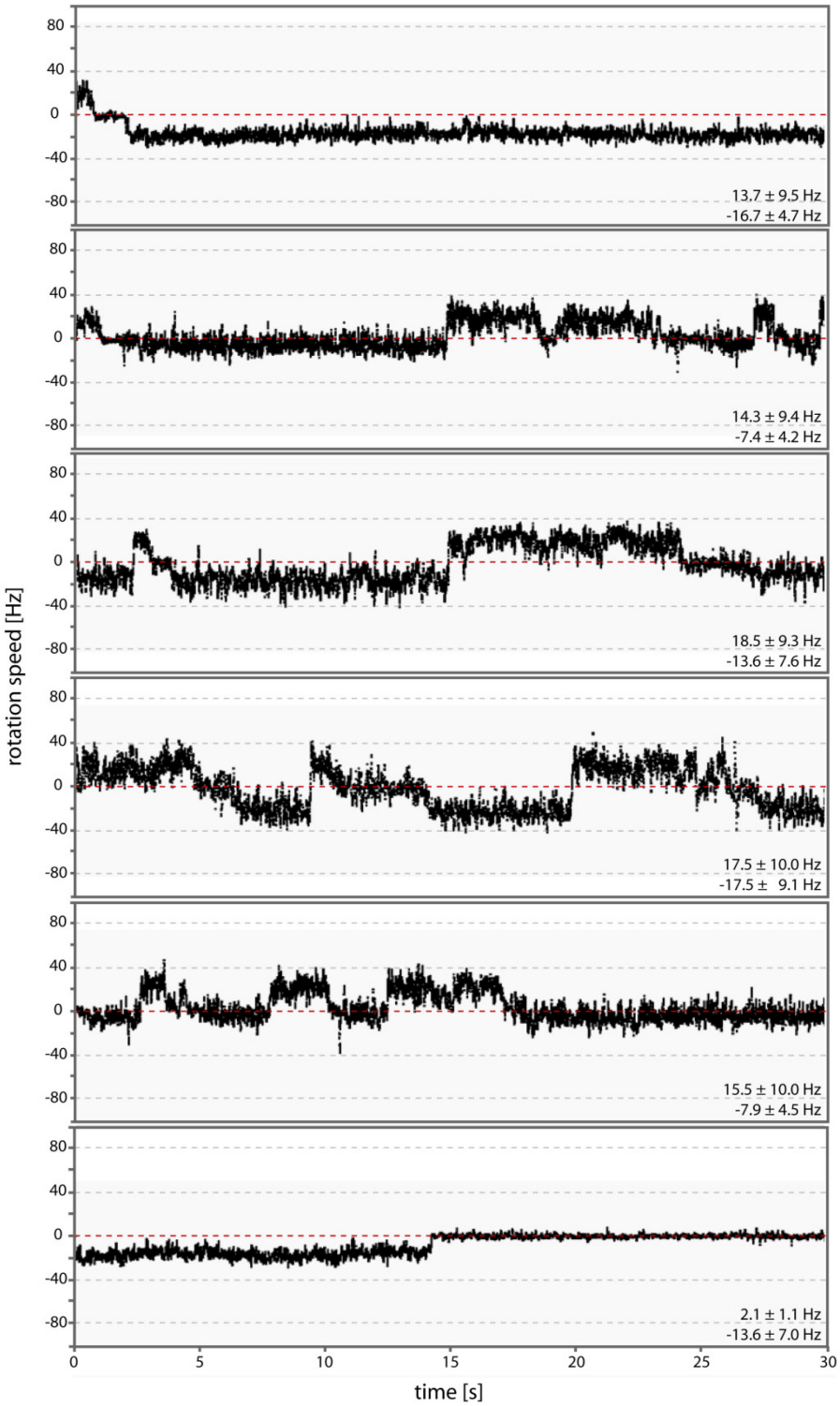

Figure 22: Speed-time traces for six additional *ΔflhF up* cells. Angular velocity for the *S. oneidensis* MR-1 flagellar motor with a 1.1 µm polystyrene bead under standard conditions (4M buffer supplemented with 200 mM sodium chloride). The averaged rotation speed above a threshold of 1 Hz is displayed in the right corner of each graph. 10,000 points per second were recorded for 30 s and the rotation speed was 200 point median filtered. The flagellar motor of *S. oneidensis* MR-1 is switching and rotates between 13.74 Hz and 18.51 Hz for CCW and 7.43 and 17.54 Hz for CW direction. Interestingly, cells slow down and even stop after a certain period of time. The rotation speed line for 0 Hz is highlighted in red.

In summary, the bead assay was established for a bacterial species harbouring a single polar flagellum. *S. oneidensis* MR-1 cells were immobilised on a Rain-X® surface and polystyrene beads were attached to the flagellar filament by immunolabeling. For this purpose and with regard to the modification of the filament in *S. oneidensis* MR-1 an antibody was raised against the whole filament. A freely rotating filament was achieved by introducing a deletion in *flhF*, a gene whose product is important for polar flagella placement. Thus, all requirements for a functional bead assay are fulfilled.

Applying the bead assay resulted in first insights into the wild-type flagellar motor performance of *S. oneidensis* MR-1 *ΔflhF up* cells. Under conditions of 200 mM sodium chloride and an attached 1.1 μm polystyrene bead, the filament stub was rotating at 17.5 Hz and 16.0 Hz for CW and CCW, respectively (averaged rotation speed). While these immobilised cells slowed down or stopped flagellar rotation, cells tethered by their filament were observed to rotate, leading to the hypothesis that surface attachment interferes with flagellar rotation in *S. oneidensis*.

However, because of the limitations in the bead assay developed for *S. oneidensis* I decided to use the tethered cell assay to biophysically characterise PomAB, MotAB and wild-type motor composition in a *ΔflhF up* background.

2.3.2 The *S. oneidensis* MR-1 tethered cell assay

In this part the tethered cell assay will be used as an alternative to the previously described bead assay. I will provide evidence that the wild-type motors outperform PomAB-driven motors at low sodium-ion concentration and that MotAB is incorporated into a PomAB-driven motor upon induction. Additionally, I observed an intriguing shift in the rotation direction in wild type cells under low sodium-ion conditions.

TETHERED CELL ASSAY

In the tethered cell assay, cells are attached to the surface by their filament (Figure 23 A). By analysing the rotation of the cell body, angular velocity is calculated. Since the motor is working against high load, the cell body, it only rotates at low frequencies. It is to note her, that 'high' describes any load which exceeds the load of a filament (maximal 0.5 μm beads).

In general, tethered cells are recorded by video microscopy and the rotation speed is calculated as angular changes over time. A MATLAB code to analyse the data was written in the Molecular Motors Group in the Department of Physics in the University of Oxford by Dr. Bradley Steel and the tethered cell assay was established in collaboration with Dr. Mostyn Brown and Dr. Nicolas Delalez. To obtain a freely rotating cell body, the delocalised *ΔflhF up* mutant was used. An overview of the performed analysis for *ΔflhF up* in 4M buffer supplemented with 5mM sodiumchloride is shown in Figure 23. This figure displays the analysis steps used to calculate the rotating speed of the cell body. Figure 23 A schematically displays the attachment of the filament to the coverslip surface. Cultures were washed in 4M buffer, supplemented with different sodium-ion concentrations and incubated on a coverslip. The anti-filament antibody was added for 15 min and finally the *tunnel slide* was flushed with 4 M buffer. Videos were recorded for each frame and rotation speed was analysed. To that end, changes of the cumulative angle over time were used for

calculation and the obtained distribution of rotation speed is shown in a histogram (Figure 23 B-E). The median for the rotation speed of all data points in CW and CCW direction was used to compare the motor performance of individual cells as presented in Figure 24. The analysed cell body was rotating at 5.7 Hz and 5.9 Hz for the CW and CCW direction, respectively. To exclude Brownian motion during stopping periods, a threshold was set to remove speeds slower than 0.25 Hz.

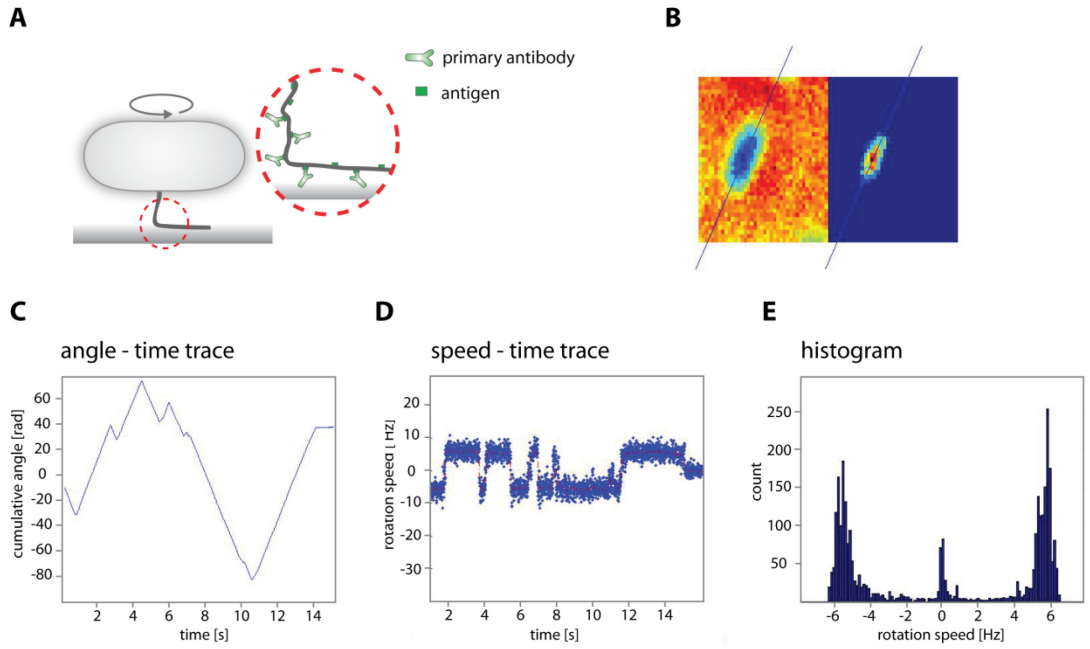

Figure 23: Calculation of rotation speed in a tethered cell. Displayed are different steps for the analysis of the rotation speed in a tethered cell. **A)** Schematically displayed is a cell tethered to a coverslip by anti-filament antibodies. **B)** A brightfield image is divided into three regions and supplemented with an axis, following rotation of the cell body. Accordingly, for the picture on the left: Orange, background; cyan, marginal area; blue, cell area. **C)** Analysis of the cumulative angle changes [rad] over time. **D)** Median-filtered rotation speed [Hz] (windowsize 3 ms). **E)** Distribution of the data points for the median-filtered rotation speed. In the next step this speed was again median-filtered for negative and positive speeds corresponding to CW and CCW direction, respectively. *ΔflhF up* cells were recorded and analysed for 15 s. The cell body in this analysis was rotating at 5.7 Hz (CW) and 5.9 Hz (CCW) in media supplemented with 5 mM sodium chloride.

To summarise, a tethered cell assay was established to analyse the rotation speed of the flagellar motor of the single polar flagella in *S. oneidensis* MR-1. The *ΔflhF up* mutant with a delocalised flagellar filament was used to obtain a freely rotating cell body, and the filament was tethered to a coverslip by an anti-filament IgG. Using this assay the rotation speed from this assay was then compared in different sodium-ion concentrations and stator compositions.

2.3.3 Wild-type motor outperforms PomAB-driven motor at low sodium ions

In order to analyse motor performance at different sodium-ion concentrations, *ΔflhF up*, *ΔflhF up ΔmotAB* and *ΔflhF up ΔpomAB* cells were tethered to a coverslip in a tunnel slide using the purified anti-filament IgG. Unlike *ΔflhF up* and *ΔflhF up ΔmotAB* cells, the cell bodies of *ΔflhF up ΔpomAB* were not rotating under these conditions. However, observations of swimming cells under the microscope revealed that those cells were motile. At least 36 tethered cells for *ΔflhF up* were analysed at different sodium-ion concentrations for 15 s. The highest rotation speed, independent of CW or CCW direction, for 200 mM, 5 mM and 0 mM sodium chloride under static buffer conditions is summarised in Figure 24 for wild type flagellar motor and *ΔflhF up* Δ*motAB*. Rotation speed of wild-type and PomAB-driven motors were not significantly different in 200 mM and 5 mM sodium chloride. In contrast, low sodium-ion conditions (0 mM sodium chloride) had significantly different rotation speeds for *ΔflhF up* and *ΔflhF up ΔmotAB* (t-Test, p-Value 0.01). Unexpectedly, cells were able to rotate at 0 mM sodium chloride, indicating that the buffer is not sodium-ion free. Notably, preliminary analyses of the distribution of wild type flagellar motor performance at high sodium-ion concentration suggest that there may be two different populations of speed, one rotating at 7.5 Hz and the other at 21.2 Hz (see appendix, Table 16).

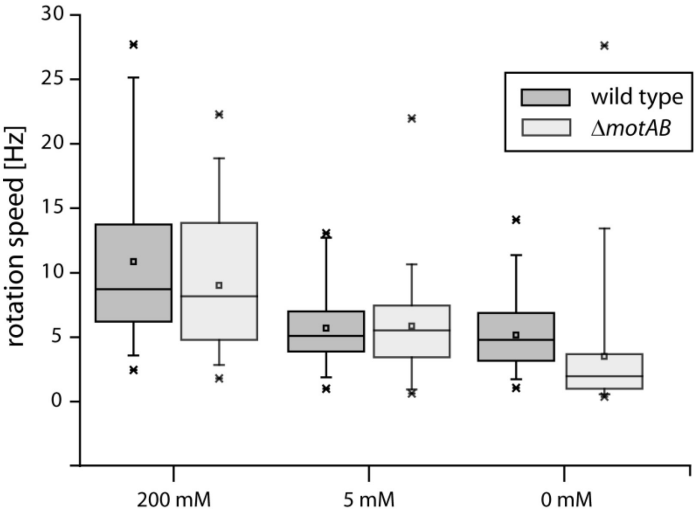

Figure 24: The wild-type flagellar motor outperforms the sodium ion-driven motor at low sodium-ion concentration. Summarised are rotations speeds obtained for *ΔflhF up* and *ΔflhF up ΔmotAB* tethered cells in a box-whisker-plot. The box and the included line represent the middle 50 % and the median of the data. The average is shown as '□', and the whiskers denote the data range of the 5th and 95th percentile. Minimum and maximum are represented by 'x'. Rotation speed of 75, 57 and 77 *ΔflhF up* cells for 200 mM, 5 mM and 0 mM sodium chloride were analysed, revealing a median angular velocity of 8.7, 5.1, and 4.8 Hz, respectively. 39, 36, and 93 *ΔflhF up ΔmotAB* cells rotated at 8.2, 5.5 and 2.0 Hz in 200 mM, 5 mM and 0 mM sodium chloride, respectively. Performance of the wild type flagellar motor at 0 mM sodium chloride is significantly different from the PomAB-driven motor (t-test, p-Value 0.01)

Taken together, my data imply that the performance of the flagellar motor in *S. oneidensis* MR-1 depends on the sodium-ion concentration. Additionally, the wild-type flagellar motor outperforms the PomAB-driven one at low sodium-ion concentration, suggesting that MotAB is functionally

incorporated into the stator ring at low sodium-ion concentration. These results are in accordance with those obtained for the swimming speed data, where full speed at low sodium-ion concentration was only achieved in the wild type [128]. Additionally, the difference of rotation speed at high and low sodium-ion concentrations in the *ΔmotAB* mutant suggests that stators are either non-active in the flagellar motor or not incorporated. Unfortunately, I was not yet able to observe the performance of a MotAB-driven motor. Previous swimming speed assays have shown that flagellar rotation of *ΔpomAB up* is independent of the sodium-ion concentrations. However, to demonstrate that MotAB is functionally incorporated into the stator ring, the *ΔflhF up ΔpomAB* mutant has also to be analysed at the single cell level.

2.3.4 Response of wild-type motor to changing sodium-ion concentrations

The tethered cell assay described in the previous part revealed that at low sodium-ion concentration a wild-type motor rotates significantly faster than a PomAB-driven motor. These results indicate that MotAB gets incorporated into the wild-type motor at low sodium-ion concentration and, therefore, flagellar motor performance is more efficient and outperforms the solely PomAB-driven motor. To address the question of whether the functional incorporation of MotAB and/or PomAB depends on the sodium-ion concentrations, the performance of a single flagellar motor in response to different sodium-ion concentrations was determined.

To this end, a *ΔflhF up* mutant was analysed in a flow cell which allows a constant exchange of buffer with different sodium-ion concentrations [79]. First, the time period required for a complete buffer exchange in the flow cell was determined, supplementing the buffer with a dye (Ponceau red) and recording the time until the stained buffer arrived in the chamber (~15 s). Subsequently, buffer with no stain was used, and the time was recorded until the liquid in the chamber was completely transparent (~20 s). The first interval equals the time until the new buffer arrived, and the second equals the time until the buffer within the chamber was replaced. Cell cultures were grown in LB and subcultured for 5 h in LM. Prior to incubation in the flow cell, the cells were washed and incubated for one hour in 4M buffer supplemented with the sodium chloride concentration which was added first. Figure 25 summarises the rotation speed upon changes of the sodium chloride concentration in *ΔflhF up*, starting in 4M buffer with 0 mM sodium chloride. The different grey areas correspond to the time interval, when the buffer was added, and grey brackets mark the timepoint when the chamber was completely replaced by the newly added buffer. At low sodium-ion concentration the rotation speed was about 3 Hz, a stepwise buffer change up to 200 mM sodium chloride increased angular velocity. Changing the sodium chloride concentration induced a response of a short drop in rotation speed, which might indicate that stators are being replaced in the stator ring. Interestingly, a reduction from 200 mM to 5 and 0 mM sodium chloride induced frequent switching of the cells between CW and CCW directions, indicating a chemotactic response.

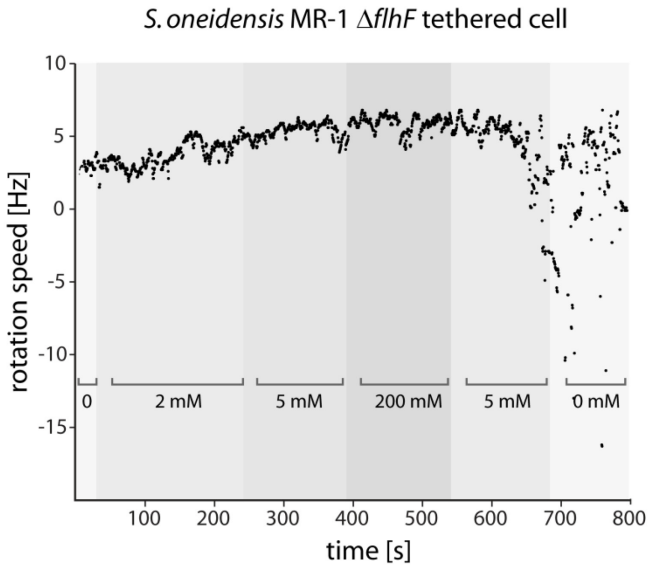

Figure 25: Response of wild-type cells to changing sodium-ion conditions. Summarised is the response of *ΔflhF up* upon buffer changes in a flow cell for 800 s. Cells were recorded by video microscopy with a frame rate of 200 Hz. Rotation speeds are powerspectral filtered with a window size of 3 s [79]. The 4M buffer was supplemented with different sodium chloride concentrations as annotated. The grey areas mark the time interval during which buffer with a defined sodium-ion concentration was added. About 20 s were required until buffer in the chamber was completely exchanged. Time periods with definable sodium-ion concentrations are marked by brackets.

Thus, the motor speed at high sodium-ion conditions in a flow cell is lower than the speed measured for the equivalent static buffer conditions. This implies that there might be two different adaptation systems responding to the external sodium chloride concentration, a short term reaction which occurs at transient buffer changes and a long term adaptation occurring in a static buffer environment in a time range that is yet to be determined.

To summarise, analyses of tethered *ΔflhF up* cells in a flow cell showed that the rotation speed of a single cell increases with increasing sodium chloride concentration. Thus, the analysis of the flagellar motor performance at the single cell level was successfully established. This work will be continued with additional measurements to increase the number of cells analysed, and to obtain further details on the flagellar motor performance in stator deletion mutants.

It was apparent that increasing sodium chloride concentration, slowly increased rotation speed. However, cells which were incubated in high sodium chloride and then suspended in low sodium chloride conditions responded with an increased switching bias and stopped rotating their flagella. Rotation was not resumed within 15 minutes. It is conceivable that incorporation of MotAB is a long term adaptation process, whereas restoration/incorporation of PomAB starting from a low sodium-ion environment occurs within a shorter period of time.

2.3.5 PomAB-driven motor has an increased CW bias

Microscopical observations revealed a chemotactic response apparent by forward and backward swimming in *S. oneidensis* MR-1. Accordingly, analysis of tethered Δ*flhFup* and Δ*flhFup* Δ*motAB* mutants displayed switching of filament rotation between CW and CCW direction at both high and

low sodium-ion conditions. Cells incubated in a tunnel slide with different sodium-ion concentration, were observed for 15 s and analysed regarding their direction of rotation. Cells, which rotated in both CW or CCW directions were scored as 0.5 in each direction, cells rotating only CW or CCW were scored as 1 in this direction and 0 in the other direction. Averaged data are summarised in Figure 26. This analysis revealed that cells harbouring a wild-type motor preferentially switched at 200 mM and 5 mM sodium chloride. 68 % and 61 % of the analysed Δ*flhFup* cells rotated in CCW at 200 mM and 5 mM sodium chloride, respectively. In contrast, 60 % and 68 % of the cells driven by a PomAB-driven motor were rotating in CW direction, at 200 mM and 5 mM, respectively. Interestingly, under low sodium-ion conditions Δ*flhFup* cells preferentially rotate in CCW direction (94 %), whereas the CW direction of the PomAB-driven motor was similar to that at high sodium-ion concentration.

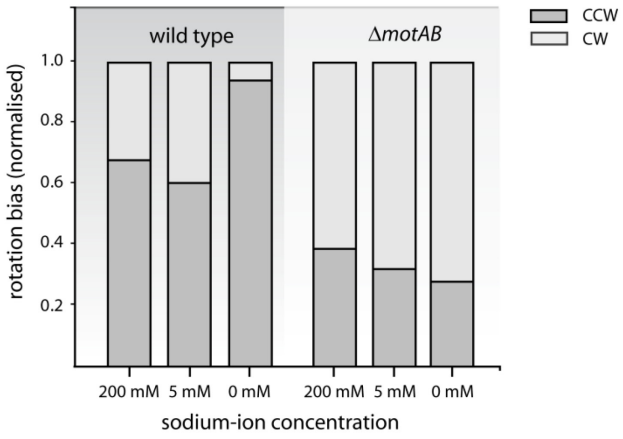

Figure 26: PomAB-driven motors have an increased CCW bias. The direction of rotation in Δ*flhFup* and Δ*flhFup* Δ*motAB* at different sodium-ion concentrations is summarised in a stacked bar chart. Cells were recorded for 15 s and analysed with respect to their direction of rotation. Cells rotating CW and CCW were scored as 0.5 in each direction; cells rotating either CW or CCW were scored as 1 in this direction and 0 in the other direction. Data were normalised to the sum of rotating cells quantified for individual conditions.

2.3.6 "Resurrection experiments"

To further characterise the properties of the two different stators, I performed "resurrection experiments" in a *pomAB*/*motAB* deletion by induced production of either PomAB or MotAB [76,107]. In order to modulate the expression levels of the stator units, *araC*-P_{BAD} cassettes were chromosomally integrated to replace the native promoter regions of *pomAB* and *motAB*, respectively. Resurrection experiments for *E. coli* revealed that up to eleven MotAB stator units are incorporated into the stator ring system and that even a single stator unit is sufficient to drive flagellar rotation [78,108]. Based on these results, I expected for *S. oneidensis* MR-1 that upon induction of either PomAB or MotAB the rotation speed would increase in a stepwise manner at a number of steps that depends on the number of stator units which are incorporated into the stator ring system. Based on *S. oneidensis* swimming speed assays and previous work with proton- or sodium-ion dependent flagellar motors the increments in speed are expected to be characteristically different for MotAB and PomAB.

The *araC*-P_{BAD} has been shown to be functional for tight regulation in *S. oneideniss* MR-1 [176]. The appropriate concentration of inducer to ectopically produce PomAB and MotAB was determined by using tethered cells, by microscopy performed on swimming cells and by analysis on motility plates. The following inducer concentrations were tested: 0.005 %, 0.01 %; 0.02 %; 0.05 %; 0.1 %, 0.2 % and 0.5 % (w/v). Upon induction of PomAB with 0.2 % arabinose most cells were motile and reached full speed, as analysed with tethered cells (data not shown). While a few motile cells were observed in a liquid non-induced culture of a *ΔmotAB pomAB::araC*-P_{BAD}-*pomAB* strain, soft agar plates did not reveal any motile cells, indicating a low level of induction only. Further quantification of the protein levels by immunoblot is necessary to characterise and to exactly modulate the number of stator complexes produced in the cell. Additionally, a vector containing a *lacIq*-P_{tac} cassette was constructed to be chromosomally integrated upstream of *pomAB* and *motAB* to replace the native promoter region. Two different inducible promoter upstream of *pomAB* and *motAB* will enable the modulation of gene expression for *pomAB* and *motAB* simultaneously.

A resurrection experiment on soft agar motility plates is displayed in Figure 27. The swimming diameter of *ΔflhF up* and the corresponding deletion mutant was compared to non-induced and arabinose-induced stator complexes. The swimming diameter on soft agar plates indirectly corresponds to swimming speed as faster swimming cells reach further distances. While induction of *motAB* in a *pomAB* deletion strain did not reveal motile cells, expression of *pomAB* in a *motAB* deletion background resulted in motile cells. Motility was further increased in a *motAB* deletion strain. In contrast, production of MotAB decreased the swimming diameter. Accordingly, production of PomAB in a *motAB* deletion background elevates motility compared to production of PomAB in a wild-type background. Thus, resurrection of a motor with PomAB was successful but the presence of MotAB decreases motility on soft agar plates compared to a PomAB-driven motor, suggesting that incorporation of MotAB slows down motor rotation.

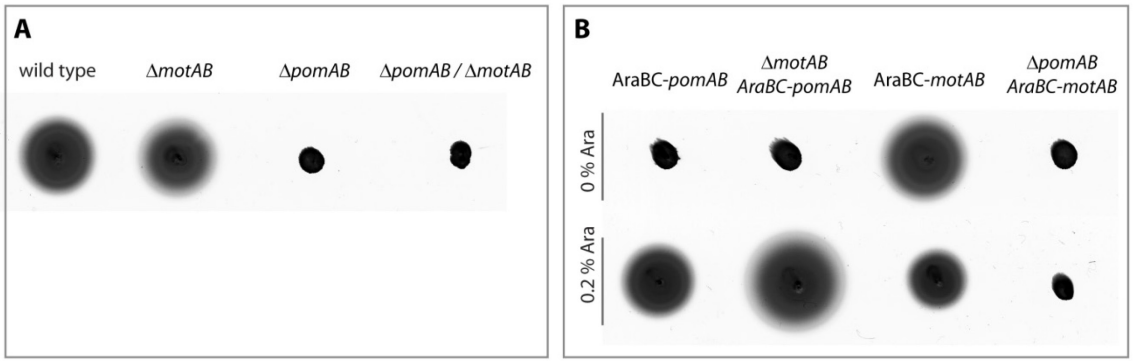

Figure 27: Resurrection of PomAB and MotAB on soft agar motility plates. A) Compared are the swimming diameters on soft agar motility plates for *ΔflhF up* and *ΔflhF up ΔmotAB* and *ΔflhF up ΔpomAB*. As a control, *ΔflhF up ΔpomAB ΔmotAB* did not swim at all. **B)** Swimming diameters upon induction of the stator complexes with 0.2 % Arabinose (w/v) in different stator deletion background. Lower panel compares the swimming phenotypes without and with induction with 0.2 % Arabinose. Cells were grown in LB overnight prior to inoculation of LB soft agar plates. While induction of *pomAB* in a *motAB* deletion strain revealed motile cells, expression of *motAB* in a *pomAB* deletion background resulted in non- motile cells. Motility is further increased in a *motAB* deletion strain compared to induction of *pomAB* in a MotAB-driven motor. In contrast, production of MotAB decreases the swimming diameter, suggesting that MotAB is incorporated into the stator ring.

2.3.7 Induction of *pomAB* resurrects the flagellar motor in a step-wise manner

In the next step rotation speed of tethered cells of the *ΔflhFup ΔmotAB pomAB::araC*-P_{BAD}-*pomAB* strain was analysed in a tunnel slide after induction with 0.2 % arabinose. Cells were kept in buffer supplemented with 0.005 % Arabinose prior induction. After 15 min of incubation, rotation of cells was recorded and increments in speed were observed as shown in the speed time-trace in Figure 28. Up to four discrete steps corresponding to stators getting incorporated into the stator ring were observed by eye. It is likely that speed intervals become smaller with increasing speed, meaning that steps at higher speed levels might be difficult to observe [72]. As most of the cells did not resurrect upon induction, only four of the recorded cells were analysed. To further analyse the biophysical characteristics of PomAB more cells have to be analysed.

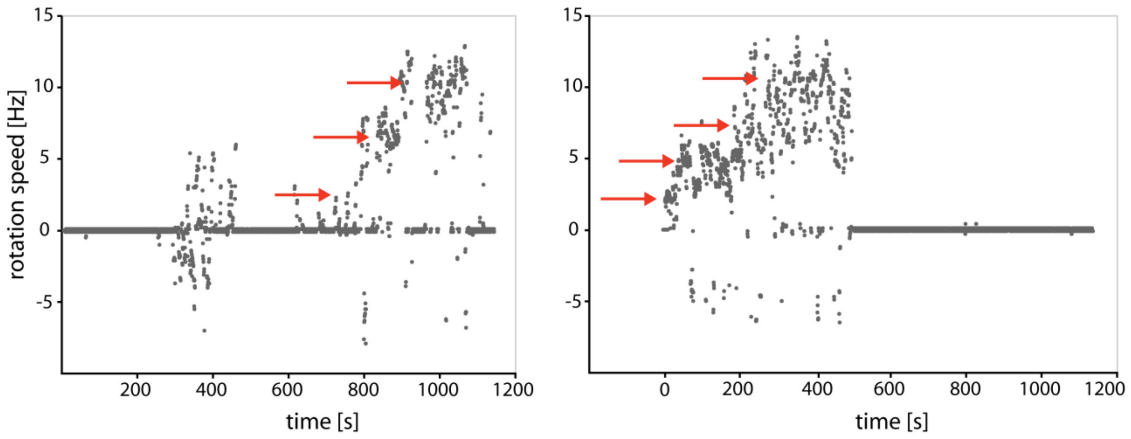

Figure 28: Induction of PomAB resurrects flagellar motor performance in a step-wise manner. Shown are powerspectral filtered speed-time traces of two different *ΔflhFup ΔmotAB pomAB::araC*-P_{BAD}-*pomAB* cells are displayed. Cells were incubated in 4M buffer supplemented with 0.005% arabinose in a tunnel slide. Recording was carried out for 1,200s with a frame rate of 200 Hz by video microscopy starting 15 min after induction with 0.2% arabinose. Red arrows indicate apparent steps in rotation speed.

In summary, motor function was resurrected by inducing PomAB production. So far, four steps in rotation speed were observed, indicating that at least four stator complexes got incorporated into the stator ring. However, recent work on *E. coli*, *R. sphaeroides* and my previous fluorescence microscopy studies with sfGfp-PomB suggest that the number of incorporated stator complexes is greater than four. It might be possible that the observed steps, pairs of stators, which is in accordance with preliminary analysis of fluorescently labeled stators in the membrane. Notably, the maximum speed observed for the cells displayed in Figure 28 was similar to the median range of rotation speed obtained in the population analysis shown in Figure 24, indicating that a full set of stator complexes entered the stator ring. However, additional experiments are needed to determine the properties of the MotAB stator.

2.3.8 MotAB gets incorporated into a PomAB-driven motor upon induction

In order to determine whether MotAB gets incorporated into a PomAB-driven flagellar motor, expression of *motAB* was induced in a *ΔflhFup* strain. Cultures were grown as described before and the analysis was performed in 4M buffer supplemented with 200 mM sodium chloride to retain rotation of the sodium-ion driven flagellar motor. The corresponding speed-time trace of one representative cell is show in Figure 29. Production of MotAB decreases rotation speed in a step-wise manner. Two such steps were observed upon production of MotAB. In accordance with the decreased swimming diameter on soft agar plates this data suggest that MotAB gets incorporated into the stator ring and subsequently slows down motor rotation.

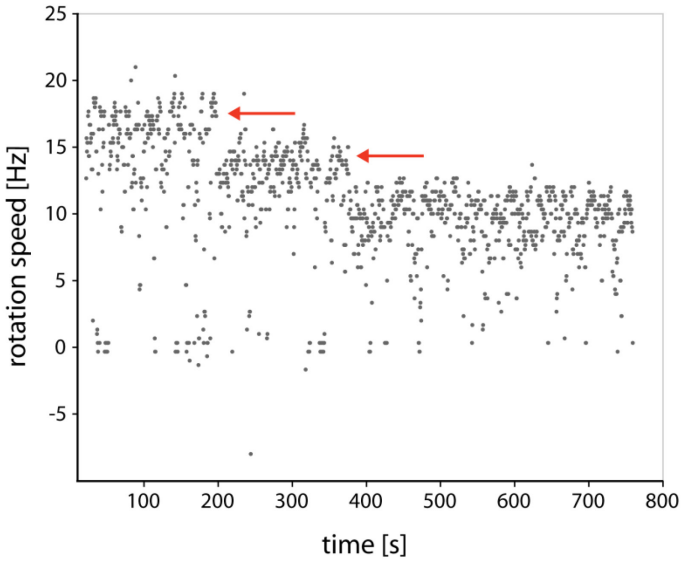

Figure 29: MotAB gets incorporated into a PomAB-driven flagellar motor and slows down motor performance. Displayed is a powerspectral-filtered speed-time trace for a single *ΔflhFup ΔpomAB motAB::araC*-P_{BAD}-*motAB* cell in 4M buffer supplemented with 200 mM sodium chloride. Expression of *motAB* was induced by 0.2 % arabinose and cells were recorded at a frame rate of 200 Hz 15 min after induction for 800 s. Red arrows indicate apparent steps in rotation speed. Induction of MotAB slows down motor rotation, indicating that MotAB gets incorporated into the PomAB stator ring.

The further characterisation of MotAB and PomAB in a tethered cell assay with fluorescently labelled stators might clearly show the number of incorporated stators as a function of the rotation speed. Additionally, immunoblot analyses are necessary to determine the copy number of expressed stator complexes, and strains with simultaneously inducible *pomAB* and *motAB* stators will help to precisely modulate the stator level in the cell.

Taken together, in accordance with the decreased swimming diameter on soft agar plates, production of MotAB in a PomAB-driven flagellar motor slows down rotation speed of a single tethered cell. This data implies that MotAB gets incorporated into the flagellar motor and causes the rotation speed to decrease. It is not yet clear whether or not MotAB is functionally incorporated. However, swimming experiments revealed that MotAB is able to drive flagellar rotation, suggesting that MotAB is functional. Additionally, my data indicate that MotAB incorporation or function might be load-dependent. MotAB might also require PomAB to be present and rotate the motor before it can be incorporated.

2.4 How common are multiple stator complexes?

Textbook knowledge suggests that most flagellated bacteria species, e.g. *E. coli* and *Salmonella* possess one or more distinct flagellar systems along with individual stator complexes. However, *S. oneidensis* MR-1 has two different stator complexes, PomAB and MotAB, along with a single polar flagellar system. To address the question how common multiple stator systems are among bacteria, I first determined how many flagellar systems and how many stator systems are present in the corresponding species. To that end, a sequence alignment of *S. oneidensis* MR-1 FliF against bacterial genomes by using BLASTP was performed. To exclude type III secretion systems that might have a considerable degree of homology to flagellar systems, an E-value cutoff < 1E-10 was used. FliF was chosen as a representative for flagellar systems, because it is an evolutionary conserved MS-ring protein and belongs to the early proteins of the flagella assembly process [4,177]. FliF is crucial for flagellar synthesis and deletion of *fliF* results in loss of the whole flagellar apparatus. Considering only fully sequenced and annotated genomes and *fliF* genes in vicinity to other flagella-related genes, 400 organisms harbouring a single and 134 harbouring two FliF homologs were identified (appendix, Table 17). For further analysis only organisms with a single FliF-encoding gene were included. Putative stator systems were identified by sequence alignment of PomA/MotA and PomB/MotB of *E. coli*, *V. alginolyticus*, and *B. subtilis* against sequenced bacterial genomes by BLASTP (E-value cutoff < 1E-10). These data were combined using the evaluated table for species harbouring a single FliF encoding gene as a master table. Only pairs of directly neighbouring putative orthologs to A- and B-stator subunits were considered to form a distinct stator locus (Table 5). It is conceivable that not all identified stator complexes are active, however, according to the literature almost all of the resulting species were shown to be motile.

Table 5: Dual stator complexes are surprisingly common.

FliF orthologs[a]	putative stator systems	species
1	2	52
1	3	12
1	4	5

[a] only the 134 suspecies, 69 species, out of 400 organisms harbouring multiple stator systems were included in the analysis.

Thus, the systematic bioinformatic analysis suggests that 33.5 % of the included 400 organisms harbour dual or multiple stator complexes along with one single flagellar system (134 different subspecies, 69 different species). Multiple stator systems are widely distributed among Gram-negative and Gram-positive bacteria (Figure 30). A complete list of all identified species can be found in the appendix (Table 18).

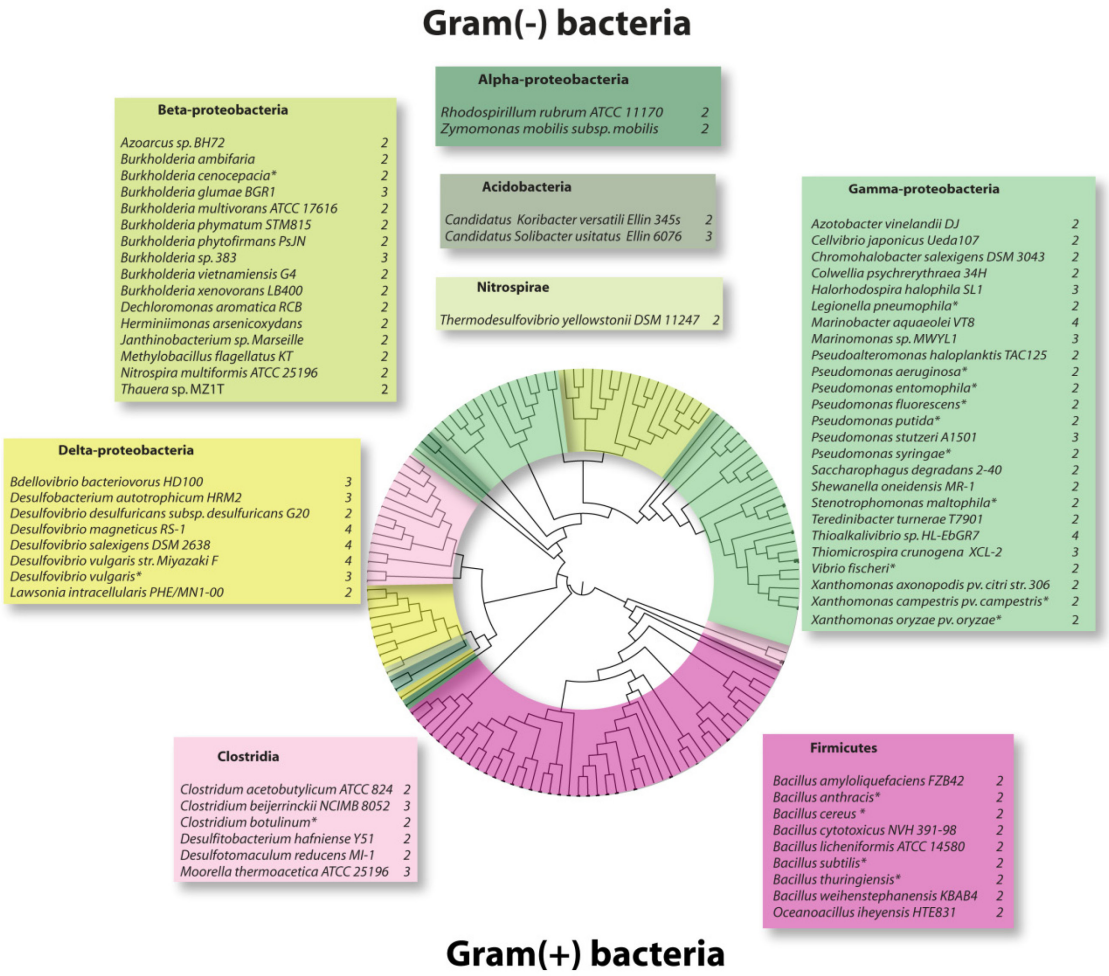

Figure 30: Bacteria with multiple stator complexes along with a single flagellar motor. Bioinformatic analysis was utilised to identify bacterial species with a single flagellar motor and multiple stator systems. Motor systems were identified by sequence alignment of FliF of *S. oneidensis* MR-1 against sequenced bacterial genomes by BLASTP with an E-value <1E-10. Candidates were then tested for their neighbouring sequence, only organisms with a single *fliF* in vicinity to other flagellar related genes were considered for further studies. Putative stator systems were identified by sequence alignment of PomA/MotA and PomB/MotB, respectively against sequenced bacterial genomes by BLASTP (E-value < 1E-10). Only pairs of directly neighbouring orthologs to A- and B-subunits were considered to form a distinct stator locus. It is conceivable that not all identified stator complexes are active. The phylogenetic tree displays distribution of FliF among the different genera (alignment CLUSTALW; phylogenetic tree with iTOL; http://itol.embl.de/). Green and yellow symbolise Gram (-) bacteria and purple stands for Gram(+) bacteria.

Although most organisms were found to have dual stator systems, the number of distinct putative stator systems for one single flagellar system can be as high as four, as found e.g. in *Desulfovibrio magneticus* RS-1. Most of the species within one genus show similarity regarding their stator to flagellar system ratio. For example, numerous *Pseudomonas* or *Bacillus* species harbour two different stator complexes with a single motor system, suggesting that this is a common feature among this species. Most of the *Desulfovibrio* species have four stator complexes. Interestingly, *D. vulgaries* and *D. desulfuricans* have three and two stator complexes, respectively, suggesting that additional stator complexes have been lost from the genome. In contrast, two stator complexes along with a single flagellar system appears to be a common feature among *Burkholderia* species, however, three stators

were identified for *B. glumae* BGR1 and *B.* sp. 383. As proposed for *S. oneidensis* MR-1, this might be due to lateral gene transfer driven by motility adaptation to different environmental conditions. Further *in vivo* analysis of these candidates might reveal the impact of multiple stator systems on the dynamics of the flagellar motor performance.

To conclude, dual or multiple stators seem to be surprisingly common among bacteria. Moreover, the overall number of four stators in *Desulfovibrio* species might suggest that stator acquisition was an early event, either by lateral gene transfer or by gene duplication. However, exceptions within this genus indicate a loss of additional stator complexes during evolution. In contrast, the additional stator complex in *S. oneidensis* as an exception among the *Shewanellae* indicates a recent uptake. The contribution to motility of additional stator complexes is not well understood yet, but as proposed for e.g. *P. aeruginosa* and *S. oneidensis* they expand the ability to enter a variety of different habitats, e.g. higher viscous environments or lower sodium-ion concentration in a fresh-water habitat.

3 DISCUSSION

Flagella-mediated motility is a widespread and effective form of active locomotion among bacteria. The flagellar motor is composed of two major structures, the rotating switch complex and the stator complexes [2,3,10]. General textbook knowledge suggests that these structures are static. Surprisingly, it has recently been demonstrated that subunits from the static and rotating part can be displaced while the flagellar motor continues to operate. Stator complexes within this stator ring system are constantly exchanged with a membrane-located pool of precomplexes that are activated upon incorporation into the motor [103,104,106,111]. This study aimed for elucidating the dynamics of the flagellar motor in *S. oneidensis* MR-1 under changing environmental conditions. To this end, the dynamic exchange of stator complexes and the flagellar performance was analysed at changing sodium chloride concentrations.

3.1 Flagellar : stator systems come at different ratios

Flagella, as an important motility organelle in bacteria, come at different flagellar- to stator systems ratios (see Table 6). *Salmonella typhimurium* for example harbours one stator system (MotAB) which interacts with the switch complex of a single flagellar system [71]. In contrast, species such as *V. alginolyticus*, *V. parahaemolyticus* , *S. putrefaciens* CN32 or *S. piezotolerans* possess more than one flagellar system with individual stator complexes [129]. In *Vibrio* species the two systems are used for movement under different conditions. In these species the polar flagellar system is driven by a sodium ion-gradient for swimming motility, whereas the lateral flagellar system is induced in addition to the polar flagellum for swarming or swimming in viscous media and uses protons for rotation of the filament [149,178]. In *S. piezotolerans* the two flagellar systems are differentially regulated by temperature and pressure. At low temperatures the lateral flagellar system is essential for motility, whereas the polar flagellar system is not. Accordingly, the primary polar system is upregulated under high pressure and downregulated under low temperature, while the secondary lateral system is regulated oppositely [129]. Unlike *Vibrio* species and *S. piezotolerans*, two flagellar systems contribute to swimming motility under nutrient-rich conditions in *S. putrefaciens* CN-32. Here, the sodium ion-dependent stator system is specific to the polar flagellar system, whereas the proton-dependent stator system belongs to the secondary flagellar system. It is proposed that expression of the two flagellar systems is linked [130].

Another way to adjust flagellar motor performance was observed in *Pseudomonas aeruginosa* PA01, *Bacillus subtilis* and *S. oneidensis* MR-1. In these organisms the number of stator systems exceeds the number of flagellar systems. *P. aeruginosa* harbours two stator systems, MotAB and MotCD, both are depending on the pmf. They are solely sufficient for swimming, but the MotCD-driven motor appears to outperform the MotAB-driven motor in liquid. However, MotAB and MotCD contribute differentially to swimming motility in highly viscous environments, to swarming and to biofilm formation [179-181]. Interestingly, for *B. subtilis* and *S. oneidensis* MR-1 two stator complexes depending on different coupling ions, protons and sodium ions, were detected. *B. subtilis* stator complexes MotAB (proton-driven) and MotPS (sodium ion-driven) are both linked to a single

peritrichous flagellar system. Here, MotAB is the dominant stator and MotPS contributes to motility in low viscous media and to biofilm formation, but not to swarming over surfaces [182]. In contrast to *B. subtilis,* my data for *S. oneidensis* suggest that the sodium ion-dependent PomAB and the proton-dependent MotAB stator complexes contribute to swimming motility in response to the sodium-ion concentration. Whereas a fraction of PomAB, the dominant stator complex, is always incorporated into the stator ring, MotAB localises in a sodium-ion dependent manner. The performed localisation studies and swimming speed assays strongly indicate that PomAB and MotAB coexist in the stator ring of *S. oneidensis* MR-1.

In order to improve the knowledge on how common multiple stators along with single flagellar systems are among bacteria, I conducted a genome-wide analysis. More than 30 % of the 400 examined species harbouring a single flagellar system were equipped with dual or multiple stator systems, suggesting a common phenomen among bacteria. For example, numerous *Pseudomonas* or *Bacillus* species display similarity regarding the number of detected stator systems. Both species harbour a dual stator system along with a single flagellar system, suggesting that the acquisition of the second stator was early event and is a common feature among this genus (Table 18). Supportively, both stator systems are optimised in terms of functionality. In *P. aeruginosa* both MotAB and MotCD are proton-dependent, but support motility in liquid and high viscous media, respectively. In contrast, *B. subtilis* changes the stators with respect to the sodium-ion concentration by either using a sodium-ion dependent or a proton-dependent one. Thus, I hypothesize that among those species the acquisition of a second set of stators was beneficial to adapt motility and was kept in the genome. In contrast, *P. stutzeri* acquired a third stator system, which was either recently integrated into the genome or integrated in an earlier process. It might also be possible that the other *Pseudomonas* species lost the third stator system. To analyse this, all identified stators should be compared among subspecies with respect to homology. The acquisition of a third would be suggested, if the two identified stators are a conserved feature among the subspecies, otherwise it would be possible that all *Pseudomonas* species had three stator complexes and lost individual ones during adaptation. However, within *Shewanella* species *S. oneidensis* recently acquired a MotAB stator system, likely in the process of adaptation to a fresh-water habitat. In contrast to *Pseudomonas* the MotAB system is still in an optimisation process as suggested by my analysis of the dual stator system. Whether the identified additional stator systems have evolved by gene duplication or horizontal gene transfer remains unanswered so far and needs additional investigations.

Flagella-mediated motility in the above described organisms demonstrates that modulation of motor performance is achieved by different strategies. In contrast to assembly of a complete new flagellar system as occurs e.g. in *V. alginolyticus* or *V. parahaemolyticus* [178,183-185], adjustment of the flagellar performance by multiple stator systems would represent a comparatively inexpensive way. In general I can think of two different possibilities for the composition of the stator ring: First, the incorporation of multiple stators is depending on the same coupling-ion and second, the simultaneous incorporation of multiple stators is depending on different coupling-ions. In *A. hydrophila* or *P. aeruginosa*, stators are depending on the same coupling ion and change the motor properties with regard to speed or performance under high load in elevated viscosity [179,186]. In *B. subtilis* and *S. oneidensis* MR-1 the same motor can interact with individual stator complexes using either protons or sodium-ions [182]. Switching the motor-driving coupling ion expands the range of flagellar function, which might contribute to the economic use of vanishing resources and increase the possibility to fine-tune flagellar motor performance. Thus, it is not surprisingly that dual or multiple stator systems are common among bacteria.

Table 6: Flagellar systems & stator systems come at different ratios. Summarised are the most important studies on species with dual or multiple stator systems.

species	flagellar system(s)	stator system(s)	energy source/ coupling ion*	ratio flagella:stator	function	reference
Aeromonas hydrophila	single polar flagellum	PomAB	smf	2:3	PomAB: swimming, swarming	[187]
		$PomA_2B_2$	smf		$PomA_2B_2$: swimming at low sodium (?)	[188]
					biofilm formation (?)	
	lateral flagella	MotAB/LafTU	pmf		LafTU: swimming, swarming	[181]
Pseudomonas aeruginosa PA01	single polar flagellum	MotAB (PA4954 / 4953)	pmf	1:2	both: swimming, swarming, biofilm formation	[179,180,189]
		MotCD (PA1460 / 1461)	pmf		MotAB: swimming in liquid	
					MotCD: swimming at elevated viscosity, swarming	
Bdellovibrio bacteriovorus	single polar flagellum	MotAB1 (Bd0144/0145)	pmf	1:3	Each individual MotAB is sufficient for motility inside the bdelloplast and during host-independent growth.	[190]
		MotAB2 (Bd3020/3019)	pmf			
		MotAB3 (Bd3254/3253))	pmf			
Bacillus subtilis	peritrichous flagella	MotAB (BSU13690/13680)	pmf	1:2	MotAB: swimming, swarming	[182]
		MotPS (BSU29730/29720)	smf		MotPS: swimming at elevated viscosity, pH and Na^+ concentrations,	
					biofilm formation	
Shewanella oneidensis MR-1	single polar flagellum	MotAB (SO4287 / 4286)	pmf	1:2	PomAB: swimming	[128]
		PomAB (SO1529 /1530)	smf		MotAB: swimming at low Na^+ concentration	
					both: biofilm formation	

* pmf, proton-motive force; smf, sodium-ion motive force.

3.2 Long term adaptation to a fresh-water environment

3.2.1 A dual stator system - the acquisition of MotAB

Although most of the *Shewanella* species were isolated from marine habitats, *S. oneidensis* MR-1 originates from a fresh-water environment, sediments in the Lake Oneida [117]. In 1835 the Erie Canal System was opened, now connecting the Sargasso Sea with the Lake Oneida, and with that a marine habitat with a fresh-water environment. There is no direct proof that *S. oneidensis* MR-1 is of marine origin, however, the closest relatives *S. sp.* MR-4 and *S. sp.* MR-7 were isolated from the Sargasso Sea [191]. Moreover, the idea that *S. oneidensis* MR-1 recently entered a fresh-water environment, is supported by the relatively high concentration of 100 to 300 mM sodium chloride required for optimal growth (marine 500 mM, fresh-water max. 35 mM NaCl) [145]. In order to drive flagellar rotation *S. oneidensis* can use the sodium ion-dependent PomAB and the proton-dependent MotAB stator complexes [128]. Bioinformatic analysis conducted in this study revealed a lower GC content of the *motAB* gene cluster compared to the overall genome, suggesting an uptake of 'foreign' DNA. Natural competence would facilitate the acquisition of 'foreign' genes, however, it has not been shown for *S. oneidensis* under *in vitro* conditions. [192]. In the phylogenetic analysis PomAB was identified to cluster with stators of other *Shewanella* species. In contrast, the closest homolog to MotAB was found in an *Aeromonas* species isolated in a fresh-water habitat [128]. Taken together, the bioinformatic data in this study suggest that the MotAB stator system has been acquired by horizontal gene transfer from *Aeromonas* species in the process of adaptation to a fresh-water habitat. Notably, the 'foreign' origin of MotAB likely is not an exception within *S. oneidensis*. The same has been proposed e.g. for the acquisition of SO_4444, a response regulator, now integrated into the existing regulatory network of *S. oneidensis* MR-1 and for two Na^+/H^+ Antiporter [193].

In general, incorporation of 'foreign' genes does not necessarily result in a functional system. The production and association of a 'foreign' stator unit into the stator ring might disrupt the effectively coordinated interaction between stator and switch complex. The acquisition of MotAB in *S. oneidensis* would even require a switch of the used coupling-ion. Interestingly, this evolutionary process was recreated in *E. coli* and *Vibrio* by constructing functional artificial stator complexes. A recent study revealed that MotAB from *E. coli* can drive the polar flagellum of *V. alginolyticus* or *V. cholera* using the pmf instead of the smf [99,100]. Moreover, a chimeric complex of PomB together with a segment of MotB converts a sodium-ion dependent motor into a proton-driven one [100]. Although the exact mechanism of motor adjustment is not known, the idea that the two different types of motors show similar mechanisms of torque generation, in concert with the finding that in 30 % of the species the number of stators exceeds the number of flagellar systems, indicate that dual or even multiple stator complexes coexist and modulate motor performance. A functional incorporation of a 'foreign' additional stator system into an existing flagellar system might provide fundamental advantages for entering a new habitat.

3.2.2 A dual stator system – dynamic stator swapping

The existence of dual or multiple stator systems along with one flagellar system raises several questions: How are the correct stators selected and recruited? Do the cells use a fixed stator-rotor configuration according to the environmental conditions or can different stator complexes work together in a single motor? Does the flagellar motor respond to environmental changes by swapping stator units?

The flagellar motor is a highly dynamic multiprotein complex regulated by external and internal signals and it has recently been demonstrated that subunits from the static and rotating part can be exchanged while the motor continues to operate [110]. The latter relies on the finding of a rapid exchange and turnover of MotB-Gfp in *E. coli,* which suggests a rapid assembly and disassembly in the stator ring [104,108]. This concept is in strong agreement with the data for the dual stator system in *S. oneidensis* obtained in this work. It is suggested that the stator ring composition in *S. oneidensis* is adjusted according to the environmental sodium-ion conditions by modulating the number of incorporated PomAB and MotAB stator complexes.

Motility assays and inhibitor studies with phenamil and CCCP have shown that both, PomAB and MotAB are individually sufficient to drive flagellar rotation in *S. oneidensis*. Furthermore the conducted localisation studies revealed that the sodium ion-driven PomAB complex is incorporated into the stator ring according to the availability of sodium ions (Figure 31; 2). The presence and abundance of PomAB affects the efficient incorporation of the proton-driven MotAB stator (Figure 31; 1). Localisation studies, tethered cell assays, and swimming speed assays suggested that under low sodium ion conditions both, PomAB and MotAB are incorporated into the stator ring, likely forming a hybrid motor (Figure 31; 3). In addition, single molecule studies with sfGfp fused to PomB suggest that at least nine PomAB complexes are associated with the stator ring in wild-type motors and that their number decreases with decreasing sodium ion concentration. I further propose that functional association of MotAB occurs in a cooperative fashion. Collectively, these data lead to novel view of motor adjustment to the environmental sodium-ion concentration by using dual stator complexes. A major question arising from the working model is: How would stator selection occur in such a system?

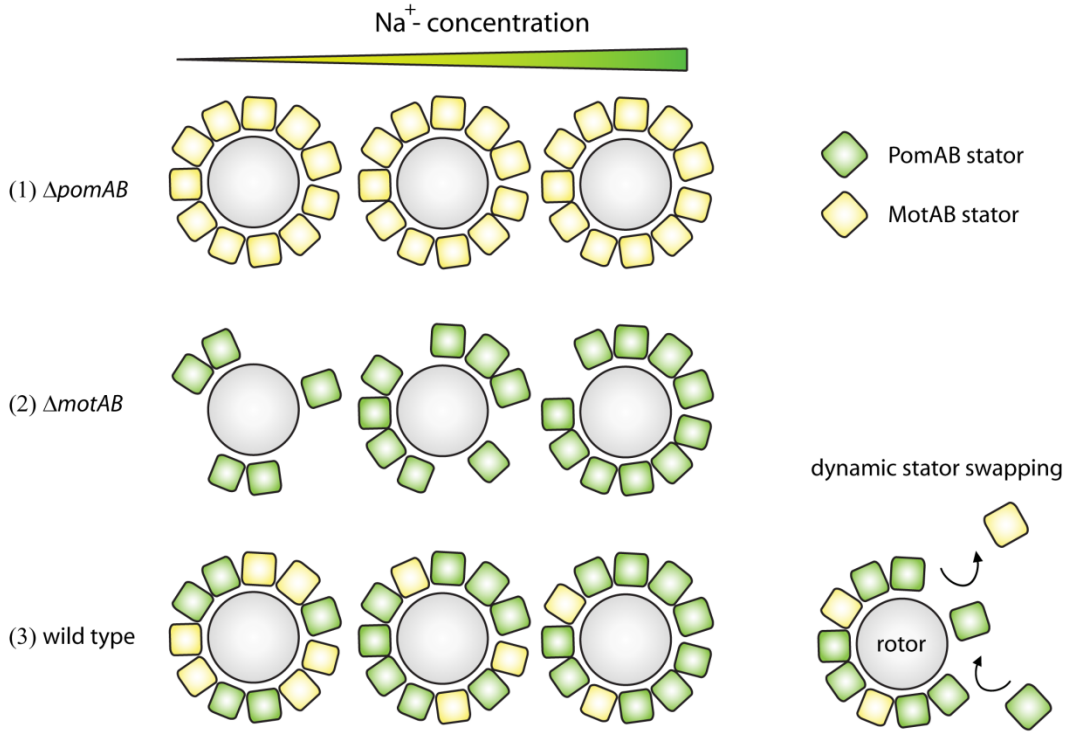

Figure 31: Current working model: A dynamic hybrid flagellar motor operates in *S. oneidensis* MR-1 to rapidly adapt to environmental changes. Recent work demonstrated that the stator complexes are rapidly exchanged within the stator ring [104,108,109]. The obtained data for the dual stator system in *S. oneidensis* suggest that the localisation of PomAB is dependent on the sodium ion concentration, whereas MotAB localisation is regulated with respect to the presence and abundance of incorporated PomAB. **(1)** MotAB localizes at low and high sodium ion concentrations at the flagellated pole in the absence of PomAB. **(2)** PomAB localizes in a sodium-ion dependent manner. With decreasing sodium-ion concentration the number of incorporated PomAB stator complexes decreases. **(3)** Stators associate and dissociate in a dynamic manner (dynamic stator 'swapping'). Collectively, the conducted localisation studies propose that under low sodium the number of incorporated PomAB stator complexes drops, to increase the incorporation efficiency of MotAB stator complexes. At low sodium-ion concentration, PomAB and MotAB are thought to coexist in the stator ring, forming a hybrid motor.

STATOR SELECTION

Stator units are diffusing as inactive precomplexes in the membrane and are activated upon incorporation into the stator ring, likely by a conformational change resulting in tight binding to the PG-layer [103,106,194]. Stator and even rotor subunits of the motor can be exchanged while the flagellar motor continues to operate, indicating that the flagellar motor is highly dynamic and can be tuned according to specific environmental conditions (Figure 32); [104,106,111].

There are two major possibilities how stator selection might be modulated: (1) by the abundance of the stator units, e.g. by altered protein or transcription levels, and (2) by the efficiency of stator localisation and incorporation into the stator ring. Higher transcription levels have been observed for the MotPS stator units in *B. subtilis,* caused by a mutation of a transcriptional terminator sequence between *ccpA* and *motPS* resulting in a readthrough and elevated transcriptional levels [195]. In contrast, as demonstrated in this work, in *S. oneidensis pomAB* and *motAB* are constitutively transcribed and the corresponding proteins are simultaneously present in the cell at similar levels. Hence, stator selection in *S. oneidensis* MR-1 is regulated at the level of efficiency of stator incorporation. In accordance with this model, fluorescence microscopy analysis performed in this study revealed that at high sodium ion concentration PomB-mCherry prevents the localisation of

MotB-mCherry to the flagellated pole and leads to a diffuse membrane localisation of inactive MotB-mCherry stator precomplexes. Under low sodium-ion conditions both PomB-mCherry and MotB-mCherry predominantly have polar foci, indicating the coexistence of PomB and MotB in the single flagellar motor of *S. oneidensis* MR-1 (Figure 32). The dynamic localisation pattern of MotB-mCherry is altered in a Δ*pomAB* strain. In the absence of PomAB, MotB-mCherry is always recruited to the flagellated pole. In addition, production of PomAB replaces polar MotB-mCherry in the motor and confines this stator to the membrane. By quantifying polar sfGfp-PomB molecules it became clear that the abundance of PomAB in the motor drops with decreasing sodium ion concentration, which allows a more efficient incorporation of MotAB. Thus, it appears that the incorporation efficiency of PomAB is directly altered in response to the sodium ion conditions, whereas MotAB recruitment depends on the abundance of PomAB in the stator ring. However, with the data obtained it cannot be excluded that incorporation efficiency of MotAB increases with lower sodium-ion concentration. A higher level of incorporated MotAB might also be a consequence of elevated turnover of PomAB due to decreased incorporation efficiency. This is supported by the observation of sfGfp-PomB bundles in the cytoplasmic membrane that might be moving faster under low sodium ion-conditions. This data corroborates the model of dynamic stator swapping according to the environmental conditions. Additionally, this suggests that the rotor-stator configuration allows a concurrent recruitment of PomAB and MotAB under appropriate conditions.

As suggested by the phylogenetic data, *S. oneidensis* acquired a second stator system likely by lateral gene transfer. Recent biophysical characterisation of PomAB and MotAB revealed that sodium-ion driven motors are rotating faster than proton-driven ones [79,84]. Thus, it is expected that the ratio of PomAB and MotAB increases or decreases the swimming speed in *S. oneidensis*. Accordingly, the performed physiological studies, the swimming speed measurements and the tethered cell analysis, revealed that under low sodium-ion conditions the wild-type motor with PomAB and MotAB significantly outperforms PomAB-only-driven cells. Although there was no significant difference in rotation speed between wild-type and PomAB-only driven motors at high sodium-ion concentrations, the swimming diameter observed under high salt on LB soft agar plates was slightly decreased in wild-type cells. This suggests that even at high sodium-ion concentration MotAB is incorporated in wild-type motors and slows down motor rotation. Notably, elevated levels of MotAB significantly decreased the swimming diameter on soft agar plates, but did not restore motility in a Δ*pomAB* background. Although MotAB was not able to restore rotation of a tethered cell in a strain lacking PomAB, a subpopulation of cells driven by MotAB-only was able to swim in liquid culture, thus indicating that MotAB is functional associated into the stator ring. Furthermore, the accomplished rotation speed measurements with tethered cells indicated a stepwise decrease of speed after expression of *motAB*. This indicates that MotAB is incorporated into the stator ring in the presence of PomAB and therefore slows down motor rotation. Although the stepwise decrease of rotation speed does not show the functionality of MotAB, it implies an incorporation into the PomAB-driven motor and strongly suggests the existence of a hybrid motor in *S. oneidensis*. Given the fact that MotAB production cannot resurrect rotation in a stator deletion strain, but MotAB production in a PomAB-driven motor slows down rotation speed in tethered cells, it is likely that MotAB incorporation into the stator ring benefits from the presence of PomAB. I recently isolated a genetically fixed Δ*pomAB* 'upmotile' mutant, characterised by an elevated number of swimming cells and an increased swimming diameter on soft agar plates. I propose that MotAB is generally functional in *S. oneidensis*, however, the 'upmotile' phenotype might be caused by a more efficient stator incorporation or an optimised alignment into the stator ring in this mutant.

Such 'upmotile' phenotypes have been described in diverse species, e.g. in *Bacillus* [182,195,196]. In *B. subtilis* a single flagellar motor is driven by two different stator complexes, coupled to different ion fluxes, sodium ions (MotPS) and protons (MotAB). The proton-dependent MotAB stator is the dominant system and disruption of MotAB leads to decreased motility. However, an 'upmotile' variant driven by MotPS was isolated and sequencing revealed a stem loop mutation between *cpA* and *motPS*, causing an increased transcription and production of the MotPS stator and an elevated number of flagella and basal bodies [195,196]. Thus, elevated motility in *B. subtilis* is either attributed to a higher abundance of the stators in the stator ring, caused by an increased transcription or production of MotPS, or to an elevated number of flagella or basal bodies. However, neither of the cases was true for *S. oneidensis* MR-1 'upmotile' mutants. Here, the protein level was not significantly altered (data not shown) and filament staining revealed a single polar flagellum only. The MotB stator subunit contains a short C-terminal cytoplasmic region, a transmembrane domain and an N-terminal periplasmic region [57,197,198]. The C-terminal part of MotB anchors the stator to the cell wall by a conserved PG-binding motive [61,199,200]. The first periplasmic alpha helix (Pro52 to Pro65 in *E. coli*) forms the so called 'plug', which interferes with $MotA_4B_2$ channel formation and is hypothesized to control the proton flow in the MotAB stator. It is thought that upon incorporation and anchoring to the PG-layer, the periplasmic region of MotB changes conformation and opens the proton channel to drive flagellar rotation [105]. Deletion of the 'plug' region or substitution of flanking amino acids in MotB of *E. coli*, and deletion of the 'plug' region of PomB in *V. alginolyticus* led to a growth defect, but did not inhibit motility [105,201]. Sequencing of the *S. oneidensis* upmotile mutant identified a substitution in the C-terminal periplasmic linker region of MotB (S56P). The substituted S56P is located in those periplasmic alpha helix, forming the 'plug' as predicted by PSIPRED [202]. As I could not detect an obvious growth defect in *S. oneidensis* Δ*pomAB* 'upmotile', it can be suggested that the ion-channel is not constantly unplugged due to the mutation. However, this substitution might facilitate PG-binding and conformational changes. Little is known about stator association into the motor, but it is thought that a linker, connecting the TM helix of MotB and the PG-binding domain, extends and interacts with the PG-layer and a part of FlgI [66,203]. This interaction might cause a twist in the linker region and therefore opens the ion channel of the stator complexes [204,205]. The substituted residue might affect stator assembly by optimising the linker region and therefore increasing the incorporation efficiency or the mounting to the PG-layer. The positive effect for motility of this mutation was verified by a targeted Δ*pomAB* S56P mutant (Volker Berndt). Although it cannot be proven that MotAB is functional incorporated, those results indicate that MotAB influences motor performance in *S. oneidensis* MR-1. As this bacterium is thought to be caught in the process of adaptation from a marine to a fresh-water environment, it can be assumed that a proton-driven motor expands motility and is still in the process of functional optimisation.

RECRUITMENT

To date, the mechanism for the dynamic recruitment of stator complexes is not understood. However, the basic mechanisms for torque generation are thought to be the same for both coupling-ions as demonstrated by biophysical characterisation of sodium ion-driven chimeric flagellar motors in *E. coli* [206]. It is conceivable that recruitment of the stators into the stator ring might be facilitated by the flux or the binding of the corresponding coupling ions, by the A- or B-subunits itself or specific charged residues within the subunits, or even by additional supporting proteins (Figure 32).

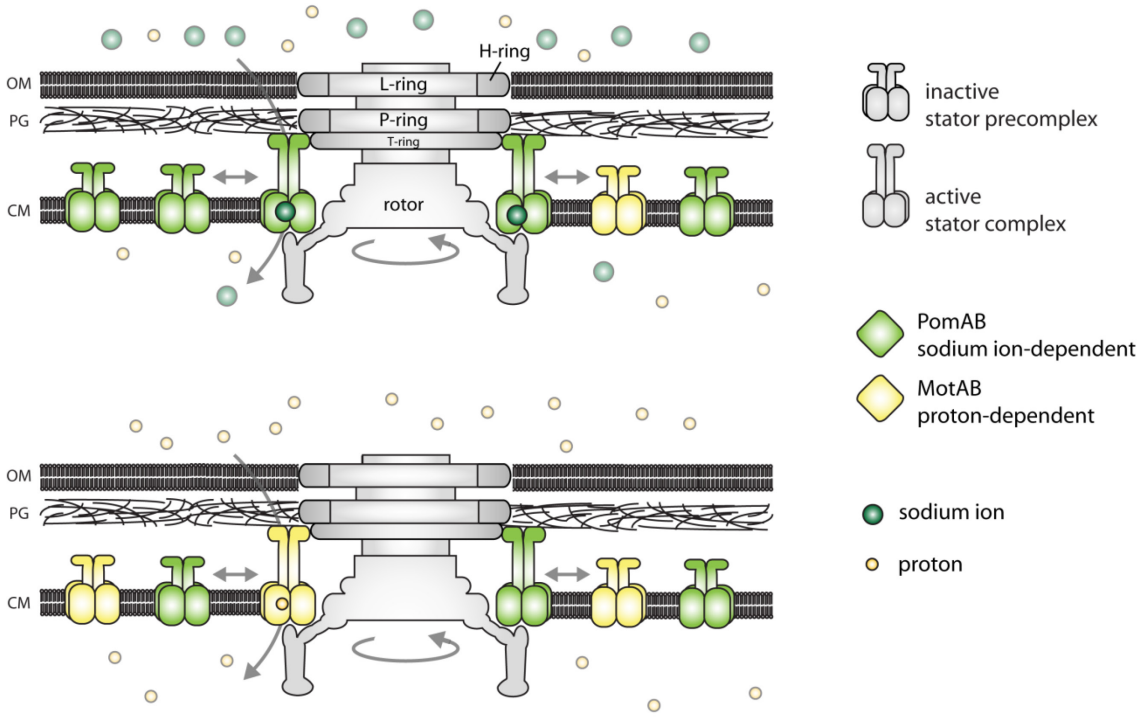

Figure 32: Regulation of stator selection in *S. oneidensis*. Additional structures in *S. oneidensis* are the H-ring (FlgT) and the T-ring (MotXY) MotXY are important for PomAB and MotAB motor function, but not for recruitment of the stator complexes in *S. oneidensis*. FlgT was identified by sequence homology only. PomAB and MotAB stators are diffusing as inactive stator precomplexes in the membrane before they get recruited and activated in the stator ring. For *S. oneidensis* it is proposed that stators are selected with respect to the environmental sodium-ion concentration. I speculate that recruitment of PomAB stators in *S. oneidensis* is facilitated by ion-binding to the specific aspartate in the B-subunit of the stator complex as hypothesized for *V. parahaemolyticus*. With decreasing sodium-ion concentrations the efficiency of PomAB incorporation drops and MotAB is recruited. OM, outer membrane; PG peptidoglycan layer, CM, cytoplasmic membrane.

A scenario underlining the concept on stator dynamics and incorporation in response to environmental sodium-ion concentration was described for *V. alginolyticus* [109]. Here, rotation of a polar flagellum is achieved by sodium ion-dependent PomAB stator complexes. PomAB stator assembly and disassembly into and from the stator ring strongly depends on the availability of the driving ion and the smf. Fukuoka *et al.* demonstrated that at high sodium-ion concentration more than 80 % of the cells display polar foci [109]. Polar localisation was rapidly lost in the absence of sodium chloride. PomAB was recruited immediately after addition of sodium ions. By substituting the critical Asp24 residue in PomB it was shown that sodium-ion binding to Asp24 is critical for efficient incorporation [15,204]. Similarly, as shown by quantification of single sfGfp-PomB molecules in *S. oneidensis* MR-1, the number of sfGfp-PomB dropped under low sodium-ion conditions. In contrast to *Vibrio*, PomAB of *S. oneidensis* is incorporated into the stator ring even at low sodium chloride concentration. Recruitment of MotAB is attributed to the presence of PomAB. Whereas PomAB stator recruitment in *V. alginolyticus* and likely also in *S. oneidensis* depends on the smf or the binding of a sodium-ion to the specific Asp24, MotAB in *E. coli* has been described to assemble independently of proton-binding to the corresponding specific Asp32 [207]. In *E. coli* neither substitutions of specific residues, disruption of the proton flow, nor depletion of the proton motive force affected the recruitment of MotAB into the motor [207], suggesting that

proton translocation is not required for stator engagement. However, as shown by localisation studies, two conserved charged residues in the cytoplasmic loop of MotA, Arg90 and Arg98, were crucial for the recruitment of the MotAB stator complex [207]. Indicating that the electrostatic interactions between FliG and MotA are not only required for torque generation, but rather for efficient assembly of MotAB around the rotor [97]. Whether or not the corresponding residues in PomA are critical for recruitment has not been tested to date, however, ion flux through and ion-binding to PomB plays a major role for incorporation of the sodium ion-dependent PomAB stator. Hence, the recruitment of PomAB and MotAB might be regulated by individual mechanisms. During previous work in our group, non-functional stator hybrids consisting of MotA/PomB-mCherry and PomA/MotB-mCherry were constructed [153]. PomB-mCherry together with MotA localised polarly, in contrast, MotB-mCherry in the presence of PomA did not [153]; (appendix Figure 34). On the one hand this might imply that the interaction of MotA-FliG recruited MotA/PomB-mCherry to the pole, on the other hand this could also mean that MotA/PomB-mCherry was engaged into the motor because of ion-binding in PomB-mCherry. To further determine whether or not the charged residues in the cytoplasmic loop of the A-subunits or the conserved Asp-residue are responsible for recruitment, the corresponding residues need to be substituted. Subsequent localisation at high and low sodium-ion concentrations should reveal which residues are important for PomAB and MotAB stator ring association in *S. oneidensis* MR-1. Although the exact mechanism for recruitment of the stators is not fully understood, tight and functional incorporation of the torque-generating units is caused by a conformational change in the periplasmic region of the B-subunits, unplugging and anchoring the stators to the cell wall [66,103,105,203]. Thus, both stators need an ion flux and ion-binding for activity. Generally, correct positioning of the stators towards the rotor in this dynamic machinery requires a high level of coordination in order to generate torque. Regarding the high rotation speed in sodium ion-dependent motors for instance, it would not be unexpected if additional proteins are supporting recruitment and tight association into the motor.

Auxiliary species-specific proteins, MotX and/or MotY, play an important role for flagellar function but not for filament assembly in some flagellar motors, suggesting a key function for stator or rotor components [63-65,156,179,208]. In *Vibrio* species MotX and MotY form an additional ring structure, the T-ring, at the basal body [11]. The N-terminal region of MotY is essential for association to the basal body and MotX, whereas the C-terminal region harbouring a PG-binding domain, stabilises the complex by binding to the PG-layer. MotX interacts with PomB and MotY (Figure 32); [66]. Moreover, it was proposed for *Vibrio* that MotX and MotY form a complex and diffuse through the periplasmic space before they interact with the basal body [209]. In *S. oneidensis* MR-1, homologous proteins to MotX and MotY have been identified [150]. Accordingly, MotX association to the motor required MotY, while MotY localised to the flagellated pole independently of MotX. Additionally, the polar localisation of MotX and MotY occurred independently of the stator complexes [156]. In contrast to the proposed model in *Vibrio*, the localisation studies performed in this work for *S. oneidensis* suggest that MotX and MotY do not form a periplasmic complex before they become associated with the basal body. MotY-mCherry localises independently of MotX to the flagellated pole, whereas MotX-mCherry localisation requires MotY. Thus, I hypothesize that MotY interacts with the basal body and subsequently recruits MotX. In *V. alginolyticus* and *V. parahaemolyticus* the T-ring is required for recruitment of the stator complexes [14,15,94]. It was further suggested that MotX and MotY are involved in incorporation and stabilisation of the PomAB complex [11]. In contrast the data obtained for *Vibrio*, my fluorescence microscopy data demonstrate that MotX and MotY in *S. oneidensis* MR-1 are

not crucial for recruitment of the stator complexes to the flagellated pole. However, at high sodium ion concentration MotAB localisation to the flagellated pole was slightly increased in the absence of MotXY, indicating that PomAB does not localise as effective in the absence of MotXY. In summary, MotX and MotY are not essential for the recruitment of PomAB and MotAB but strictly required for functionality in *S. oneidensis*.

Although the proton-driven MotAB in *E. coli* and *Salmonella* are not dependent on ancillary proteins, MotX and MotY are not exclusive factors of sodium-ion dependent flagellar motors. In *S. oneidensis*, as shown in this work, and in *V. parahaemolyticus*, MotXY and LafY (a MotY homolog) are involved in proton-dependent flagellar rotation [67,156]. It is suggested that the requirement of MotX and MotY arises from the periplasmic domain of the B-subunits. An *E. coli* MotAB stator complex drives flagellar rotation in a proton-dependent manner in *V. alginolyticus* and *V. cholerae* lacking PomAB and MotXY. Additionally, chimeras with PomA and a fusion of the C-terminal region of PomB to the N-terminal periplasmic part of MotB, is functional in the absence of MotXY in *E. coli* and *V. alginolyticus* [2,96,99,100]. On the other hand, the abolished motility in the absence of MotXY, as found for *S. oneidensis* in this work, together with the observation that MotAB of *E. coli* is functional in *V. cholera*, suggest that the presence of MotXY is not hindering functionality of the proton-dependent stator complex and might be required for functionality as well, for example by correct positioning of the stators [100].

Notably, analysis of the direction of rotation in tethered *S. oneidensis* cells revealed a shift towards CCW direction at low sodium ion concentrations for wild-type in comparison to *ΔmotAB* cells. According to the current working model, at low sodium ion concentration MotAB stators are incorporated into the stator ring. In contrast, the flagellar motor of *ΔmotAB* cells is driven by the remaining PomAB stators, suggesting that the direction of rotation is caused by the interaction of MotAB with the switch complex. Both strains had a wild-type phenotype with respect to chemotaxis. The molecular mechanism for switching is widely discussed and highly complex. To date, it is thought that switching induces a tilting of the FliM middle domain and by that therefore reorientates FliG, the stator-rotor interaction site. This causes the electrostatic interaction sites to be reversed [210,211]. Flagellar rotation is achieved by an electrostatic interaction of the stator A-subunit with charged residues of FliG and it is likely that the A-subunit pushes against FliG to support rotation [52,61,94]. FliG subunits are arranged in a wheel-like structure, with the electrostatic interaction sites exposed to the A-subunits of the stators [210]. Improper alignment of the MotAB stators relatively to the motor-switch complex, especially to the electrostatic interaction sites, might explain this observed shift in direction of rotation. Although MotX and MotY cannot explain the switch in direction of rotation, they support the hypothesis that proper alignment in the stator ring towards the switch complex is essential not only for functionality. MotXY likely generate a more robust structure allowing a rapid dynamic exchange of stator units during flagellar rotation.

STATOR RING DYNAMICS

According to the current working model presented in this study the stator ring composition in *S. oneidensis* is modified in response to environmental sodium ion concentrations. The obtained data for the distribution of sfGFP-PomB at high sodium ion concentration suggest the existence of two subpopulations, one with 6.8 ± 0.2 and one with 11.7 ± 0.6 stators associated, whereas the median number revealed 9.4 stators. Thus, there are two possible major scenarios for the stator ring

occupation in *S. oneidensis* MR-1: (1) the maximal number of incorporated stators, PomAB and/or MotAB is nine; (2) the maximal number exceeds nine stator complexes. The reported stator dynamic and rapid turnover promotes the second scenario. Two subpopulations with 6.8 and 11.7 stators might be explained by different stator ring occupancies and heterogeneity. The structural core of the flagellar motor is conserved among species, however, divergent structures and symmetries of proteins surrounding the rotor, e.g. stator complexes, have been reported [9]. Chen and co-workers observed stator symmetries of 13 and 16 copies for *H. gracilis* and the spirochaete *B. burgdorferi*, respectively. TIRF microscopy on fluorescently labelled *E. coli* MotB stators revealed 11 copies, which is in accordance with freeze-fracturing electron microscopy results [5,104]. Thus, the hypothesized stator number of at least nine stators is in the expected range. Furthermore, the conducted resurrection experiments of MotAB in a PomAB-driven motor of *S. oneidensis* agree with the hypothesis of Blair and Berg that the stator ring is not necessarily fully occupied under wild type expression levels of stator complexes [107]. In *E. coli* the rotation speed was about 20 % increased when MotAB was ectopically produced in comparison to that of the wild type. Supportively, freeze-fracturing experiments displaying the symmetry of stators in *E. coli* indicate vacant spots in the stator ring [5]. For *S. oneidensis* I observed a decreased swimming diameter on soft agar plates in addition to a step-wise decrease of rotation speed in tethered cells upon production of MotAB in a PomAB-driven motor. Biophysical characterisation of PomAB and MotAB revealed that in general sodium-ion driven motors rotate faster than proton-driven ones [84]. My obtained data for the resurrection of MotAB in a PomAB-driven motor of *S. oneidensis,* indicate a decrease in rotation speed. These results indicate that upon production of MotAB, vacant spots in the stator ring are occupied and therefore rotation speed is slowed down. However, to validate that the stator ring is not fully occupied either PomAB should be overproduced in a Δ*pomAB* background to determine potential speed increments or the native PomAB and MotAB levels should be quantified and rotation speed under elevated and wild-type levels should be compared. The current working model proposes that the number of PomAB stators determine the number of incorporated MotAB. The question how MotAB is distributed under high sodium ion conditions in the presence of PomAB is in the focus of a future project in our working group. A dual labelling with different fluorophores (e.g. mCherry-MotB and sfGfp-PomB) will facilitate the direct analysis of the stator number at different sodium ion concentrations. In addition, combining fluorescent microscopy with rotation speed measurements of a tethered cell at the single cell level will give direct insights into the composition of the stator ring and reveal whether MotAB is functionally incorporated or not. Furthermore, the determination of the number of units in a stator ring consisting of PomAB or MotAB only in the corresponding deletion backgrounds might reveal a discrete number for the occupancy of the stator ring and reveal whether the number of incorporated MotAB stators is variable at different sodium-ion concentrations in the absence of PomAB.

3.3 Motor performance at the single cell level – two assays

The physiological and localisation studies on *S. oneidensis* MR-1 performed in this work provide evidence that the flagellar motor configuration is modified according to environmental sodium-ion concentrations by an exchange of stator units. The obtained data suggest that at low sodium-ion concentration two different stator complexes simultaneously drive the flagellar motor. Functionality of both stator complexes has been verified in a swimming speed assay. Thus, the single polar flagellum is likely powered by a hybrid motor, concurrently using sodium ions and protons.

To demonstrate this novel kind of motor tuning, the composition and rotation speed of the flagellar filament had to be determined at the single cell level with changing sodium chloride concentrations. The two major approaches to study flagellar performance at the single cell level are: The bead assay, in which cells are irreversible attached to a microscope coverslip and a polystyrene bead is attached to the filament and used as a marker for rotation [78]. The second approach is the tethered cell assay, in which cells are tethered by their filament and the cell body rotation is measured [70]. These approaches have been successfully established for *E. coli* and *R. sphaeroides* [18,78] but not for a polarly flagellated species so far. At this point it is to add that beads have been attached to the sheathed polar filament of *V. alginolyticus*, however, it was not possible to perform long term studies as the cell body was not firmly attached to the surface [74]. The establishment of the two assays for *S. oneidensis* encountered several obstacles. Therefore, the initial aim of this thesis to demonstrate a functional hybrid motor in *S. oneidensis* MR-1 was expanded and further included the establishment of an approach to study flagellar performance in a polarly flagellated species.

Significant effort was made to delocalise the polar flagellar filament in order to obtain reliable rotation data. This was successfully accomplished by deletion of *flhF*, a gene whose product has shown to play a role in flagella placement for *V. cholera*, *V. alginolyticus*, *P. aeruginosa* and *P. putida* [166-172]. Lack of the GTPase FlhF resulted in displacement of the polar flagella to a lateral position and drastically reduced the number of flagellated cells, while overproduction of FlhF leads to an increased number of polar flagella in *V. alginolyticus* [167,168]. In *S. oneidensis*, deletion of *flhF* resulted in displacement as well as in reduction of the number of flagellated cells. Thus, a suppressor mutant was isolated in which 10 % of the cells possessed delocalised filaments. The exact mechanism for placement of the flagella remains unknown to date. Based on studies of flagellar assembly, the first structure formed is the MS-ring, followed by the C-ring, the rod, other rings and finally late structures like the filament [10]. Once the basal body is formed FlgM is secreted and the transcription of genes encoding late structures starts. In *S. oneidensis* MR-1 *ΔflhF* FliN-Gfp localised in distinct foci, likely forming a part of the C-ring. Moreover, cells harbouring a flagellum were able to swim, although the diameter on soft agar plates was decreased, which is likely caused by an elevated drag of the cell body when the cell has to push itself in a lateral position. Since it is likely that the flagellar motor structure is not altered in these mutants, a major prerequisite for a functional assay was successfully accomplished. Additionally, beads were successfully attached to the delocalised filament and the cell body was irreversible stuck to a surface. Hence, prerequisites for the bead assay as well as for the tethered cell assay were fullfilled and both were successfully established within the framework of this thesis.

However, measuring flagellar rotation rates using the bead assay in *S. oneidensis* MR-1 indicated that the microorganism senses surface attachment, as flagellar rotation slowed down or even stopped, once the microorganisms attached to the coverslip. Interestingly, cells attached by their filament stub did not stop or slow down, suggesting that the cell body plays an important role in surface

sensing. This might be due to a control mechanism dependent on the "life style" of the cell slowing down or stopping motor function. Surface attachment as the first step in biofilm formation is a highly regulated process and it is thought that extracellular polymeric substances like proteins, polysaccharides, lipids and DNA as well as processes effecting flagellar regulation and performance play an important role [212-215]. A protein called EpsE has been found for *B. subtilis* and it is involved in controlling motor performance and biofilm formation [213]. Here, EpsE directly interacts with FliG and stops flagellar rotation, in a clutch-like mechanism [213,216,217]. A homolog of EpsE has been identified in *S. oneidensis* MR-1 (SO_3180, E-value 7E-13). However, in contrast to *B. subtilis eps* genes of *Shewanella* are not significantly regulated in the early biofilm stages, as indicated by microarray data of Julia Gödeke [213]. Corresponding deletions will show whether or not EpsE of *S. oneidensis* has a similar role as in *B. subtilis* and whether a Δ*epsE* strain might help in optimising the bead assay.

To conclude, two assays were established to measure flagellar rotation. So far, the bead assay is limited to short-term measurement, however, the tethered cell assay is now suitable as a basis to study flagellar motor performance in the polarly flagellated species *S. oneidensis* MR-1. The tethered cell assay was optimised in a way that now allows a constant exchange of buffer as well as the resurrection and modulation of motor function by chromosomal integration of *araC*-P_{BAD} cassette replacing the native promoter. The proposed dependency of PomAB incorporation on the sodium chloride concentration was reflected by a stepwise increase of rotation speed according to the sodium chloride concentration in the exchanged buffer. In accordance to resurrection experiments in *E. coli* [78], a stepwise increase of rotation speed was observed upon induction of PomAB in *S. oneidensis*. Furthermore, production of MotAB in a PomAB-driven motor indicated the incorporation and co-existence of both stator systems simultaneously. However, to verify that both stator complexes are simultaneously and functional incorporated, both stator complexes have to be characterised biophysically with respect to the rotation speed. Based on the swimming speed and tethered cell assays in addition to previous work with proton- or sodium ion dependent flagellar motors, the increments in speed are expected to be characteristically different for MotAB and PomAB. Therefore, it can be expected for *S. oneidensis* MR-1 that upon induction of either PomAB or MotAB the rotation speed will increase stepwise, depending on the number of stator units that are incorporated into the stator ring system. Additionally, the rotation speed of either MotAB or PomAB has to be measured to directly calculate the number of active stator units in the ring system under different ionic conditions. To further analyse how many proton- or sodium ion-driven stator complexes are incorporated into the motor, *motAB* should be expressed at low levels and *pomAB* at higher levels. Removal of sodium ions by buffer exchange will then result in a drop of the motor speed to a level that can be used to calculate how many active MotAB stator complexes are incorporated into the stator ring. Increasing the sodium-ion concentration should result in the stepwise speed increase characteristic for PomAB stator complexes incorporated into the stator ring. These rotation speed measurements of the flagellar filament will directly demonstrate whether a functional hybrid-motor, which concurrently uses protons and sodium ions, exists in nature.

4 MATERIAL AND METHODS

4.1 Materials

4.1.1 Reagents and Enzymes

Common reagents used in this studies were purchased from Bioline (Germany), Carl-Roth (Germany), GE Healthcare (Germany), Invitrogen (Germany), Merck (Germany), Millipore (Germany), Perkin Elmer (USA), Peqlab (USA), SIGMA-Aldrich (Germany), Thermo Scientific (USA) or Zymo Research Europe GmbH (Germany). Specific chemicals used in this thesis are described in the respective parts.

Enzymes required for the molecular manipulation and cloning of DNA were acquired from NewEngland Biolabs (NEB, USA), Fermentas (Canada) or Thermo Scientific (USA).

Size standards for DNA and proteins were obtained from NEB (USA) and Fermentas (Germany), respectively.

4.1.2 Buffers and solutions

Standard buffers and solutions were prepared according to Sambrook *et al.* [218]. When required, buffers and solutions were autoclaved (20 min at 121 °C) or filter sterilized (Sarstedt, Germany; pore size 0.22 µm). Specific buffers and solutions are described along with the respective method.

4.1.3 Media

Complex media used for growth of *E. coli* and *S. oneidensis* are listed in Table 7. Media were autoclaved for 21 min at 121°C and 2 bar, unless otherwise stated. Media additives are listed in Table 8 and Table 9. To solidify media 1.5 % (w/v) agar was added prior to autoclaving.

Table 7: Media.

media	component		reference
LB (**l**ysogeny **b**roth, Miller)	Tryptone Yeast Extract NaCl pH	10 g/l 5 g/l 10 g/l 7.0	[219]

media	component		reference
SOB (**s**uper **o**ptimal **b**roth)	Tryptone Yeast Extract $MgCl_2$ NaCl KCl pH	20 g/l 5 g/l 0.95 g/l 0.5 g/l 0.186 g/l 7.0	[220]
SOC (SOB with **c**atabolite repression)	SOB Glucose	 20 mM	[220]
LM (**L**actate **M**edium)	Yeast Extract Peptone HEPES NaCl Lactate (85 % (v/v) pH	0.2 g/l 0.1 g/l 10 mM 100 mM 15 mM 7.5	[128]
4M (**M**yers and **M**yers **M**inimal **M**edium)*	HEPES NaCl Lactate (85 % (v/v) NaOH [10 N] add sterile: K_2HPO_4 [1.27 mM] KH_2PO_4 [0.73 mM] $(NH_4)_2SO_4$ [10 mM] $MgSO_4$ x $7H_2O$ [100 mM] $CaCl_2$ x $2H_2O$ [50 mM] trace element solution [100x]	 25 mM 150 mM 40 mM 3 ml/l 10 ml/l 10 ml/l 10 ml/l 2 ml/l 1 ml/l 10 ml/l	[221]
trace element solution [100x]	Na_2EDTA x $2H_2O$ $MnSO_4$ $FeCl_2$ x $4H_2O$ $CoCl_2$ x $5H_2O$ $ZnSO_4$ $CuSO_4$ x $5H_2O$ H_3BO_3 Na_2MO_4 x $2H_2O$ $NiCl_2$ x $6H_2O$ Na_2SeO_4	6.72 mM 0.13 mM 0.54 mM 0.5 mM 0.1 mM 0.02 mM 5.66 mM 0.39 mM 0.5 mM 0.15 mM	[221]

* stock concentration is displayed in brackets []

Antibiotics were prepared as stock solutions and added to the media in the following concentration. If not otherwise stated the same final concentration was used for both, *E. coli* and *S. oneidensis* (Table 8).

Table 8: Antibiotics.

antibiotic	stock concentration	final concentration	solvent
Ampicillin-sodium salt	100 mg/ml	100 µg/ml	ddH_2O
Chloramphenicol	30 mg/ml	*E. coli* 30 µg/ml *S. oneidensis* 10 µg/ml	96 % (v/v) EtOH
Kanamycinsulfate	25 mg/ml	50 µg/ml	ddH_2O
Tetracyclinhydrochlorid	10 mg/ml	2.5 µg/ml	96 % (v/v) EtOH
Gentamycinsulfat	10 mg/ml	10 µg/ml	ddH_2O

Filter sterilized (Sarstedt, Germany; pore size 0.22 µm) additives are listed in Table 9.

Table 9: Additives.

other additives	stock concentration	final concentration	solvent
IPTG (isopropyl-beta-D-thiogalactopyranoside)	1 M	1 mM	ddH_2O
L-Arabinose	20 % (w/v)	0.2 % (w/v)	ddH_2O
DAP (Meso-diaminopimelic acid)	60 mM	300 µM	ddH_2O
Sucrose	80 % (w/v)	10 % (w/v)	ddH_2O
CCCP (carbonyl cyanide *M*-chlorophenyl hydrazone)		10 µM	DMSO
Phenamil sulphonamide		50 µM	DMSO

4.1.4 Kits

The *kits* used for this work are listed in Table 10.

Table 10: 'Kits'.

label and company	application
DNA Clean & Concentrator (Zymo Research, Germany)	DNA purification
Zymo Clean™ Gel DNA Recovery Kit (Zymo Research, Germany)	Isolation and purification of DNA from agarose gels
Zyppy™ Plasmid Miniprep Kit (Zymo Research, Germany)	Isolation and purification of plasmid DNA
Western Lightning™ Chemiluminescence Reagent Plus (Perkin Elmer, Germany)	Chemiluminescent reagent for HRP-dependent immunodetection
CDP-Star® Reagent (New England Biolabs, Germany)	Chemiluminescent reagent for HRP-dependent immunodetection
PCR DIG Probe Synthesis Kit (Roche, Germany)	Synthesis of DNA probes for Southern Blotting
DIG Nucleic Acid Detection Kit (Roche, Germany)	Hybridization and detection of DIG-labelled probes for Southern Blotting

4.1.5 Laboratory equipment and software

Standard equipment and software used during this work is listed in Table 11. Specific equipment and software is listed with the respective method.

Table 11: Equipment and software.

equipment or software	label and manufacturer
Agarose gel photochamber	2UV-Transilluminator (UVP, USA)
Fluorescence microscope	Axio Imager.M1 (Zeiss, Göttingen)
Bioanalyzer	Tecan infinite M200 (Tecan, Crailsheim)
PCR cycler	Mastercycler personal (Eppendorf, Hamburg) Mastercycler epgradient

pH meter	CyberScan 510 (USA)
Spectral photometer	Ultrospec 2100 pro (Amersham Biosciences, Germany) NanoDrop® ND-1000 (Peqlab, Germany)
Thermo mixer	Thermomix compact (Eppendorf, Hamburg)
Centrifuges	Sorvall RC 5B Plus (Kendro laboratory products, Germany) Multifuge 1 S-R (Heraeus, Germany) Biofuge fresco (Heraeus, Germany) Biofuge pico (Heraeus, Germany)
Electro power supply for electroporation	Consort Power Supply E835/E865 (Peqlab, Germany)
Electroblotter for western transfer	TE 77 ECL Semi Dry (Amersham Biosciences, Germany)
Imaging software	MetaMorph® 7.1.2 (Molecular Device; USA) Adobe® Illustrator® CS2 12.0.1 (Adobe Systems Software, Ireland) Adobe® Photoshop® CS2 9.0.2 (Adobe Systems Software, Ireland)
In silico cloning	Vector NTI Advance™ 11 (Invitrogen, Germany)
Biophysical analysis rotating cells and /or beads	MATLAB (MathWorks, USA), LabView (National Instruments, USA)
Statistical analysis	Origin 6.1 (OriginLab, USA)

4.1.6 Oligonucleotides and plasmids

Oligonucleotides were designed using OligoCalc [222] and generated by SIGMA-Aldrich (Germany). Vector NTI Advance™ 11 (Invitrogen, Germany) was used for *in silico* plasmid construction. A complete list for the synthesised oligonucleotides can be found in Table 21. Plasmids used in this study are summarised in the appendix (Table 20).

4.1.7 Strains

S. oneidensis MR-1 was used as the wild-type strain during this work [117]. The host strains for molecular cloning were *E. coli* DH5αλpir [223] and *E. coli* WM 3064 (W. Metcalf, University of Illinois,USA). A list summarizing all strains used and constructed during this work can be found in the appendix (Table 19).

4.2 Microbiological and cell biological methods

4.2.1 Cultivation of *E. coli*

E. coli strains were grown aerobically in LB medium at 37 °C overnight. Liquid cultures were incubated in a shaker at 210 rpm. When necessary, liquid media were solidified using 1.5 % (w/v) agar and supplemented with the respective antibiotics/additives (Table 8 and Table 9).

4.2.2 Cultivation of *S. oneidensis* MR-1

S. oneidensis strains were cultivated aerobically at 30 °C in LB, LM, and 4M in a shaking culture (210 rpm). For growth on solid media 1.5 % (w/v) agar was added. Media were supplemented with the listed additives and antibiotics when necessary (Table 8 and Table 9). Before inoculation in liquid media from a frozen stock, *S. oneidensis* strains were streaked on LB 1.5 % (w/v) agar plates, with the respective antibiotics.

Optical density of bacterial cultures was measured in a spectral photometer at 600 nm (OD_{600}).

4.2.3 Storage of bacteria

For long-term storage in the strain collection, strains were grown to mid log phase and supplemented with DMSO to a final concentration of 10 % (v/v) and stored at -80 °C.

4.2.4 Motility assays

Motility of different *S. oneidensis* mutants was analysed either on soft agar plates or in a tunnel slide (see section 4.6.1). For screening on soft agar plates precultures were grown over night in the appropriate media (LM or LB) supplemented with the respective antibiotics and additives. Motility screening was carried out by spotting 3 µl of liquid culture on LM or LB soft agar plates containing 0.25 % (w/v) agar and when necessary additives. Strains directly compared were spotted on the same plate and incubated over night at 30 °C. Note that the used soft agar plates are commonly referred as 'swarming plates', however, the actual motility monitored for *S. oneidensis* is flagella-mediated swimming motility.

Enrichment of Δ*pomAB* and Δ*flhF* was carried out by restreaking cells from edges of elevated motility on fresh soft agar plates.

4.2.5 Filament isolation

The protocol for the purification of intact flagella was modified after De Pamphilis and Schirm [40,224]. Motile *S. oneidensis* pili deletion mutants, (Δ*pilM-Q* Δ*mshA*) were enriched on soft agar

plates and inoculated in 40 ml LB over night at 30 °C. Cells were harvested by centrifugation at 4,500 rpm for 30 min and resupended in 8 ml TBS buffer. The resulting pellet was subjected 10 times to 1 min shearing cycles at maximal output in a blender at 4 °C and a final vortexing step of 30 min. Whole cells were centrifuged (30 min, 13,000 rpm) and the supernatant was retained. A final ultracentrifugation step (1 h, 100,000 x g) recovered flagellar filaments from the supernatant. The pellet containing crude flagellar filaments was resuspended in 200 µl TBS. By using Ryu stain (see section 4.5.1) Successful isolation of filaments was confirmed under the microscope and the size integrity was confirmed by SDS-PAGE [173,225].

TBS buffer (**T**ris-**B**uffered **S**aline), pH 7.0	Tris/HCl	0.02 M
	NaCl	0.15 M

4.3 Molecular biological methods

Molecular biological methods carried out according to standard protocols [218,226] or by following manufacturer´s instructions. The used kits are listed in Table 10.

4.3.1 Isolation of DNA

Plasmid DNA from *E. coli* was isolated using the Zyppy™ Plasmid Miniprep Kit (Zymo Research, Germany).

S. oneidensis MR-1 chromosomal DNA was isolated following the protocol by Prospiech *et al.* [226]. Cells were grown over night in 10 ml LB, harvested by centrifugation (10 min, 3,000 x g) and resuspended in 2 ml SET-buffer. Lysozyme was added to a concentration of 1 mg/ml and the suspension was supplemented with 10 µl RNase (stock concentration: 20 µg/ml) and incubated at 37°C for one hour. Subsequently, 200 µl of 10 % (w/v) SDS (1/10 of the volume) and 0.5 mg/ml proteinase K were added to the mixture and incubated at 55°C for two hours. Afterwards, 1/3 volumes 5 M NaCl and 1 volume chloroform were added and incubated at room temperature for 0.5 hours with frequent inversions. After centrifugation (15 min, 5000 x g) the upper (aqueous) phase was transferred to a new reaction cup using a clipped pipette tip. The DNA was then precipitated by adding 1 volume of isopropanol, gentle inversion and transferred to a 2 ml reaction cup with a Pasteur pipette, rinsed with 70% (v/v) EtOH, dried at room temperature and dissolved in 500 µl TE buffer. The concentration of the extracted DNA was determined using a NanoDrop ND-100 (Peqlab, Germany) and/or by agarose gel-electrophoresis.

SET buffer (**S**alt-**E**DTA-**T**ris), pH 7.5	NaCl	75 mM
	EDTA	25 mM
	Tris/HCl	20 mM

TE buffer (**T**ris-**E**DTA), pH 7.5	Tris/HCl	10 mM
	EDTA	1 mM

4.3.2 Polymerase Chain Reaction – PCR

PCR amplification of specific gene regions of chromosomal or plasmid DNA was carried out using the Phusion™ Polymerase (Biozym Scientific GmbH, Germany) along with the supplied Phusion HF reaction buffer (5 x) following the manufacturer´s instructions.Successful amplification of PCR fragments was verified by agarose gel electrophoresis 4.3.4. Gene fragments were purified by using the DNA Clean & Concentrator Kit (Zymo Research, Germany).

Plasmid uptake or correct integration into the genome of *E. coli* or *S. oneidensis* was verified by 'colony'-PCR. *E. coli* colony material was directly added to the reaction mix, whereas *S. oneidensis* colonies were resuspended in 100 µl ddH_2O and denatured by boiling the suspension at 95°C for 5 min. Two micro litres were added to the reaction mix and a standard PCR (35 cycles) was performed using Taq- Polymerase

1 µl	Forward primer (10µM)
1 µl	Reverse primer (10 µM)
2.5 µl	10x Taq buffer
1.25 µl	$MgSO_4$ (2 mM)
1 µl	dNTP's (10 mM)
1 µl	Taq- Polymerase
2 µl	chromosomal DNA
15.25 µl	ddH_2O

To construct either N- or C-terminal protein fusions or markerless *in frame* deletions of specific genes in *S. oneidensis* MR-1 an 'overlap-PCR' with Phusion™ polymerase was performed. For this purpose, fragments 500-600 bps upstream and downstream of the target gene were PCR-amplified and fused in a second PCR by overlap extension (9-12 bps) using the outer primer pairs with respective restriction sites. 5'-overhanging regions of the primers were designed in a manner that each fragment was supplemented with an outer restriction site and an inner 9-12 bp overlapping region.

4.3.3 Restriction digestion and ligation of DNA

DNA fragments or plasmids (2-5 µg) were digested with the respective restriction endonucleases (New England Biolabs, Germany; Fermentas, Germany) with the recommended buffer for 3 to 12 h at 37 °C following the manufacturer's instructions. Restricted DNA fragments or plasmid separated by gel electrophoresis were excised and purified with the Zymo CleanTM Gel DNA Recovery Kit (Zymo Research, Germany).

Ligation of PCR fragments and plasmid DNA was performed using T4 Ligase and appropriate buffer systems (New England Biolabs, Germany) according to the manufacturer's instructions. Ligation mixtures were incubated on melting ice over night or at room temperature for 2 h. In general, a 5-fold molar excess of DNA insert was incubated with 50 ng recipient vector.

$$\text{mass of DNA insert (ng)} = \frac{5 \times 50 \text{ ng (recipient vector)} \times \text{size of insert (bp)}}{\text{size of vector (bp)}}$$

4.3.4 Agarose gel electrophoresis

DNA probes were supplemented with 5x loading dye (50 % (v/v) glycerine, 0.25 % (w/v) bromphenol blue added to 1 x TAE) and separetd by size in 1 % agarose gels prepared in 0.5 x TAE (0.175 % acetic acid, 20 mM Tris base, 0.5 mM EDTA) and 0.005 % EtBr. DNA fragments were visualised using a 2UV-Transilluminator (UVP, USA).

4.3.5 DNA sequencing

DNA fragments or plasmids were sequenced using a method that is based on chain-termination sequencing by Sanger [227]. DNA sequencing was outsourced to MWG Operon (Germany) and digital raw data were analyzed by VectorNTI™ software (Invitrogen, Germany).

4.3.6 Plasmid construction

In silico generation of plasmids was done using Vector NTI Advance™ 11 (Invitrogen, Germany). A list of the constructed plasmids can be found in Table 20. Specific oligonucleotides used for plasmid construction carried restriction enzyme recognition sites at their 5'-end, as annotated in Table 21.

High-copy plasmids for arabinose-inducible gene expression

To achieve high levels of proteins or fusion proteins in the cell, genes of interest or fluorescent gene fusions were inserted into pBAD33, a self-replicating plasmid. To this end the corresponding target gene was PCR amplified with oligonucleotides carrying the specific restriction enzyme recognition sites at their 5'-end. The resulting fragment as well as pBAD33 were restricted and ligated, following the protocol in section 4.3.3. Fluorescent gene fusions were constructed using the 'overlap-PCR' and then cloned into pBAD33 as described above. The resulting vectors were transferred into *S. oneidensis* by electroporation.

Plasmids for C-terminal gene fusions with mCherry

For C-terminal gene fusions with mCherry, a fragment lacking the stop codon of the respective gene was PCR amplified and cloned into the corresponding restriction sites of the suicide vector pJP5603-mCherry. The construct was transferred into *E. coli* DH5α and then, for mating purposes into *E. coli* WM3064.

Plasmids for markerless *in frame* gene deletion and insertion

In frame deletion and insertions fragments were constructed using the 'overlap-PCR' described in 4.3.2. Overlap-fragments and the suicide vector were restricted with the corresponding enzymes, purified by agarose gel electrophoresis and subsequently ligated (see section 4.3.3).

For markerless *in frame* insertions three fragments: the DNA fragment containing the insertion without a stop codon and the up- and downstream region flanked by restriction enzyme recognition sites (500-600 bps) were PCR amplified and purified. A second PCR amplification using all three DNA fragments in a 1:1:1 ratio was done by overlap extension using the outer primer pairs of the upstream and downstream fragment. The resulting gene fusion was restricted and ligated into a suicide vector (see section 4.3.3). The following suicide vector backbones have been used: pNPTS138-R6KT and pGP704Sac28Km. The vector pCR2.1-mCherry-SO (adjusted to the codon-usage of *S. oneidensis*) was usedas a template for PCR-amplification of mCherry. The following other plasmids were used as a template for fluorescence gene constructs: pET21-sfGfp, pN-eGfp-Tn7mini, pET21-mOrange and pUC57-mAzami (synthesized following the *S. oneidensis* codon usage by GenScript, USA).

To generate N-terminal *sfgfp*-stator fusions the *sfgfp* gene was inserted without a stop codon behind the sequence encoding the N-terminal cytoplasmic region of MotB or PomB. A $(GGS)_x$ linker was introduced downstream of *sfgfp* and the sequence encoding the cytoplasmic region was repeated. Three fragments using the respective oligonucleotides were PCR amplified: the fragment upstream of the target region including the N-terminal region of the B-subunit (first ~50 cytoplasmic nucleotides), the *sfgfp* gene fragment flanked by oligonucleotides introducing upstream the overlapping region and downstream the $(GGS)_x$ linker. The downstream fragment, repeating the cytoplasmic region of the B-subunit, was framed by the $(GGS)_x$ linker and restriction enzyme recognition sites. After the second PCR amplification using the resulting purified DNA fragments in a 1:1:1 ratio, the fragment was cloned into pNPTS138-R6KT in the corresponding restriction sites.

The resulting vectors were propagated in *E. coli* DH5α and, for the purpose of conjugation, transferred in *E. coli* WM3064. The vector was then transferred to *S. oneidensis* MR-1 by mating as described in 4.3.9.

4.3.7 Preparation and transformation of chemically competent *E. coli* cells

Preparation of chemically competent *E. coli* cells was done using an optimized protocol of Inoue *et al.* [228]. *E. coli* was grown to an OD_{600} in 250 ml SOB media at 18 °C and placed onto ice for 10 min. Subsequently, cells were centrifuged (10 min, 4,600 x g, 4 °C) and the cell pellet was resuspended in 80 ml ice-cold TB buffer and incubated on ice for 10 min. After an additional centrifugation step the cell pellet was resuspended in 20 ml TB buffer supplemented with 7 % (v/v) DMSO. The cells were again placed on ice for 10 min before aliquoted (100 µl) and shock-frozen in liquid nitrogen.

E. coli WM3064 cells were grown in SOB media containing 300 µM DAP.

TB (**T**ransformation **B**uffer), pH 6.7	Pipes	10 mM
	$MnCl_2$	55 mM
	$CaCl_2$	15 mM
	KCl	250 mM

Transformation of chemically competent *E. coli* cells was done according to the protocol of Inoue *et al* [228]. To introduce plasmids, 100 µl of chemically competent *E. coli* cells were thawed on ice, mixed with 20 µl of the ligation mixture or 20 ng plasmid and incubated for 30 min on ice. After performing a heat-shock at 42 °Cfor 30 s, cells were placed on ice and supplemented with 1 ml SOB (SOB with 300 µM DAP for WM3064). The cultures were allowed to recover for 1 to 2 h at 37 °C under shaking conditions and spread on LB agar plates supplemented with the appropriate additives. After 12 h single colonies of recombinant *E. coli* cells were restreaked on fresh LB plates and verified by colony PCR.

4.3.8 Preparation and transformation of electrocompetent *S. oneidensis* MR-1 cells

To prepare fresh electrocompetent *S. oneidensis* cells, recipient cells were cultured over night, reinoculated in LB media and grown to an OD_{600} of 0.6. Afterwards 1.5 ml of the cells were centrifuged and washed two times in Sorbitol buffer (1 min, 13,000 x rpm). Subsequently, the electrocompetent cells were resuspended in 35 µl sorbitol and kept on ice. To transform *S. oneidensis* cells, 10 ng plasmid DNA was added, transferred to a sterile electroporation cuvette and electroporated at 1.8 kV, 200 Ω and 25 µF. Cells were allowed to recover for 2-3 h at 30 °C and selected for recombinant *S. oneidensis* cells on LB-agar plates supplemented with the appropriate selection reagents. Single recombinant colonies were restreaked on the respective LB-agar plates and verified by colony PCR.

Sorbitol buffer, pH 7.5	Sorbitol	1 M
	EDTA	0.1 M

4.3.9 Conjugation of *S. oneidensis* MR-1 cells

Conjugation of *S. oneidensis* was performed using an optimized protocol of Thormann *et al.* [229]. Plasmids were introduced in *S. oneidensis* by mating, using *E. coli* WM3064 as a donor strain. After overnight incubation of recipient and donor strain, 1 ml of the culture was centrifuged (1 min, 13,000 x rpm) and washed three times in LB. Both pellets were unified in 250 µl LB and spotted as one drop on a LB-agar plate containing 300 µM DAP. After incubation for 12 h at 30 °C, colonies were resuspended in 2 ml LB, washed three times in LB and plated on LB-agar plates supplemented with the respective antibiotics for selection. Single crossover integration mutants were restreaked on LB-agar plates, containing the appropriate antibiotics and finally verified by colony PCR. For single crossover, pJP5603-based constructs were used.

For the purpose of markerless *in frame* deletions or insertions by using pGP704Sac28Km or pNPTS138-R6KT the protocol described above was expanded. Kanamycin resistant colonies were cultured overnight in LB without antibiotics and plated on LB containing sucrose (10 % (w/v)) to select for double crossover events. Subsequently, cells were restreaked in parallel on LB and LB-kanamycin plates to screen for kanamycin-sensitive colonies. *In frame* deletions or insertions were confirmed by colony PCR.

4.3.10 Southern Blotting and DIG detection

Southern blotting was performed according to the protocol of Southern [230]. Chromosomal DNA was prepared according to 4.3.1, 5 µg were digested with the respective restriction endonuclease and separated by gel electrophoresis (see section 4.3.3 and 4.3.4). The gel was documented by UV light in order to correlate the DNA fragment size to the corresponding signal after DIG detection. It was then successively incubated for 30 min in denaturation solution and neutralization solution, with washing steps in ddH_2O in between, and finally equilibrated in 20 x SSC (0.3 M sodium citrate, 3 M NaCl, pH 7). Restricted DNA fragments were transferred overnight by capillary force from the agarose gel to a positively charged nylon membrane (Amersham Hybond™-N^+ nylon membrane, GE Healthcare, UK) by using a 20 x SSC based buffer system. Afterwards, the separated DNA fragments were covalently bound to the membrane by incubation at 80 °C for 2 h.

DNA probes were synthesized and labeled using PCR DIG Probe Synthesis Kit (Roche, Germany) following the manufacturer's instructions with the respective oligonucleotides. After incubating the membrane in hybridization solution (2 h at 45 °C) the single stranded probe (5 min, 95 °C and subsequently chilled on ice) was added to the blot and incubated overnight at 42 °C.

For hybridization and detection the DIG Nucleic Acid Detection Kit (Roche, Germany) was utilized. To this end, the blot was washed 2 x in 2 x SSC, 0.1 % SDS (15 min), 2 x in 0.2 SSC, 0.1 % SDS (15 min, 60 °C) and 3 x briefly in DIG wash buffer (0.3 % Tween-20 in maleic acid buffer). After incubation in blocking solution for 30 min, the membrane was transferred for 30 min in antibody solution. Two additional washing steps for 15 min in DIG wash buffer were followed by an equilibration in detection buffer (100 mM diethanolamine, 10 mM $MgCl_2$, 100 mM NaCl, pH 10) and finally 1:1,000 in detection buffer diluted CDP-Star® reagent (New England Biolabs, Germany) was added and chemiluminescence was documented using the Immunoblot-Imager LAS 400 (FujiFilm, Germany).

Table 12: Used buffers for Southern Blotting.

Denaturation solution	
NaCl NaOH	1.5 M 0.5 M
Neutralization solution	
NaCl Tris/HCl	1.5 M 0.5 M
Hybridization solution	
20 x SSC ddH_2O	15 ml 45 ml
Blocking reagent	Blocking reagent (bottle 5 in kit) was dissolved in maleic acid buffer (0.1 M maleic acid, 0.15 M NaCl) to a final concentration of 10 % (w/v) and autoclaved.
Blocking solution	Blocking reagent was diluted 1:10 in maleic acid buffer
Antibody solution	Antibody solution was diluted 1:5000 (4 µl in 20 ml, 150 mU/ml) in blocking solution

4.3.11 Promoter activity

Measurement of *pom*- and *mot*-promoter activity was carried out by a transcriptional fusion to *lucB*, using a modified protocol of Feustel *et al.* [231]. LB-grown cultures were harvested at an OD_{600} 1.0-1.5 and resuspended in 150 µl K_2HPO_4 (50 mM, pH 7.0). Aliquots of 45 µl were transferred as triplicates into a 96 well polypropylene microtitre plate (Greiner, Germany). By using an Infinite M200 plate reader equipped with two microinjectors (Tecan, Switzerland) the following solutions were addedto each well: 50 µl 2 x assay buffer (62.5 mM glycyl glycine, 25 mM $MgCl_2$, pH 7.8) and 12.4 µl ATP-solution (100 mM), subsequently a mixing step for 1 s was applied, followed by the injection of 50 µl D-luciferin solution (330 µM D-luciferin, 10 mM K_2HPO_4, pH 6.5). After mixing for 3 s, the luminescence was measured with an exposure time of 5 s. Luciferase activity in RLU (**R**elative **L**ight **U**nits) was calculated by dividing luminescence with the measured optical density (OD_{600}). The experiments were done in triplicates and repeated two times, *S. oneidensis* MR-1 cells harbouring pBBR-*lucB* was used as a negative control.

4.4 Biochemical methods

4.4.1 SDS-PAGE

Protein samples were separated by **S**odium-**D**odecyl **S**ulphate **P**oly**a**crylamide **G**el-**E**lectrophoresis (SDS-PAGE) according to Lämmli [232]. Protein lysates were obtained from logarithmically growing cultures. Cells corresponding to an OD_{600} 0.25 were sedimented by centrifugation and resuspended in 25 µl 2 x SDS sample buffer (0.125 M Tris base, 20 % (w/v) Glycerine, 4 % SDS, 10 % (v/v) β-mercaptoethanol, 0.02 % bromphenol blue, pH 6.8). Subsequently, cells were boiled for 5 min and stored at -20°C. Frozen samples (10 µl) were boiled for 5 min prior to loading on a SDS-gel, consisting of a 5 % stacking and an 11 % resolving gel. For Coomassie staining and for immunoblot analysis 5 µl of an unstained and prestained molecular weight marker were loaded as a standard, respectively (PageRuler™ Prestained Protein Ladder/ Unstained Protein Ladder, Fermentas, St. Leon-Rot). Electrophoresis was performed in a Tris/Glycine based buffer system at 50 mAh^{-1} (100 to 150 V) in a custom-made electrophoresis system. The resulting SDS-PAGES were either stained for 2-3 h in Coomassie (Coomassie Brillliant Blue R-250, BIO-RAD, US) and destained overnight in dH_2O for visualisation of proteins or used for specific protein detection by immunoblot analysis (see section 4.4.2.).

Table 13: Used buffers for SDS-PAGE.

11 % SDS-PAGE	11 % resolving gel	5 % stacking gel
ddH_2O	3.8 ml	2.8 ml
4 x resolving buffer	2.5 ml	
4 x stacking buffer		1.25 ml
30 % Rotiphorese® NR-Acrylamide/Bis-(29:1)	3.7 ml	840 µl
10 % (w/v) APS (Ammonium persulfate)	80 µl	50 µl
TEMED (N,N,N,N-Tetramethylethylenediamine)	6 µl	3.8 µl
4 x resolving buffer, pH 8.8		
SDS	0.4% (w/v)	
Tris base	1.5 M	
4 x stacking buffer, pH 6.8		
SDS	0.4 % (w/v)	
Tris base	0.5 M	

4.4.2 Immunoblot assays

Resolved proteins on a SDS-PAGE were transferred onto a polyvinylidene fluoride (PVDF)-membrane (Millipore Immobilion™ P Transfer Membrane, (Millipore, USA)) by semidry western blot transfer (Electroblotter TE 77 ECL Semi Dry (Amersham Biosciences, Germany). Prior assembly PVDF membranes were first incubated for 30 s in 100 % Methanol, washed in ddH_2O for 2 min and saturated for 5 min in Western transfer buffer (25 mM Tris base, 192 mM glycine, 10 % (v/v) Methanol). The activated PVDF membrane and the SDS-gel were sandwiched between blotting papers soaked in Western transfer buffer (6 x) according to manufacturer´s instructions. Proteins were blotted onto the PVDF membrane by applying an electric current of 2 mA/cm² for 1-2 h. Afterwards, the membrane was blocked overnight at 4 °C in 5 % (w/v) milk powder dissolved in PBST (6.6 mM Na_2HPO_4 x 7 H_2O, 1.8 mM KH_2PO_4, 137 mM NaCl, 2.7 mM KCl, 1 % (v/v) Tween-20, pH 7.5).

Table 14: used antibodies.

Antibody	Dilution	Company/Comment
primary antibodies		
anti-MotB	1:250	SO_MotB-1; polyclonal antibody raised against internal peptide fragments (Q240 to N254), antibody dilution was
anti-PomB	1:250	SO_PomB2; polyclonal antibody raised against internal peptide fragments (Q240 to N254)
anti-filament	1:500*	polyclonal antibody raised against whole flagellar filaments of *S. oneidensis* MR-1 (rabbit 036)
	1:50	immunostaining (see section 4.5.2)
	1:10	for biophysical approaches antibody was purified with an IgG-purification KitA (probior GmbH, Germany) according to manufacturer´s instructions
		Eurogentec, Germany
anti-surface	1:50	Immunostaining (see section 4.5.2)
	1:10	Polyclonal antibody raised against whole cells fixed with 2.5 % paraformaldehyde (in 30 mM $NaPO_4$, pH 7.5) antibody was purified with an IgG-purification KitA (probior GmbH, Germany) according to manufacturer´s instructions
		Eurogentec, Germany
anti-Gfp	1:10,000	SIGMA-Aldrich, Germany
anti-dsRed	1:500	Clontech, USA
anti-6 x His	1:2,000	Pierce, Germany
secondary antibodies		
anti-rabbit-HRP	1:20,000	Perkin Elmer, USA

* whole blood was used for immunoblot analysis

In order to detect specific proteins, the membrane was briefly washed in TBST and incubated for at least 1 h with the primary antibody at the desired dilution. Afterwards, membranes were washed trice with TBST and incubated for 1 h with the secondary anti-rabbit IgG, coupled to horseradish peroxidase (HRP). Antibodies were diluted in TBST supplemented with 2.5 % (w/v) milk powder as listed in Table 14. Subsequently, membranes were washed three times in TBST and incubated with chemiluminescence substrate (Western Lightning™ Chemiluminescence Reagent Plus (Perkin Elmer, USA)) according to manufacturer´s instructions. Signals were visualized by exposure to autoradiography films (Amersham Hyperfilm™, GE Healthcare, Germany).

4.5 Microscopical methods

Microscopy and image acquisition was carried out on an Axio Imager.M1 microscope (Zeiss, Germany). Fluorescence and Differential Interference Contrast (DIC) images were acquired by using a Zeiss Plan Apochromate 100 x/1.40 Oil DIC objective and a Cascade 1K CCD camera (Photometrics, USA). Fluorescence imaging was performed by combining a mercury short-arc reflector lamp LQ-HXP 120 (LEj, Germany) with ET-GFP, ET-YFP and ET-TexasRed filter cubes (Chroma, USA). Images were processed with the MetaMorph® 7.1.2 software (Molecular Device, USA).

4.5.1 Flagellar filament staining

Flagellar filaments were stained either by a wet-mount method with Ryu stain, by AlexaFluor^{488} carboxylic acid succinimidyl ester [128] or by immunolabelling after Heimbrook *et al.* [173,225]; (see section 4.5.1).

Ryu stain is a mordant dye, thus, cells have to be fixed in order to allow the dye to adhere to them. Five microlitres of a culture were spotted on a slide and covered with a coverslip. After two to five min Ryu stain was added to the edges so that capillary forces drew the stain under the coverslip.

In order to colocalise stained filaments with fluorescently tagged motor proteins, AlexaFluor^{488} carboxylic acid succinimidyl ester (Invitrogen, Germany) was chosen. After 15 ml of cells were carefully washed two times (10 min, 2,000 x g) in 4M medium with no $(NH_4)_2SO_4$ added. Susequently, they were resuspended in 0.5 ml and diluted to an appropriate working concentration for microscopy. Next, 12.5 µl staining solution (4 M containing no $(NH_4)_2SO_4$, 0.08 mg Alexa Fluor^{488}) was added to the cells and incubated with low agitation for 1 h (RT). The cell suspension was washed two times in 4 M and finally resuspended in 100 µl. Five microlitres were applied on an agarose pad (1% (w/v) agarose dissolved in 4 M media) and visualised by fluorescence microscopy. Visualisation of the flagellar filaments was enhanced by using the 'sharpen' function of Metamorph (Molecular Device; USA).

4.5.2 Immuno fluorescence

The standard immuno fluorescence protocol was modified to allow staining of *S. oneidensis* cells without fixation. In order to stain the filament by immunofluorescence, cultures were grown overnight and carefully sedimented by centrifugation (6 min, 3,000 x g). After resuspension in a BSA-containing 4 M buffer (1 % (w/v) BSA, 50 mM HEPES, 15 mM Lactate 85 % (w/v), 200 mM NaCl, pH 7.0), cells were incubated on a rotary device for 1 h. Then the cells were centrifuged again and supplemented with an appropriate antibody dilution in 4 M buffer with 1 % (w/v) BSA (see Table 14). Incubation on a rotary device for 1 h was followed by three additional washing steps and an incubation with the secondary antibody for one hour (1:300 anti-rabbit-Alexa Fluor^{488} (Invitrogen, Germany). Finally, cells were gently washed three times in 4 M buffer (50 mM HEPES, 15 mM Lactate, 100 mM NaCl, pH 7.0) and prepared for microscopy on an agarose pad.

4.5.3 Determination of the stator complex stoichiometry

Fluorescently labeled PomB complexes were visualized and quantified in collaboration with the Molecular Motors Group of the Physics Department in the University of Oxford. Overnight cultures of *sfgfp-pomB* grown in LB were washed two times (4 M buffer, 0 mM NaCl, 200 mM KCl, 6 min, 3,000 x g) and subcultured in LM media supplemented with the appropriate NaCl concentration (0 mM, 5 mM, 200 mM). Cells grown to mid-exponential phase were sedimented and washed in 4 M buffer. Cells were incubated on a 4 M agar pad supplemented with the respective NaCl concentration for 20 min. Fluorescent movies were recorded in Oxford, using a custom-made inverted microscope with a Plan Fluor100 x/1.45 Oil objective (Nikon, UK) and a 473 nm DPSS laser modified after Leake *et al.* [104]. Movies were recorded for 500 frames or until the fluorescent foci were completely bleached. Individual frames were exposed for 0.05 s, by applying a laser power of 2.5 mW.

The quantification of fluorescent foci was carried out by using a MATLAB code written by Bradley Steel (Molecular Motors Group, Physics Department, University of Oxford). Based on an algorithm as described in Leake *et al.*, this code allows to quantify single fluorescent molecules. Briefly, intensity trajectories over time were filtered (Chung Kennedy, median filter) and the initial intensity was calculated. The filtered intensity trajectories were used to calculate the pairwise difference distribution (PDDF) and the power spectrum of each PDDF histogram was calculated. The dominant peak corresponds to the step size of bleached molecules and was used to calculate the number of Gfp molecules by dividing the initial intensity by the step size. Statistical analysis of the distribution of of stators at various NaCl concentrations was performed using the two-tailored 't-test' tool (independent two population t-test, p=0.01) in Origin 6.1.

4.6 Biophysical methods

The following buffers derived from 4 M media were used for the single cell analysis:

4 M-0	(50 mM HEPES, 15 mM Lactate, 200 mM KCl, pH 7.0)
4 M-5	(50 mM HEPES, 15 mM Lactate, 5 mM NaCl, 195 mM KCl pH 7.0)
4 M-200	(50 mM HEPES, 15 mM Lactate, 200 mM NaCl, pH 7.0)
4 M-200-BSA	(50 mM HEPES, 15 mM Lactate, 200 mM NaCl, 0.1 % (w/v) BSA, pH 7.0)
4 M-200-BSA-1	(50 mM HEPES, 15 mM Lactate, 200 mM NaCl, 1 % (w/v) BSA, pH 7.0)

4.6.1 Bead assay

An unconjugated anti-rabbit IgG (AbCam, UK) was crosslinked by using EDAC (1-**E**thyl-3-(3-**d**imethyl**a**minopropyl) **c**arbodiimide hydrochloride, Invitrogen, Germany) to carboxy-modified polystyrene beads (Invitrogen, Germany). To this end 1.5 mL MES buffer (50 mM MES, pH 6.0) was supplemented with 100 µl polystyrene beads and centrifuged (7 min, 13,000 x rpm). Meanwhile, 50 µl containing 50 mg/ml EDAC were prepared and added to the beads (50 µl MES, 2.5 g EDAC). Subsequently, the beads were sonicated for 15-30 min to avoid clumping. Three additional washing steps in 1.5 ml MES buffer (7 min, 13,000 x rpm) were followed by sonication in anti-rabbit IgG antibody solution (0.6 mg/ml anti-rabbit IgG in MES buffer) for 15 min. The 'anti-rabbit IgG beads' stock was kept on a rotary device overnight at 4 °C and stored at 4 °C.

Next, a tunnel slide was prepared by mounting a cleaned coverslip (5 M NaOH for 15 min, briefly rinsed in ddH_2O) to a slide using 'sticky tape' (Scotch, Germany), (Figure 33). To increase the number of cells attaching to the surface, the coverslip was silanized with RainX® (RainX, UK) [175].

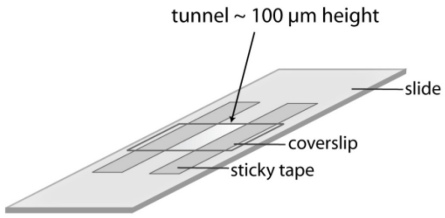

Figure 33: Tunnel slide.

Cells were cultured overnight in LB, washed in LM media without NaCl and grown in LM (200 mM NaCl) to an OD_{600} of 0.6. Subsequently, 250 µl of the culture were centrifuged (5 min, 6,000 x rpm) and resuspended in 100 µl 4 M-200. The tunnel slide was flushed two times with 50 µl 4 M-200, followed by 20 µl cell suspension. After 5 min of incubation, 100 µl 4 M-200-BSA was

flushed through, followed by the incubation with 20 µl anti-filament IgG diluted 1:10 in 4 M-200-BSA for 10 min. Meanwhile, 10 µl of 'anti-rabbit-IgG beads' stock solution was added to 1.5 ml 4 M-200-BSA, sedimented (7 min, 13,000 x rpm), and resuspended in 50 µl 4 M-200-BSA prior to sonication (15 min). After cells were washed with 100 µl 4 M-200-BSA-1, 20 µl of beads were added (diluted 1:5) and incubated for 5 min before being flushed out with 4 M-200-BSA.

Bead rotation was measured in an optical trap built by Pilizota *et al.* in the Physics Department at the University of Oxford [233]. The optical trap mainly consists of a custom-made inverted microscope and a 1064 nm Ytterbium fibre laser (IPG Photonics, USA). Position of the bead was detected by Back Focal Plane interferometry (BFP). The laser beam was focused into the specimen plane by the objective and collimated by the condenser to the quadrant photodiode in the BFP of the condensor.

Rotation data were analysed by applying a LabView code, written in the Physics Department in the University of Oxford. Bead positions were analysed by fitting an ellipse to the bead´s trajectory. Data were 200 point median filtered and angular velocity (ω) was calculated from the angle versus time data ($\omega = d\theta/dt$) [18].

4.6.2 Tethered cell assay

Overnight cultures were subcultured in LB or LM and 1 ml was harvested in mid-exponential phase (OD_{600} 0.6). After two additional washing steps, cells were resuspended in 4 M supplemented with the appropriate NaCl concentration. Cells were tethered by their filament (without shearing) in a flow cell or in a tunnel slide. Cells flushed into a tunnel slide (20 µl) were allowed to settle for 5 min, and antibody solution diluted 1:20 in 4 M buffer was added. After 20 min of incubation in a humidity chamber, 50 µl of 4 M buffer was flushed through two times. Cells tethered in a flow cell [79] were incubated for 5 min on a coverslip and supplemented with antibody solution to a final dilution of 1:20 for 20 min in a humidity chamber. The coverslip was then invertedly mounted onto the flow chamber and 4 M buffer was flowed through. Cells were recorded using a Nikon Optiphot Phase-Contrast Microscope with a 40 x magnification (Nikon, Japan) with a digital DALSA Genie-HM640 camera, capable of high-speed image acquisition (up to 295 Hz). Movies of tethered cells were taken at 200 Hz with an exposure time of 4 ms.

Tethered cells in a tunnel slide were used to compare rotation speed in cell populations depending on the NaCl concentration, the flow cell was used to analyse the response of a single cell to different NaCl concentrations. Expression of stator genes from *araC*-P_{BAD}-controlled promoters was induced by using 0.2 % arabinose.

Rotation speed of tethered cells was extracted from the video data by aMATLAB code written by Bradley Steel in the Molecular Motors Group in the University of Oxford according to Berg *et. al* [79]. Rotation speeds are powerspectral-filtered with a windowsize of 3 s. This code was used to calculate the rotation speed from changes of the cumulative angle of the cells over time. The distribution of the rotation speed was median-filtered and a threshold of 0.25 Hz was set to exclude Brownian motion.

4.7 Bioinformatical methods

Bacterial nucleotide- and protein sequences were obtained from NCBI (http://www.ncbi.nlm.nih.gov) and analysed using the NCBI BLASTP- or BLASTN algorithm and the EMBL SMART algorithm (http://smart.embl-heidelberg.de/).

Phylogenetic trees were generated with iTOL (http://itol.embl.de)

The ESPRIPT 2.2 workbench was used for protein sequence alignment with ClustalW and for graphically modifications (http://espript.ibcp.fr/ESPript/cgi-bin/ESPript.cgi). Structures of FlaB and FlaA of *S. oneidensis* were built on the full length flagellar filament atomic model of *Salmonella typhimurium* by using the SWISS-MODEL workspace (http://swissmodel.expasy.org/workspace).

Transmembrane domains, signal peptides were predicted by using SignalP (both at http://www.cbs.dtu.dk/services/SignalP/), TMHMM and TOPCONS (http://topcons.cbr.su.se/).

Statistical analysis and the distribution of rotation speed obtained from the tethered cell assay and the bead assay were performed using Origin 6.1 (OriginLab, USA). The boxplot- and the t-test analysis tool were used (independent two-tailored t-test, significance level $p=0.01$).

APPENDIX

Results:

The constructed PomB-Gfp fusions as described in section 2.1.5.

Table 15: Construction of a functional PomB-Gfp fusion.

	variation[a]	polar localisation[b]	Functionality[c]
wild type stator complex		-	++++
different fluorophores[c]	Gfp-mut3 (N-terminal)	-	(+) cleaved
	Gfp-mut2 (N-terminal)	-	(+) cleaved
	sfGfp (N-terminal)	+	(+)
	mAzami (C- and N-terminal)	(-)	n.d.
	mCherry (C-terminal)	+	++++
	mOrange (C- and N-terminal)	(-)	n.d.
repetition of cytoplasmic region[e]	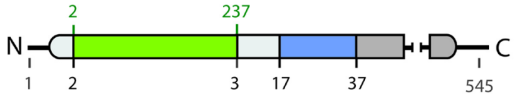	+	-
	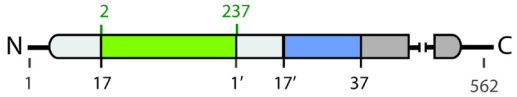	+	+
	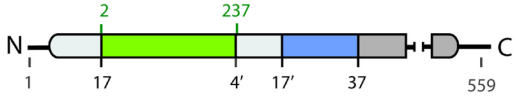	+	+
variation in linker sizes $(GGS)_x$ [f]	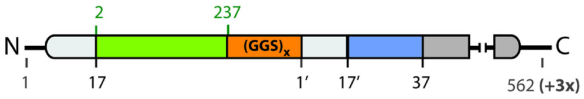		
	linker GGS	+	+
	linker $(GGS)_2$	+	+
	linker $(GGS)_3$	+	++
	linker $(GGS)_4$	+	++

[a] colour code: light grey, N-terminal cytoplasmic region of B-subunit; green, fluorophore; blue, transmembrane domain; dark grey, C-terminal region periplasmic region

[b] polar localisation was verified by fluorescent microscopy; - no polar foci; + polar localisation

[c] swimming motility was tested on 0.25 % soft agar plates. ++++ wild-type; ++ decreased motility on soft agar plates; - no swimming diameter on soft agar plates.

[d] N-terminal: genes encoding different fluorophores were inserted after the second or seventeenth residues of the B-subunit. C-terminal fusions were fused directly downstream of the stop-codon.

[e] N-terminal fusion were constructed using sfGfp. To exclude a cleavage site within the first three residues, which was predicted with really low possibility by using SignalP [234], the first three aa have not been repeated in the last fusion.

[f] N-terminal fusions were constructed using sfGfp. GGS-linker with one, two and three repetitions were introduced. Introducing a linker of (GGS)3 or (GGS)4 increased motility and was used for the stoichiometry analysis.

Stator complexes are composed of two A- and four B-subunits. To analyse whether PomA formed a functional complex with MotB and vice versa, stator subunit strains were constructed and MotB-mCherry and PomB-mCherry were ectopically expressed from a plasmid [128]. The observed motility patterns suggest that *S. oneidensis* does not have functional hybrid stators in order to drive flagellar rotation. However, PomB-mCherry localises polarly in the presence of Mot, suggesting that PomB might interact with MotA. Polar loalisation of MotB-mCherry in the presence of only PomA was not observed. PomB-mCherry and MotB-mCherry restored motility and localised polarly in the presence of PomA and MotA, respectively, indicating that the ectopically expressed fusions can restore the functionality of the stator complexes.

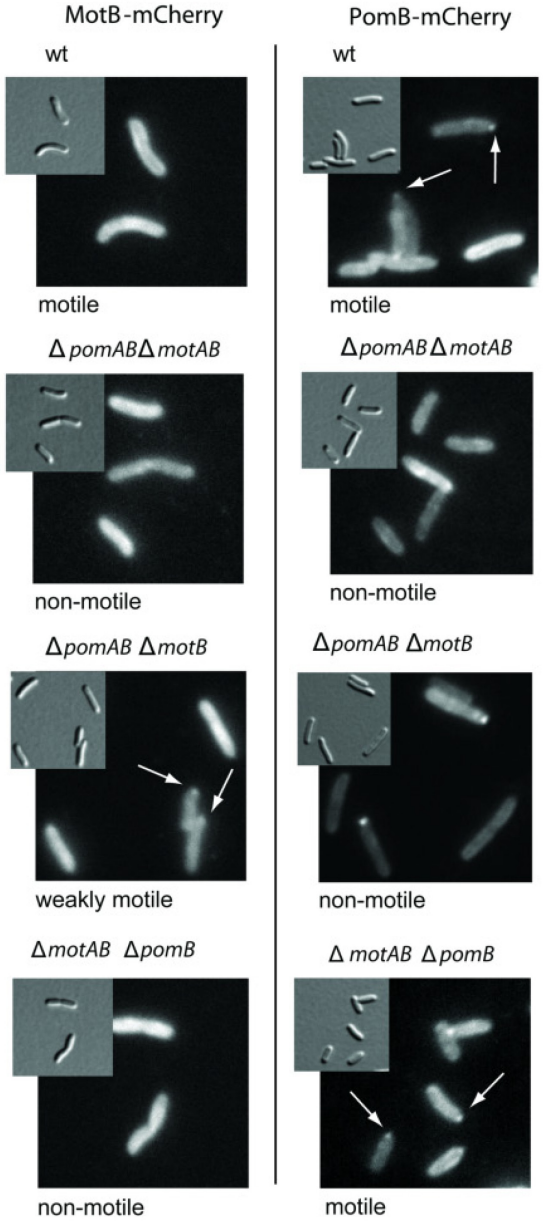

Figure 34: The A- and B-subunits of the stator complexes do not form functional hybridstators in *S. oneidensis* MR-1. Displayed are micrograohs of cells producing MotB- and PomB-mCherry, left and right panel, respectively. The corresponding stator deletion background is annotated above the micrographs. Swimming ability was microscopically analysed and is not below the fluorescence pictures. Arrows indicate positions of the tagged B-subunits.

Sequence alignment of flagellin of *S. oneidensis* MR-1 as described in section 2.3.1.

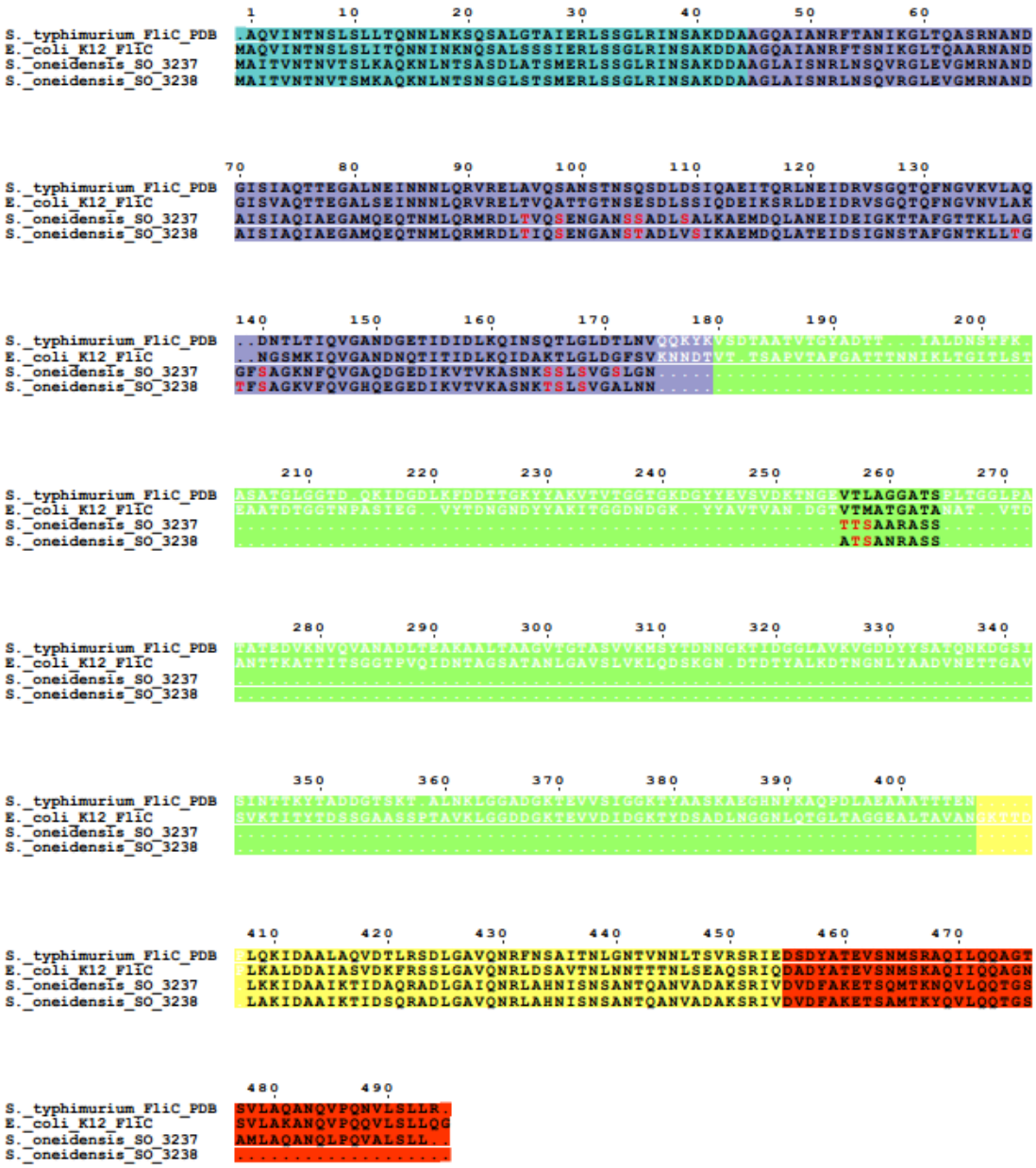

Figure 35: Sequence alignment of *S. oneidensis* FliC. Aligned FlaA (SO_3238) and FlaB (SO_3237) of *S. oneidenis* MR-1 and FliC of *E. coli* and *S. typhimurium*. Alignment was performed by using ClustalW and ESPRIPT. Putative modified residues of *S. oneidensis* flagellin are highlighted in red. Amino acids are coloured according to the corresponding flagellin domains: N-D0 and C-D0, cyan and red; N-D1 and C-D1, purple and yellow; D2 and D3 domains, green. In *S. oneidensis* MR-1 most of the D2 and the complete D3 domains are missing.

To get insights into the flagellar motor performance the rotation speed of tethered cells was analysed. Shown are the statistics for the cells included in the analysis in section 2.3.3.

Table 16: statistics for tethered cell experiments.

Strain	Sodiumchloride [mM]	Median speed [Hz]		Number of cells		High speed [Hz]*	Number of cells
		CW	CCW	CW	CCW		
ΔflhF up	200	8.64	5.66	69	40	8.72	75
	5	4.35	5.77	34	25	5.09	57
	0	4.86	3.52	67	7	4.79	77
ΔflhF up ΔmotAB	200	6.42	5.88	30	31	8.17	39
	5	3.49	6.41	23	22	5.53	36
	0	1.08	2.28	32	70	1.95	93

* median speed for CCW and CW direction was compared and only the highest rotation speed was considered as the maximum output of the flagellar motor of the analysed tethered cell.

Raw data for the genome wide analysis in section 2.4 are listed below. Fully sequenced and annotated organisms harbouring one FliF were used as a master table to identify the number of stator complexes, consisting of A- and B-subunits.

Table 17: Raw data bioinformatic analysis of obtained FliF, PomAB and MotAB orthologs.

number of putative FliFs	number of organisms (raw data)	number of organisms(annotated and fully sequenced)	stator complex	number of orthologs
1	663	400	PomA	821
2	102	134	PomB	1219
3	1	0	MotA	1218
			MotB	1226

Listed are all organisms obtained in the genome-wide bioinformatic analysis harbouring one flagellar system and multiple stator complexes (section 2.4).

Table 18: Dual or multiple stator systems are common among bacteria.

organism with one putative motor system**	number of putative stator system***
Gram (-) bacteria	
Proteobacteria	
Alpha-proteobacteria	
Rhodospirillum rubrum ATCC 11170	2
Zymomonas mobilib subsp. mobilis	2
Beta-proteobacteria	
Azoarcus sp. BH72	2
Burkholderia ambifaria	2
*Burkholderia cenocepacia**	2
Burkholderia glumae BGR1	3
Burkholderia multivorans ATCC 17616	2
Burkholderia phymatum STM815	2
Burkholderia phytofirmans PsJN	2
Burkholderia sp. 383	3
Burkholderia vietnamiensis G4	2
Burkholderia xenovorans LB400	2
Dechloromonas aromatica RCB	2
Herminiimonas arsenicoxydans	2
Janthinobacterium sp. Marseille	2
Methylobacillus flagellatus KT	2
Nitrospira multiformis ATCC 25196	2
Thauera sp. MZ1T	2
Gamma-proteobacteria	
Azotobacter vinelandii DJ	2
Cellvibrio japonicus Ueda107	2
Chromohalobacter salexigens DSM 3043	2
Colwellia psychrerythraea 34H	2
Halorhodospira halophila SL1	3
*Legionella pneumophila**	2
Marinobacter aquaeolei VT8	4
Marinomonas sp. MWYL1	3
Pseudoalteromonas haloplanktis TAC125	2
*Pseudomonas aeruginosa**	2
*Pseudomonas entomophila**	2
*Pseudomonas fluorescens**	2
*Pseudomonas putida**	2
Pseudomonas stutzeri A1501	3
*Pseudomonas syringae**	2
Saccharophagus degradans 2-40	2
Shewanella oneidensis MR-1	2
*Stenotrophomonas maltophila**	2
Teredinibacter turnerae T7901	2
Thioalkalivibrio sp. HL-EbGR7	4
Thiomicrospira crunogena XCL-2	3

organism with one putative motor system**	number of putative stator system***
*Vibrio fischeri**	2
Xanthomonas axonopodis pv. citri str. 306	2
*Xanthomonas campestris pv. campestris**	2
*Xanthomonas oryzae pv. oryzae**	2
Delta-proteobacteria	
Bdellovibrio bacteriovorus HD100	3
Desulfobacterium autotrophicum HRM2	3
Desulfovibrio desulfuricans subsp. desulfuricans G20	2
Desulfovibrio magneticus RS-1	4
Desulfovibrio salexigens DSM 2638	4
Desulfovibrio vulgaris str. Miyazaki F	4
*Desulfovibrio vulgaris**	3
Lawsonia intracellularis PHE/MN1-00	2
Nitrospirae	
Thermodesulfovibrio yellowstonii DSM 11247	2
Acidobacteria	
Candidatus Koribacter versatili Ellin 345s	2
Candidatus solibacter usitatus Ellin 6076	3
Gram(+) bacteria	
Firmicutes	
Bacillus amyloliquefaciens FZB42	2
*Bacillus anthracis**	2
*Bacillus cereus **	2
Bacillus cytotoxicus NVH 391-98	2
Bacillus licheniformis ATCC 14580	2
*Bacillus subtilis**	2
*Bacillus thuringiensis**	2
Bacillus weihenstephanensis KBAB4	2
Oceanoacillus iheyensis HTE831	2
Clostridia	
Clostridum acetobutylicum ATCC 824	2
Clostridium beijerrinckii NCIMB 8052	3
*Clostridium botulinum**	2
Desulfitobacterium hafniense Y51	2
Desulfotomaculum reducens MI-1	2
Moorella thermoacetica ATCC 25196	3

* different strains in this species, exhibiting the same number of putative stator complexes, are combined

** Identification of the putative motor systems was done by sequence alignment of FliF of *S. oneidensis* MR-1 using the BLASTP homepage, with an E-value of $1E^{-10}$. Putative MS-ring proteins for sequenced genomes were checked for the neighbour genes in a flagellar cluster.

*** Identification of the putative stator systems was done by sequence alignment of PomA / MotA and PomB / MotB subunits of *E. coli*; *V. alginolyticus* and *B. subtilis* using the BLASTP homepage, with an E-value of $1E^{-10}$. Putative stator subunits located in a close neighbourhood are referred to stator complexes.

Material and Methods:

Strains, plasmids and oligonucleotides used and constructed in this work.

Table 19: Strains.

Strain	Relevant genotype or phenotype	Source or reference
E. coli		
DH5αλpir	*recA1 gyrA* (*lacIZYA-argF*) (80d *lac* [*lacZ*] M15) *pir* RK6	[223]
WM3064	*thrB1004 pro thi rpsL hsdS lacZ* ΔM15 RP4-1360 Δ(*araBAD*) 567Δ*dapA* 1341::[*erm pir*(wt)]	W. Metcalf, University of Illinois,Urbana-
***In frame* deletions for the characterisation of flagellar motor components**		
***S. oneidensis* MR-1**	**wild type**	**[117]**
MR-1 *egfp*	wild type, labeled with enhanced Gfp integrated in Tn7 region	[214]
Δ*flag*	Δ*flag*	[128]
Δ*pil*/Δ*mshA*	Δ*pil;* Δ*mshA*	[147]
Δ*pomAB*	ΔSO_1529-30	[128]
Δ*motAB*	ΔSO_4287-86	[128]
Δ*pomAB*/Δ*motAB*	ΔSO_1529-30*;* ΔSO_4287-86	[128]
Δ*pomAB-up*	ΔSO_1529-30, "upmotile" mutant enriched from edges of elevated motility on soft agar plates	this work
Δ*motX*	ΔSO_3936	[153]
Δ*motY*	ΔSO_2754	[153]
Δ*motXY*	ΔSO_3936; ΔSO_2754	[153]
Δ*motAB*/Δ*motX*	ΔSO_4287-86; ΔSO_3936	this work
Δ*motAB*/Δ*motY*	ΔSO_4287-86; ΔSO_2754	this work
Δ*motAB*/Δ*motXY*	ΔSO_4287-86; ΔSO_3936; ΔSO_2754	this work
Δ*pomAB*/Δ*motX*	ΔSO_1529-30	this work
Δ*pomAB*/Δ*motY*	ΔSO_1529-30; ΔSO_2754	this work
Δ*pomAB*/Δ*motXY*	ΔSO_1529-30; ΔSO_3936; ΔSO_2754	this work
Δ*flbF*	ΔSO_3212	This work
Δ*flbG*	ΔSO_3211	This work
Δ*flbFG*	ΔSO_3212; ΔSO_3211	Nathalie Heß
Δ*flbFup*	ΔSO_3212; upmotile muatnt, enriched from edges of elevated motility on soft agar plates	this work
Δ*flbFup*/Δ*pomAB*	ΔSO_3212 up; ΔSO_1529-30	this work
Δ*flbFup*/Δ*motAB*	ΔSO_3212 up; ΔSO_4287-86	this work
Δ*flbFup*/Δ*pomAB*/ Δ*motAB*	ΔSO_3212 up; ΔSO_1529-30*;*	this work
Δ*flbFup*/ Δ*CheA1,3*	ΔSO_3212 up; ΔSO_2121 (Δ*cheA1*)*;* ΔSO_3207 (Δ*cheA3*)	this work

Strain	Relevant genotype or phenotype	Source or reference
In frame* insertion of *AraBC* for inducible expression of *pomAB* and *motAB		
pomAB-AraBC	*pomAB::araC*-P_{BAD}-*pomAB*	this work
Δ*motAB* *pomAB-AraBC*	ΔSO_4287-86 *pomAB::araC*-P_{BAD}-*pomAB*	this work
motAB-AraBC	*motAB::araC*-P_{BAD}-*motAB*	this work
Δ*pomAB* *motABAB-AraBC*	ΔSO_1529-30*;* *motAB::araC*-P_{BAD}-*motAB*	this work
Δ*flhFup/* *pomAB-AraBC*	*pomAB::araC*-P_{BAD}-*pomAB*	this work
Δ*flhFup*/Δ*motAB* *pomAB-AraBC*	ΔSO_4287-86 *pomAB::araC*-P_{BAD}-*pomAB*	this work
Δ*flhFup/* *motAB-AraBC*	*motAB::araC*-P_{BAD}-*motAB*	this work
Δ*flhFup*/Δ*pomAB* *motAB-AraBC*	ΔSO_1529-30*;* *motAB::araC*-P_{BAD}-*motAB*	this work
***In frame* insertion of fluorescence protein fusions**		
motB-mCherry	*motB::mCherry*; Km^r; C-terminal fusion *mCherry* to *motB*	[150]
pomB-mCherry	*pomB::mCherry*; Km^r; C-terminal fusion *mCherry* to pom*B*	[150]
Δ*pomAB* *motB-mCherry*	ΔSO_1529-30*;* *motB::mCherry*; Km^r; C-terminal fusion *mCherry* to *motB*	[128]
motX-mCherry	*motX::mCherry*; Km^r; C-terminal fusion *mCherry* to *motX*	[156]
motY-mCherry	*motY::mCherry;* Km^r; C-terminal fusion *mCherry* to *motY*	[156]
Δ*motX* *motB-mCherry*	ΔSO_3936*;* *motB::mCherry*; Km^r; C-terminal fusion *mCherry* to *motB*	This work
Δ*motY* *motB-mCherry*	ΔSO_2754*;* *motB::mCherry*; Km^r; C-terminal fusion *mCherry* to *motB*	This work
Δ*motXY* *motB-mCherry*	ΔSO_3936*;* ΔSO_2754*;* *motB::mCherry*; Km^r; C-terminal fusion *mCherry* to *motB*	This work
Δ*motX* *pomB-mCherry*	ΔSO_2754*;* *pomB::mCherry*; Km^r; C-terminal fusion *mCherry* to *pomB*	[156]
Δ*motY* *pomB-mCherry*	ΔSO_2754*;* *motB::mCherry*; Km^r; C-terminal fusion *mCherry* to *pomB*	[156]
Δ*motXY* *pomB-mCherry*	ΔSO_3936*;* ΔSO_2754*;* *pomB::mCherry*; Km^r; C-terminal fusion *mCherry* to *pomB*	This work
fliN-Gfp	*fliN::gfp*	This work
Δ*flhF* *fliN-Gfp*	ΔSO_3212; *fliN::gfp*	This work
Δ*flhFup* *fliN-Gfp*	ΔSO_3212 up; *fliN::gfp*	Nathalie Heß
Δ*flhfG* *fliN-Gfp*	ΔSO_3211; *fliN::gfp*	Nathalie Heß
Δ*flhFG* *fliN-Gfp*	ΔSO_3212; ΔSO_3211; *fliN::gfp*	Nathalie Heß
pomB-sfGfp-3aa	*pomB::sfGfp;* N-terminal fusion with GGS-linker, *sfGfp* inserted after cytoplasmic aa (first 17 aa) and repetition of first 17 aa downstream of linker	This work

Table 20: Plasmids.

plasmid	relevant genotype or phenotype	Source or reference
pCR2.1-mCherry-SO	synthesized *mCherry* (monomeric), codon usage *S. oneidensis*	GenScript
pET21-sfGfp	fast maturating *gfp*	[235]
pUC18-R6KT-miniTn7T-egfp	enhanced *gfp* inserted in miniTn7T	[214]
pET21-mOrange	*mOrange* (monomeric)	Thanbichler
pUC57-mAzami-SO	Synthesized *mAzami* (monomeric); codon usage *S. oneidensis*; blunt end inserted in pUC57	GenScript (USA)
pNPTS138-R6KT	pUC origin pNPTS138 exchanged with γ-origin from pUC18R6KT-mini-Tn7T	[128]
pGP704Sac28Km	*mob*RP4$^+$ *ori*-R6K *sacB*, suicide plasmid for in frame deletions, Km^r	[229]
pBAD33	araC, oriV_{p15A} P_{BAD} promoter; Cm^r	Invitrogen (Germany)
pNPTS-*lacIq*	*lacIq* integrated in pNPTSR6KT	Lassak
Fluorescent protein fusion constructs		
pJP5603-*motB*::*mCherry*	C-terminal fusion of *motB* to *mCherry* in pJP5603, Km^r	[150]
pJP5603-*pomB*::*mCherry*	C-terminal fusion of *pomB* to *mCherry* in pJP5603, Km^r	[150]
pNPTSR6KT-*fliN-gfp*	C-terminal fusion of *gfp* to *fliN*	This work
pNPTS-*pomB17*(GGS)-*sfgfp*	N-terminal fusion of *sfgfp to pomB*; linker (GGS) inserted downstream; first 17 aa repeated	This work
pNPTS-*pomB17*$(GGS)_2$-*sfgfp*	N-terminal fusion of *sfgfp to pomB*; linker $(GGS)_2$ inserted downstream; first 17 aa repeated	This work
pNPTS-*pomB17*$(GGS)_2$-*sfgfp*	N-terminal fusion of *sfgfp to pomB*; linker $(GGS)_3$ inserted downstream; first 17 aa repeated	This work
pJP-*pomB-mAzami*	C-terminal fusion of *mAzami* to *pomB*	This work
pNPTS-*motB18-mAzami*	N-terminal fusion of *mAzami* to *motB*; first 18 aa repeated	This work
pNPTS-*pomB17-mAzami*	N-terminal fusion of *mAzami* to *pomB*; first 17 aa repeated	This work
pNPTS-*motB-gfpmut2*	N-terminal fusion of *gfpmut2* to *motB*; inserted after 2nd aa	This work
pNPTS-*motB-gfpmut3*	N-terminal fusion of *gfpmut3* to *motB*; inserted after 2nd aa	This work
pNPTS-*pomB-mOrange*	N-terminal fusion of *mOrange* to *pomB*; inserted after 2nd aa	This work
***In frame* deletion constructs**		
pGPSac28Km-Δ*pomAB*	*in frame pomAB* deletion fragment in pGPSac28Km; Km^r	[128]
pGPSac28Km-Δ*motAB*	*in frame motAB* deletion fragment in pGPSac28Km; Km^r	[128]
pGP704Sac28Km-Δ*motX*	*in frame motX* deletion fragment in pGP704Sac28-Km, Km^r	[156]
pGP704Sac28Km-Δ*motY*	*in frame motY* deletion fragment in pGP704Sac28-Km, Km^r	[156]
pNPTSR6KT-Δ*flhF*	*in frame flhF* deletion fragment in pNPTSR6KT; Km^r	This work
pNPTSR6KT-Δ*flhG*	*in frame flhG* deletion fragment in pNPTSR6KT; Km^r	This work
pNPTSR6KT-Δ*cheA1*	*in frame cheA1* deletion fragment in pNPTSR6KT; Km^r	This work
pNPTSR6KT-Δ*cheA3*	*in frame cheA3* deletion fragment in pNPTSR6KT; Km^r	This work

plasmid	relevant genotype or phenotype	Source or reference
Inducible expression constructs		
pNPTSR6KT-*motAB-AraBC*	*in frame* fusion of *araBC-*P_{BAD} to *motAB* in pNPTSR6KT; Km^r; *AraBC* amplified of pBAD33; *motAB* from MR-1	This work
pNPTSR6KT-*pomAB-AraBC*	*in frame* fusion of *araBC-*P_{BAD} to *pomAB* in pNPTSR6KT; Km^r; *AraBC* amplified of pBAD33; *pomAB* from MR-1	This work
pNPTS-R6KT-*lacIq-motAB*	*in frame* fusion of *lacIq* to *motAB* in pNPTSR6KT; Km^r; *lacIq* amplified of pNPTS-*lacIq*; *motAB* from MR-1	This work
pNPTS-R6KT-*lacIq-pomAB*	*in frame* fusion of *lacIq* to *pomAB* in pNPTSR6KT; Km^r; *lacIq* amplified of pNPTS-*lacIq*; *pomAB* from MR-1	This work
pBAD33-pomAB	*pomAB* in pBAD33; Cm^r	[128]

Table 21: Oligonucleotides

name	Sequence 5'-3'*	Restriction endonuclease
***In frame* deletion**		
PspOMI-flhF-KO-up-fw	GCG CAA GGG CCC CAA CTT ATG GAT ATG CTT GCG AAG C	*PspOMI*
flhF-up-ol-rev	CAC AGG TCA TAT TAT CTG AAC GCA TAT CTT TGG CAA AAA AAC GTT TAA TC	-
flhF-dwn-ol-fw	TTG CCA AAG ATA TGC GTT CAG ATA ATA TGA CCT GTG CAT TCG AG	-
NheI-flhF-dwn-rev	CGC TAG CAT AGG CGT CAG TAA TAG ACG TTG G	*NheI*
PspOMI-flhG-KO-up-fw	TCG TAT GGG CCC CGG TGC CTA TGA GCA ATT AGC AA	*PspOMI*
flhG-up-ol-rv	GAA AAT CTG GTC GAT GAT AGG GTT GAT TCA TCA TAC GTA AAC CAC TTG C	-
flhG-dwn-ol-fw	CAA CCC TAT CAT CGA CCA GAT TTT CAA GAG GAA AAA AC	-
NheI-flhG-KO-dwn-rev	AGC TAG CTC GTA GTA TAA CGA TAG CAC TAG C G	*NheI*
PspOMI-CheA1-KO-fw	GAT CTA GGG CCC CGG ATG ATT GGG TAA AAG TGT GC	*PspOMI*
OL-CheA1-KO-rv	CTG TGC CAG CAT ATT AAT GGA CAT AGT GCC CC	-
OL-CheA1-KO-fw	CAT TAA TAT GCT GGC ACA GCA AAT TAA GAA TTA ACT G	-
NheI-CheA1-KO-rv	GTG CAT GCC TCT TCA TCT TGG TGT TGG CG	*NheI*
PspOMI-CheA3-KO-up-fw	GAT CTA GGG CCC TGA ACA CTC TCA AGC TGA TGA TTT ATT TAG	*PspOMI*
CheA3-KO-OL-up-rv	CTA ACT TTT ATC AAA GGC CAT CAA ATT GAC TCC CA	-
CheA3-KO-OL-dwn-fw	ATG GCC TTT GAT AAA AGT TAG TTT CCA AGT TAA GGA ATG GAA	-
NheI-CheA3-KO-dwn-rv	TGC TAG CCG ATG TGC CAA TCA GCA GTA ATT TAT A	*NheI*
Inducible expression constructs		
PspOMI-pomAB-AraBC-OL-up-fw	CAT ACT GGG CCC GGT GGC TTC ATC GAA AGC GAT ATG TAC A	*PspOMI*
pomAB-AraBC-OL-up-rv	GAC GGA GGA CAT AAT ACT GAC TCT ATT GGT AAA ATA ACA CT	-
pomAB-AraBC-OL-dwn-fw	TTA TGT CCT CCG TCA AGC CGT CAA TTG TCT GAT	-
SphI-pomAB-AraBC-OL-dwn-rv	TTG CAT GCC GGT GGA CAG TTG CAC TTA GCC AT	*SphI*
SphI-motAB-AraBC-OL-dwn-rv	TTG CAT GCC ATC TTA TTA GTG CTC TAA ATA TGG ATT TAA TTG AGC T	*SphI*

name	Sequence 5'-3'*	Restriction endonuclease
motAB-AraBC-OL-dwn-fw	TTC GCC CTC CGT CAA GCC GTC AAT TGT CTG AT	-
PspOMI-motAB-AraBC-OL-up-fw	CAT ACT GGG CCC GAT GCG CTA CAG TTT ACA TCT GAT GCA AT	*PspOMI*
motAB-AraBC-OL-up-rv	TGA CGG AGG GCG AAT TTT GTT CCA AAG TAC ACA TTA TAA G	-
pomAB-RBS-Ptac-OL-dwn-fw	ATT CGA GCT CAG GAG GAT CGT TGT GGA TTT AGC TAC AAT AAT AGG ACT AGT CG	-
pomAB-RBS-Ptac-OL-dwn-SphI-rv	A AGC ATG CGC CTT CTA TCA CCC TAG GAT TTT GGC CA	*SphI*
pomAB-RBS-Ptac-OL-mid-fw	ACC GAA CCT GCA GGA TAT CTG GAT CCG TTG ACA	-
pomAB-RBS-Ptac-OL-mid-rv	AAC GAT CCT CCT GAG CTC GAA TTC CAA GCT TCT GCT GGG A	-
NheI-pomB-Ptac-OL-up-fw	A GCT AGC ACT GAG GAG CTG TAT CTT CGA GTG TAC TAA	*NheI*
pomB-Ptac-OL-up-rv	GAT ATC CTG CAG GTT CGG TTT AAC CGA CAT AAT ACT GAC TC	-
Fluorescent protein fusions		
FliN-I-fw-SphI	CAA TGC ATG CGC CAC CAT TGT CAG CCC AAC CGA AG	*SphI*
FliN-I-rv-Eco	CAT CGA ATT CCA TCT CAC TTC ACC TTT ATA ATT CTG	*EcoRI*
FliN-II-fw-Bam	AAG TGG ATC CAG TAC AGA TGA CGA TTG GGC AGC	*BamHI*
FliN-II-rv-Pst	GTT ACT GCA GCC GTT GCC GCA CTA CCT TCA TTG	*PstI*
Gfp138-fw-Eco-NL	CTT GAA TTC CGT AAA GGA GAA GAA CTT TTC AC	*EcoRI*
Gfp138-rv-G-Bam	GAA GGA TCC TCC TCC GCC TCC TTT GTA TAG	*BamHI*
PspOMI-motAB-fw	GAT CTA GGG CCC GAG GCA ATG GGT GGC TAT TGT CC	*PspOMI*
motAB-sfGFP-OL-rv	CCT TTG CTC ATA CGC TCA TGA TTT TCT GGT GGA TCA AC	-
sfGFP-motB´-OL-fw	ATC ATG AGC GTA TGA GCA AAG GAG AAG AAC TTT TCA CTG	-
sfGFP-noHis-GGS-OL-rv	CCG CCA CTG CCA CCG CTG CCG CCG GAT CCT TTG TAG AGC TCA TCC ATG CCA T	-
GGS-motB- noLys-OL-fw	GC AGT GGC GGT AGC GGC GGC TCA AAG AAA GTT GAT CCA CCA GAA AAT CAT GAG	-
motB-dwn-NheI-rv	AGC TAG CGC AGA TCC AGA TGC AAA AAA AGT ATT GTT GTC	*NheI*
PspOMI-pomAB-fw	TGA CTG GGG CCC GGA TAT TAC GCT TAC AGA GGA TCG C	*PspOMI*
pomAB-sfGFP-OL-rv	CCT TTG CTC ATC AAC CAG AGT GGC GCT CCG GG	-
sfGFP-pomB´-OL-fw	CAC TCT GGT TGA TGA GCA AAG GAG AAG AAC TTT TCA CTG	-
GGS-pomB- no3aa-OL-fw	GCA GTG GCG GTA GCG GCG GCT CAT GCA ACT GTC CAC CGC CCG GA	-
pomB-dwn-NheI-rv	AGC TAG CCT TGC TGA TTG ATC TTA TCC TGA GC	*NheI*
GGS-pomB- 3aa-OL-fw	GCA GTG GCG GTA GCG GCG GCT CAA TGG CTA AGT GCA ACT GTC CAC C	-
Bam-motB-mAz-fw	AGG ATC CGA GAG TAA TAA TGA CCT AAC AAA TGC C	*BamHI*
motB-GGS-OL-mAz-rv	AAT CAC GCT CAC GCT ACC ACC CTC AGG AAT GGG AAT ATG GCT TTC AAC	-
motB-GGS-OL-mAz-fw	CCC ATT CCT GAG GGT GGT AGC GTG AGC GTG ATT AAA CCA GAA ATG AA	-
mAzami-Kpn-rv	CTG GTA CCT TAC TTG GCT TGG CTT GGT AAC ATG	*KpnI*
Bam-pomB-mAz-fw	GGG ATC CGT TAA AGC TGA AGC TGC TGC GG	-
pomB-GGS-OL-mAZ-rv	TCA CGC TCA CGC TAC CAC CAT TTG GTT TAT CCA CTT GAA TCT CTT CC	-
pomB-GGS-OL-mAz-fw	AAC CAA ATG GTG GTA GCG TGA GCG TGA TTA AAC CAG AAA TGA	-
PspOMI-motB18-up-fw	GAT CTA GGG CCC ACG AAC TGA TTT AAA CGA GCG TGC	*PspOMI*
motB18-sfGFP-up-rv	TCT CCT TTG CTA GAA ATT AAC CAA CGC TCA TGA TTT TC	-

name	Sequence 5'-3'*	Restriction endonuclease
motB18-sfGFP-OL-fw	GTT AAT TTC TAG CAA AGG AGA AGA ACT TTT CAC TGG	-
motB18-dwn-fw	GTG GCA GTG GCG GTA GCA AAA AAA AGA AAG TTG ATC CAC CAG AAA ATC AT	-
NheI-motB-dwn-rv	TGC TAG CGT CAG CAT AAA TCT CCA TTG GCA A	*NheI*
motB18-mAzami-up-rv	TAA TCA CGC TCA CAG AAA TTA ACC AAC GCT CAT GAT TTT C	-
motB18-mAzami-OL-fw	TTA ATT TCT GTG AGC GTG ATT AAA CCA GAA ATG A	-
mAzami-GGS3-OL-rv	ACT GCC ACC GCT GCC GCC CTT GGC TTG GCT TGG TAA CAT G	-
PspOMI-pomB17-up-fw	GAT ACG GGG CCC ATT CCT TGC CCT TGA GGA AGC	*PspOMI*
pomB17-sfGFP-up-rv	TCT CCT TTG CTT GTA GCC AAC CAG AGT GGC G	-
pomB17-sfGFP-OL-fw	TGG CTA CAA GCA AAG GAG AAG AAC TTT TCA CTG G	-
pomB17-sfGFP-dwn-fw	CAG TGG CGG TAG CGC TAA GTG CAA CTG TCC ACC G	-
NheI-pomB-sfGFP-dwn-rv	TGC TAG CCA ATT TCA ATC GCA CCA TCG	*NheI*
pomB17-mAzami-up-rv	TCA CGC TCA CTG TAG CCA ACC AGA GTG GCG	-
pomB17-mAzami-OL-fw	GTT GGC TAC AGT GAG CGT GAT TAA ACC AGA AAT GA	-
"check" Primer		
chk-pomB-sfGFP-GGS-fw	ACT ATG GCC GAT GCC GCT CGT	-
chk-pomB-sfGFP-GGS-rev	CAT TCA AGC TGC TTA GGG CGT G	-
chk-motB-sfGFP-GGS-fw	CCT AAC AAA TGC CAA GAG TAA TGA CAC	-
chk-motB-sfGFP-GGS-rev	ACT ACT CTG CCT GGC ACA GAT GC	-
motB-N-chk-fw	GAG GTA ATC GCA TCT GTG CCA G	-
pomB-N-chk-fw	CGT TGT GCG CTC TGT TGG TGA	-
mAzami-chk-rv	TAC ATC TTT TCG GTG CTT GGT TCC	-
CheA1-chk-fw	GCT ATC GAC CAT GGA GTC CTT GA	-
CheA1-chk-rv	CGG CCT TAT TGG CAT AAA TGA TAT TAC G	-
chk-pomAB-SO-rv	GCA CGC CAA TCG CAT CGG TAA	-
chk-pomAB-SO-fw	TGC ATT GAC TAA CAC GCT GAT TCG	-
chk-motAB-SO-fw	ACG TTA ATG GAG CGT CAC TTT AGT TC	-
chk-motAB-SO-rv	CTG ACA CAG AAT TAT GAA CAG CCT CT	-
CheA3-SO_3207-chk-fw	CAT CAC GCT CGA GCA TGC TCA	-
CheA3-SO_3207-chk-rv	CCA TAG TGA TCA CTT GGG GAT TGA GA	-
pomAB-OE-chk-fw	GCA CGC CAA TCG CAT CGG TAA	-
pomAB-OE-chk-rv	TGC ATT GAC TAA CAC GCT GAT TCG	-
motAB-OE-chl-fw	ACG TTA ATG GAG CGT CAC TTT AGT TC	-
motAB-OE-chk-rv	CTG ACA CAG AAT TAT GAA CAG CCT CT	-

* restriction endonuclease recognition sites are underlined.

REFERENCES

1. Dobell C: **Antony van Leeuwenhoek and His "Little Animals."**. *Sonse&Danielsson, Reprinted by Dover, New York, 1960* 1932.

2. Berg HC: **The rotary motor of bacterial flagella**. *Annu Rev Biochem* 2003, **72**:19-54.

3. Bardy SL, Ng SY, Jarrell KF: **Prokaryotic motility structures**. *Microbiology* 2003, **149**:295-304.

4. Aldridge P, Hughes KT: **Regulation of flagellar assembly**. *Curr Opin Microbiol* 2002, **5**:160-165.

5. Khan S, Dapice M, Reese TS: **Effects of *mot* gene expression on the structure of the flagellar motor**. *J Mol Biol* 1988, **202**:575-584.

6. Liu J, Lin T, Botkin DJ, McCrum E, Winkler H, Norris SJ: **Intact flagellar motor of *Borrelia burgdorferi* revealed by cryo-electron tomography: evidence for stator ring curvature and rotor/C-ring assembly flexion**. *J Bacteriol* 2009, **191**:5026-5036.

7. Minamino T, Imada K, Namba K: **Molecular motors of the bacterial flagella**. *Curr Opin Struct Biol* 2008, **18**:693-701.

8. Thomas DR, Francis NR, Xu C, DeRosier DJ: **The three-dimensional structure of the flagellar rotor from a clockwise-locked mutant of *Salmonella enterica* serovar Typhimurium**. *J Bacteriol* 2006, **188**:7039-7048.

9. Chen S, Beeby M, Murphy GE, Leadbetter JR, Hendrixson DR, Briegel A, Li Z, Shi J, Tocheva EI, Muller A, et al.: **Structural diversity of bacterial flagellar motors**. *EMBO J* 2011, **30**:2972-2981.

10. Macnab RM: **How bacteria assemble flagella**. *Annu Rev Microbiol* 2003, **57**:77-100.

11. Terashima H, Fukuoka H, Yakushi T, Kojima S, Homma M: **The *Vibrio* motor proteins, MotX and MotY, are associated with the basal body of Na-driven flagella and required for stator formation**. *Mol Microbiol* 2006, **62**:1170-1180.

12. Terashima H, Koike M, Kojima S, Homma M: **The flagellar basal body-associated protein FlgT is essential for a novel ring structure in the sodium-driven *Vibrio* motor**. *J Bacteriol* 2010, **192**:5609-5615.

13. Blocker A, Komoriya K, Aizawa S: **Type III secretion systems and bacterial flagella: insights into their function from structural similarities**. *Proc Natl Acad Sci U S A* 2003, **100**:3027-3030.

14. McCarter LL: **Polar flagellar motility of the *Vibrionaceae***. *Microbiol Mol Biol Rev* 2001, **65**:445-462, table of contents.

15. Yorimitsu T, Homma M: **Na(+)-driven flagellar motor of *Vibrio***. *Biochim Biophys Acta* 2001, **1505**:82-93.

16. Blair DF: **Flagellar movement driven by proton translocation**. *FEBS Lett* 2003, **545**:86-95.

17. Xie L, Altindal T, Chattopadhyay S, Wu XL: **Bacterial flagellum as a propeller and as a rudder for efficient chemotaxis**. *Proc Natl Acad Sci U S A* 2011, **108**:2246-2251.

18. Pilizota T, Brown MT, Leake MC, Branch RW, Berry RM, Armitage JP: **A molecular brake, not a clutch, stops the *Rhodobacter sphaeroides* flagellar motor**. *Proc Natl Acad Sci U S A* 2009, **106**:11582-11587.

19. Schmitt R: ***Sinorhizobial* chemotaxis: a departure from the enterobacterial paradigm**. *Microbiology* 2002, **148**:627-631.

20. Chilcott GS, Hughes KT: **Coupling of flagellar gene expression to flagellar assembly in *Salmonella enterica* serovar typhimurium and *Escherichia coli***. *Microbiol Mol Biol Rev* 2000, **64**:694-+.

21. Komeda Y: **Transcriptional Control of Flagellar Genes in *Escherichia coli* K-12**. *J Bacteriol* 1986, **168**:1315-1318.

22. Kutsukake K, Ohya Y, Iino T: **Transcriptional Analysis of the Flagellar Regulon of *Salmonella typhimurium***. *J Bacteriol* 1990, **172**:741-747.

23. Hughes KT, Erhardt M: **Bacterial Flagella**. In *eLS*. Edited by: John Wiley & Sons, Ltd; 2011.

24. Wilhelms M, Molero R, Shaw JG, Tomas JM, Merino S: **Transcriptional Hierarchy of *Aeromonas hydrophila* Polar-Flagellum Genes**. *J Bacteriol* 2011, **193**:5179-5190.

25. Dasgupta N, Wolfgang MC, Goodman AL, Arora SK, Jyot J, Lory S, Ramphal R: **A four-tiered transcriptional regulatory circuit controls flagellar biogenesis in *Pseudomonas aeruginosa***. *Mol Microbiol* 2003, **50**:809-824.

26. Prouty MG, Correa NE, Klose KE: **The novel sigma54- and sigma28-dependent flagellar gene transcription hierarchy of *Vibrio cholerae***. *Mol Microbiol* 2001, **39**:1595-1609.

27. McCarter LL: **Regulation of flagella**. *Curr. Opin. Microbiol.* 2006, **9**:180-186.

28. Syed KA, Beyhan S, Correa N, Queen J, Liu J, Peng F, Satchell KJ, Yildiz F, Klose KE: **The *Vibrio cholerae* flagellar regulatory hierarchy controls expression of virulence factors**. *J Bacteriol* 2009, **191**:6555-6570.

29. Apel D, Surette MG: **Bringing order to a complex molecular machine: The assembly of the bacterial flagella**. *Biochim Biophys Acta* 2008, **1778**:1851-1858.

30. Kutsukake K: **Hook-length control of the export-switching machinery involves a double-locked gate in *Salmonella typhimurium* flagellar morphogenesis**. *J Bacteriol* 1997, **179**:1268-1273.

31. Chevance FFV, Hughes KT: **Coordinating assembly of a bacterial macromolecular machine**. *Nat Rev Micro* 2008, **6**:455-465.

32. Yonekura K, Maki S, Morgan DG, DeRosier DJ, Vonderviszt F, Imada K, Namba K: **The bacterial flagellar cap as the rotary promoter of flagellin self-assembly**. *Science* 2000, **290**:2148-2152.

33. Yonekura K, Maki-Yonekura S, Namba K: **Structure analysis of the flagellar cap-filament complex by electron cryomicroscopy and single-particle image analysis**. *J Struct Biol* 2001, **133**:246-253.

34. O'Brien EJ, Bennett PM: **Structure of straight flagella from a mutant *Salmonella***. *J Mol Biol* 1972, **70**:133-152.

35. Kamiya R, Hotani H, Asakura S: **Polymorphic Transition in Bacterial Flagella**. *Symposia of the Society for Experimental Biology* 1982:53-76.

36. Asakura S: **Polymorphism of bacterial flagella**. *Tanpakushitsu Kakusan Koso* 1970, **15**:1372-1381.

37. Maki-Yonekura S, Yonekura K, Namba K: **Conformational change of flagellin for polymorphic supercoiling of the flagellar filament**. *Nat Struct Mol Biol* 2010, **17**:417-U450.

38. Yonekura K, Maki-Yonekura S, Namba K: **Complete atomic model of the bacterial flagellar filament by electron cryomicroscopy**. *Nature* 2003, **424**:643-650.

39. Samatey FA, Imada K, Nagashima S, Vonderviszt F, Kumasaka T, Yamamoto M, Namba K: **Structure of the bacterial flagellar protofilament and implications for a switch for supercoiling**. *Nature* 2001, **410**:331-337.

40. DePamphilis ML, Adler J: **Fine structure and isolation of the hook-basal body complex of flagella from *Escherichia coli* and *Bacillus subtilis***. *J Bacteriol* 1971, **105**:384-395.

41. Ueno T, Oosawa K, Aizawa S: **M-ring, S-ring and proximal rod of the flagellar basal body of *Salmonella typhimurium* are composed of subunits of a single protein, FliF**. *J Mol Biol* 1992, **227**:672-677.

42. Ueno T, Oosawa K, Aizawa S: **Domain structures of the MS-ring component protein (FliF) of the flagellar basal body of *Salmonella typhimurium***. *J Mol Biol* 1994, **236**:546-555.

43. Francis NR, Sosinsky GE, Thomas D, DeRosier DJ: **Isolation, characterization and structure of bacterial flagellar motors containing the switch complex**. *J Mol Biol* 1994, **235**:1261-1270.

44. Suzuki H, Yonekura K, Namba K: **Structure of the rotor of the bacterial flagellar motor revealed by electron cryomicroscopy and single-particle image analysis**. *J Mol Biol* 2004, **337**:105-113.

45. Yamaguchi S, Aizawa S, Kihara M, Isomura M, Jones CJ, Macnab RM: **Genetic evidence for a switching and energy-transducing complex in the flagellar motor of *Salmonella typhimurium***. *J Bacteriol* 1986, **168**:1172-1179.

46. Brown PN, Terrazas M, Paul K, Blair DF: **Mutational analysis of the flagellar protein FliG: Sites of interaction with FliM and implications for organization of the switch complex**. *J Bacteriol* 2007, **189**:305-312.

47. Marykwas DL, Berg HC: **A mutational analysis of the interaction between FliG and FliM, two components of the flagellar motor of *Escherichia coli***. *J Bacteriol* 1996, **178**:1289-1294.

48. Passmore SE, Meas R, Marykwas DL: **Analysis of the FIiM/FIiG motor protein interaction by two-hybrid mutation suppression analysis**. *Microbiology-Sgm* 2008, **154**:714-724.

49. Paul K, Gonzalez-Bonet G, Bilwes AM, Crane BR, Blair D: **Architecture of the flagellar rotor**. *EMBO J* 2011, **30**:2962-2971.

50. Francis NR, Irikura VM, Yamaguchi S, Derosier DJ, Macnab RM: **Localization of the *Salmonella* typhimurium Flagellar Switch Protein FliG to the Cytoplasmic M-Ring Face of the Basal Body**. *Proc Natl Acad Sci U S A* 1992, **89**:6304-6308.

51. Kihara M, Miller GU, Macnab RM: **Deletion analysis of the flagellar switch protein FliG of *Salmonella***. *J Bacteriol* 2000, **182**:3022-3028.

52. Kojima S, Blair DF: **Solubilization and purification of the MotA/MotB complex of *Escherichia coli***. *Biochemistry* 2004, **43**:26-34.

53. Sato K, Homma M: **Multimeric structure of PomA, a component of the Na+-driven polar flagellar motor of *Vibrio alginolyticus***. *J Biol Chem* 2000, **275**:20223-20228.

54. Braun TF, Al-Mawsawi LQ, Kojima S, Blair DF: **Arrangement of core membrane segments in the MotA/MotB proton-channel complex of *Escherichia coli***. *Biochemistry* 2004, **43**:35-45.

55. Sato K, Homma M: **Functional reconstitution of the Na+-driven polar flagellar motor component of *Vibrio alginolyticus***. *J Biol Chem* 2000, **275**:5718-5722.

56. Dean GE, Macnab RM, Stader J, Matsumura P, Burks C: **Gene Sequence and Predicted Amino-Acid-Sequence of the MotA Protein, a Membrane-Associated Protein Required for Flagellar Rotation in *Escherichia coli***. *J Bacteriol* 1984, **159**:991-999.

57. Sharp LL, Zhou J, Blair DF: **Tryptophan-scanning mutagenesis of MotB, an integral membrane protein essential for flagellar rotation in *Escherichia coli***. *Biochemistry* 1995, **34**:9166-9171.

58. Lloyd SA, Tang H, Wang X, Billings S, Blair DF: **Torque generation in the flagellar motor of *Escherichia coli:* evidence of a direct role for FliG but not for FliM or FliN**. *J Bacteriol* 1996, **178**:223-231.

59. Yorimitsu T, Mimaki A, Yakushi T, Homma M: **The conserved charged residues of the C-terminal region of FliG, a rotor component of the Na+-driven flagellar motor**. *J Mol Biol* 2003, **334**:567-583.

60. Zhou J, Lloyd SA, Blair DF: **Electrostatic interactions between rotor and stator in the bacterial flagellar motor**. *Proc Natl Acad Sci U S A* 1998, **95**:6436-6441.

61. De Mot R, Vanderleyden J: **The C-terminal sequence conservation between OmpA-related outer membrane proteins and MotB suggests a common function in both gram-positive and gram-negative bacteria, possibly in the interaction of these domains with peptidoglycan**. *Mol Microbiol* 1994, **12**:333-334.

62. Braun TF, Blair DF: **Targeted disulfide cross-linking of the MotB protein of *Escherichia coli*: evidence for two H(+) channels in the stator complex**. *Biochemistry* 2001, **40**:13051-13059.

63. McCarter LL: **MotX, the channel component of the sodium-type flagellar motor**. *J Bacteriol* 1994, **176**:5988-5998.

64. McCarter LL: **MotY, a component of the sodium-type flagellar motor**. *J Bacteriol* 1994, **176**:4219-4225.

65. Okabe M, Yakushi T, Asai Y, Homma M: **Cloning and characterization of *motX*, a *Vibrio alginolyticus* sodium-driven flagellar motor gene**. *J Biochem* 2001, **130**:879-884.

66. Kojima S, Furukawa Y, Matsunami H, Minamino T, Namba K: **Characterization of the periplasmic domain of MotB and implications for its role in the stator assembly of the bacterial flagellar motor**. *J Bacteriol* 2008, **190**:3314-3322.

67. Stewart BJ, McCarter LL: **Lateral flagellar gene system of *Vibrio parahaemolyticus***. *J Bacteriol* 2003, **185**:4508-4518.

68. Kim EA, Price-Carter M, Carlquist WC, Blair DF: **Membrane segment organization in the stator complex of the flagellar motor: implications for proton flow and proton-induced conformational change**. *Biochemistry* 2008, **47**:11332-11339.

69. Delalez N, Armitage JP: **Parts exchange: tuning the flagellar motor to fit the conditions**. *Mol Microbiol* 2009, **71**:807-810.

70. Silverman M, Simon M: **Flagellar rotation and the mechanism of bacterial motility**. *Nature* 1974, **249**:73-74.

71. Larsen SH, Adler J, Gargus JJ, Hogg RW: **Chemomechanical coupling without ATP: the source of energy for motility and chemotaxis in bacteria**. *Proc Natl Acad Sci U S A* 1974, **71**:1239-1243.

72. Sowa Y, Berry RM: **Bacterial flagellar motor**. *Q Rev Biophys* 2008, **41**:103-132.

73. Lowe G, Meister M, Berg HC: **Rapid Rotation of Flagellar Bundles in Swimming Bacteria**. *Nature* 1987, **325**:637-640.

74. Sowa Y, Hotta H, Homma M, Ishijima A: **Torque-speed relationship of the Na+-driven flagellar motor of *Vibrio alginolyticus***. *J Mol Biol* 2003, **327**:1043-1051.

75. Blair DF, Berg HC: **The MotA protein of *E. coli* is a proton-conducting component of the flagellar motor**. *Cell* 1990, **60**:439-449.

76. Block SM, Berg HC: **Successive incorporation of force-generating units in the bacterial rotary motor**. *Nature* 1984, **309**:470-472.

77. Chen X, Berg HC: **Torque-speed relationship of the flagellar rotary motor of *Escherichia coli***. *Biophys J* 2000, **78**:1036-1041.

78. Ryu WS, Berry RM, Berg HC: **Torque-generating units of the flagellar motor of *Escherichia coli* have a high duty ratio**. *Nature* 2000, **403**:444-447.

79. Berg HC, Turner L: **Torque generated by the flagellar motor of *Escherichia coli***. *Biophys J* 1993, **65**:2201-2216.

80. Berry RM, Berg HC: **Torque generated by the flagellar motor of *Escherichia coli* while driven backward**. *Biophys J* 1999, **76**:580-587.

81. Washizu M, Kurahashi Y, Iochi H, Kurosawa O, Aizawa S, Kudo S, Magariyama Y, Hotani H: **Dielectrophoretic Measurement of Bacterial Motor Characteristics**. *Ieee Transactions on Industry Applications* 1993, **29**:286-294.

82. Silverman M, Matsumura P, Simon M: **The identification of the *mot* gene product with *Escherichia coli*-lambda hybrids**. *Proc Natl Acad Sci U S A* 1976, **73**:3126-3130.

83. Yuan J, Berg HC: **Resurrection of the flagellar rotary motor near zero load**. *Proc Natl Acad Sci U S A* 2008, **105**:1182-1185.

84. Magariyama Y, Sugiyama S, Muramoto K, Maekawa Y, Kawagishi I, Imae Y, Kudo S: **Very fast flagellar rotation**. *Nature* 1994, **371**:752.

85. Meister M, Lowe G, Berg HC: **The proton flux through the bacterial flagellar motor**. *Cell* 1987, **49**:643-650.

86. Blair DF: **Structure and Mechanism of the Flagellar Rotary Motor**. In *Pili and Flagella: Current Research and Future Trends*. Edited by Jarrell KF: Caister Academic Press; 2009.

87. Porter SL, Wadhams GH, Armitage JP: **Signal processing in complex chemotaxis pathways**. *Nat Rev Microbiol* 2011, **9**:153-165.

88. Dyer CM, Vartanian AS, Zhou H, Dahlquist FW: **A molecular mechanism of bacterial flagellar motor switching**. *J Mol Biol* 2009, **388**:71-84.

89. Sarkar MK, Paul K, Blair D: **Chemotaxis signaling protein CheY binds to the rotor protein FliN to control the direction of flagellar rotation in *Escherichia coli***. *Proc Natl Acad Sci U S A* 2010, **107**:9370-9375.

90. Welch M, Oosawa K, Aizawa S, Eisenbach M: **Phosphorylation-dependent binding of a signal molecule to the flagellar switch of bacteria**. *Proc Natl Acad Sci U S A* 1993, **90**:8787-8791.

91. Bai F, Branch RW, Nicolau DV, Jr., Pilizota T, Steel BC, Maini PK, Berry RM: **Conformational spread as a mechanism for cooperativity in the bacterial flagellar switch**. *Science* 2010, **327**:685-689.

92. Cluzel P, Surette M, Leibler S: **An ultrasensitive bacterial motor revealed by monitoring signaling proteins in single cells**. *Science* 2000, **287**:1652-1655.

93. Thomas DR, Morgan DG, DeRosier DJ: **Rotational symmetry of the C-ring and a mechanism for the flagellar rotary motor**. *Proc Natl Acad Sci U S A* 1999, **96**:10134-10139.

94. Asai Y, Kojima S, Kato H, Nishioka N, Kawagishi I, Homma M: **Putative channel components for the fast-rotating sodium-driven flagellar motor of a marine bacterium**. *J Bacteriol* 1997, **179**:5104-5110.

95. Lloyd SA, Blair DF: **Charged residues of the rotor protein FliG essential for torque generation in the flagellar motor of *Escherichia coli***. *J Mol Biol* 1997, **266**:733-744.

96. Sowa Y, Rowe AD, Leake MC, Yakushi T, Homma M, Ishijima A, Berry RM: **Direct observation of steps in rotation of the bacterial flagellar motor**. *Nature* 2005, **437**:916-919.

97. Zhou J, Blair DF: **Residues of the cytoplasmic domain of MotA essential for torque generation in the bacterial flagellar motor**. *J Mol Biol* 1997, **273**:428-439.

98. Zhou J, Sharp LL, Tang HL, Lloyd SA, Billings S, Braun TF, Blair DF: **Function of protonatable residues in the flagellar motor of *Escherichia coli*: a critical role for Asp 32 of MotB**. *J Bacteriol* 1998, **180**:2729-2735.

99. Asai Y, Yakushi T, Kawagishi I, Homma M: **Ion-coupling determinants of Na+-driven and H+-driven flagellar motors**. *J Mol Biol* 2003, **327**:453-463.

100. Gosink KK, Hase CC: **Requirements for conversion of the Na(+)-driven flagellar motor of *Vibrio cholerae* to the H(+)-driven motor of *Escherichia coli***. *J Bacteriol* 2000, **182**:4234-4240.

101. Yakushi T, Yang J, Fukuoka H, Homma M, Blair DF: **Roles of charged residues of rotor and stator in flagellar rotation: comparative study using H+-driven and Na+-driven motors in *Escherichia coli***. *J Bacteriol* 2006, **188**:1466-1472.

102. Yorimitsu T, Sowa Y, Ishijima A, Yakushi T, Homma M: **The systematic substitutions around the conserved charged residues of the cytoplasmic loop of Na+-driven flagellar motor component PomA**. *J Mol Biol* 2002, **320**:403-413.

103. Fukuoka H, Yakushi T, Kusumoto A, Homma M: **Assembly of motor proteins, PomA and PomB, in the Na+-driven stator of the flagellar motor**. *J Mol Biol* 2005, **351**:707-717.

104. Leake MC, Chandler JH, Wadhams GH, Bai F, Berry RM, Armitage JP: **Stoichiometry and turnover in single, functioning membrane protein complexes**. *Nature* 2006, **443**:355-358.

105. Hosking ER, Vogt C, Bakker EP, Manson MD: **The *Escherichia coli* MotAB proton channel unplugged**. *J Mol Biol* 2006, **364**:921-937.

106. Van Way SM, Hosking ER, Braun TF, Manson MD: **Mot protein assembly into the bacterial flagellum: a model based on mutational analysis of the *motB* gene**. *J Mol Biol* 2000, **297**:7-24.

107. Blair DF, Berg HC: **Restoration of torque in defective flagellar motors**. *Science* 1988, **242**:1678-1681.

108. Reid SW, Leake MC, Chandler JH, Lo CJ, Armitage JP, Berry RM: **The maximum number of torque-generating units in the flagellar motor of *Escherichia coli* is at least 11**. *Proc Natl Acad Sci U S A* 2006, **103**:8066-8071.

109. Fukuoka H, Wada T, Kojima S, Ishijima A, Homma M: **Sodium-dependent dynamic assembly of membrane complexes in sodium-driven flagellar motors**. *Mol Microbiol* 2009, **71**:825-835.

110. Fukuoka H, Inoue Y, Terasawa S, Takahashi H, Ishijima A: **Exchange of rotor components in functioning bacterial flagellar motor**. *Biochem Biophys Res Commun* 2010, **394**:130-135.

111. Delalez NJ, Wadhams GH, Rosser G, Xue Q, Brown MT, Dobbie IM, Berry RM, Leake MC, Armitage JP: **Signal-dependent turnover of the bacterial flagellar switch protein FliM**. *Proc Natl Acad Sci U S A* 2010, **107**:11347-11351.

112. Derby H. HB: **Bacteriology of butter. IV. Bacteriological studies of surface taint butter**. *Iowa Agric. Ecp. Stn. Res. Bull.* 1931, **145**:387-416.

113. Long H. HB: **Classification of organisms important in dairy products. III. *Pseudomonas putrefaciens.*** *Iowa Agric. Exp. Stn. Res. Bull.* 1941, **285**:176-195.

114. Baumann L, Baumann P, Mandel M, Allen RD: **Taxonomy of aerobic marine eubacteria**. *J Bacteriol* 1972, **110**:402-429.

115. MacDonell M. CR: **Phylogeny of the *Vibrionaceae*, and recommendation for two new genera, *Listonella* and *Shewanella***. *Syst. appl. Microbiol* 1985, **6**:171-182.

116. Hau HH, Gralnick JA: **Ecology and biotechnology of the genus *Shewanella***. *Annu Rev Microbiol* 2007, **61**:237-258.

117. Venkateswaran K, Moser DP, Dollhopf ME, Lies DP, Saffarini DA, MacGregor BJ, Ringelberg DB, White DC, Nishijima M, Sano H, et al.: **Polyphasic taxonomy of the genus *Shewanella* and description of *Shewanella oneidensis* sp. nov**. *Int J Syst Bacteriol* 1999, **49 Pt 2**:705-724.

118. Lovley DR: **Dissimilatory metal reduction**. *Annu Rev Microbiol* 1993, **47**:263-290.

119. Myers CR, Nealson KH: **Bacterial manganese reduction and growth with manganese oxide as the sole electron acceptor**. *Science* 1988, **240**:1319-1321.

120. Caccavo F, Blakemore RP, Lovley DR: **A Hydrogen-Oxidizing, Fe(III)-Reducing Microorganism from the Great Bay Estuary, New Hampshire**. *Appl Environ Microbiol* 1992, **58**:3211-3216.

121. Wielinga B, Mizuba MM, Hansel CM, Fendorf S: **Iron promoted reduction of chromate by dissimilatory iron-reducing bacteria**. *Environ Sci Technol* 2001, **35**:522-527.

122. Farrenkopf AM, Dollhopf ME, NiChadhain S, Luther GW, Nealson KH: **Reduction of iodate in seawater during Arabian Sea shipboard incubations and in laboratory cultures of the marine bacterium *Shewanella putrefaciens* strain MR-4**. *Marine Chemistry* 1997, **57**:347-354.

123. Wildung RE, Gorby YA, Krupka KM, Hess NJ, Li SW, Plymale AE, McKinley JP, Fredrickson JK: **Effect of electron donor and solution chemistry on products of dissimilatory reduction of technetium by *Shewanella putrefaciens***. *Appl Environ Microbiol* 2000, **66**:2451-2460.

124. Lloyd JR, Yong P, Macaskie LE: **Biological reduction and removal of Np(V) by two microorganisms**. *Environ Sci Technol* 2000, **34**:1297-1301.

125. Boukhalfa H, Icopini GA, Reilly SD, Neu MP: **Plutonium(IV) reduction by the metal-reducing bacteria *Geobacter metallireducens* GS15 and *Shewanella oneidensis* MR-1**. *Appl Environ Microbiol* 2007, **73**:5897-5903.

126. Klonowska A, Heulin T, Vermeglio A: **Selenite and tellurite reduction by *Shewanella oneidensis***. *Appl Environ Microbiol* 2005, **71**:5607-5609.

127. Carpentier W, Sandra K, De Smet I, Brige A, De Smet L, Van Beeumen J: **Microbial reduction and precipitation of vanadium by *Shewanella oneidensis***. *Appl Environ Microbiol* 2003, **69**:3636-3639.

128. Paulick A, Koerdt A, Lassak J, Huntley S, Wilms I, Narberhaus F, Thormann KM: **Two different stator systems drive a single polar flagellum in *Shewanella oneidensis* MR-1**. *Mol Microbiol* 2009, **71**:836-850.

129. Wang F, Wang J, Jian H, Zhang B, Li S, Zeng X, Gao L, Bartlett DH, Yu J, Hu S, et al.: **Environmental adaptation: genomic analysis of the piezotolerant and psychrotolerant deep-sea iron reducing bacterium *Shewanella piezotolerans* WP3**. *PLoS One* 2008, **3**:e1937.

130. Bubendorfer S, Held S, Windel N, Paulick A, Klingl A, Thormann KM: **Specificity of motor components in the dual flagellar system of *Shewanella putrefaciens* CN-32**. *Mol Microbiol* 2011.

131. Venkateswaran K, Dollhopf ME, Aller R, Stackebrandt E, Nealson KH: ***Shewanella amazonensis sp. nov.*, a novel metal-reducing facultative anaerobe from Amazonian shelf muds**. *Int J Syst Bacteriol* 1998, **48 Pt 3**:965-972.

132. Brettar I, Moore ER, Hofle MG: **Phylogeny and Abundance of Novel Denitrifying Bacteria Isolated from the Water Column of the Central Baltic Sea**. *Microb Ecol* 2001, **42**:295-305.

133. Brettar I, Christen R, Hofle MG: ***Shewanella denitrificans* sp. nov., a vigorously denitrifying bacterium isolated from the oxic-anoxic interface of the Gotland Deep in the central Baltic Sea**. *Int J Syst Evol Microbiol* 2002, **52**:2211-2217.

134. Bowman JP, McCammon SA, Nichols DS, Skerratt JH, Rea SM, Nichols PD, McMeekin TA: ***Shewanella gelidimarina sp. nov.* and *Shewanella frigidimarina sp. nov.*, novel Antarctic species with the ability to produce eicosapentaenoic acid (20:5 omega 3) and grow anaerobically by dissimilatory Fe(III) reduction**. *Int J Syst Bacteriol* 1997, **47**:1040-1047.

135. Gao H, Obraztova A, Stewart N, Popa R, Fredrickson JK, Tiedje JM, Nealson KH, Zhou J: ***Shewanella loihica sp. nov.*, isolated from iron-rich microbial mats in the Pacific Ocean**. *Int J Syst Evol Microbiol* 2006, **56**:1911-1916.

136. Heidelberg JF, Paulsen IT, Nelson KE, Gaidos EJ, Nelson WC, Read TD, Eisen JA, Seshadri R, Ward N, Methe B, et al.: **Genome sequence of the dissimilatory metal ion-reducing bacterium *Shewanella oneidensis***. *Nat Biotechnol* 2002, **20**:1118-1123.

137. Leonardo MR, Moser DP, Barbieri E, Brantner CA, MacGregor BJ, Paster BJ, Stackebrandt E, Nealson KH: ***Shewanella pealeana* sp. nov., a member of the microbial community**

associated with the accessory nidamental gland of the squid *Loligo pealei*. *Int J Syst Bacteriol* 1999, **49 Pt 4**:1341-1351.

138. Wang F, Wang P, Chen M, Xiao X: **Isolation of extremophiles with the detection and retrieval of *Shewanella* strains in deep-sea sediments from the west Pacific**. *Extremophiles* 2004, **8**:165-168.

139. Obuekwe CO, Westlake DW: **Effects of medium composition on cell pigmentation, cytochrome content, and ferric iron reduction in a *Pseudomonas sp.* isolated from crude oil**. *Can J Microbiol* 1982, **28**:989-992.

140. Zhao JS, Manno D, Beaulieu C, Paquet L, Hawari J: ***Shewanella sediminis sp nov.*, a novel Na+-requiring and hexahydro-1,3,5-trinitro-1,3,5-trinitro-degrading bacterium from marine sediment**. *Int J Syst Evol Microbiol* 2005, **55**:1511-1520.

141. Saltikov CW, Cifuentes A, Venkateswaran K, Newman DK: **The ars detoxification system is advantageous but not required for As(V) respiration by the genetically tractable *Shewanella species* strain ANA-3**. *Appl Environ Microbiol* 2003, **69**:2800-2809.

142. Nealson KH, Myers CR, Wimpee BB: **Isolation and identification of manganese-reducing bacteria and estimates of microbial Mn(IV)-reducing potential in the Black-Sea**. *Deep-Sea Research Part a-Oceanographic Research Papers* 1991, **38**:S907-S920.

143. Murray AE, Lies D, Li G, Nealson K, Zhou J, Tiedje JM: **DNA/DNA hybridization to microarrays reveals gene-specific differences between closely related microbial genomes**. *Proc Natl Acad Sci U S A* 2001, **98**:9853-9858.

144. Makemson JC, Fulayfil NR, Landry W, Van Ert LM, Wimpee CF, Widder EA, Case JF: ***Shewanella woodyi sp. nov.*, an exclusively respiratory luminous bacterium isolated from the Alboran Sea**. *Int J Syst Bacteriol* 1997, **47**:1034-1039.

145. Liu Y, Gao W, Wang Y, Wu L, Liu X, Yan T, Alm E, Arkin A, Thompson DK, Fields MW, et al.: **Transcriptome analysis of *Shewanella oneidensis* MR-1 in response to elevated salt conditions**. *J Bacteriol* 2005, **187**:2501-2507.

146. Bencharit S, Ward MJ: **Chemotactic responses to metals and anaerobic electron acceptors in *Shewanella oneidensis* MR-1**. *J Bacteriol* 2005, **187**:5049-5053.

147. Thormann KM, Saville RM, Shukla S, Pelletier DA, Spormann AM: **Initial Phases of biofilm formation in *Shewanella oneidensis* MR-1**. *J Bacteriol* 2004, **186**:8096-8104.

148. Li J, Romine MF, Ward MJ: **Identification and analysis of a highly conserved chemotaxis gene cluster in *Shewanella* species**. *FEMS Microbiol Lett* 2007, **273**:180-186.

149. Atsumi T, McCarter L, Imae Y: **Polar and lateral flagellar motors of marine *Vibrio* are driven by different ion-motive forces**. *Nature* 1992, **355**:182-184.

150. Paulick A: **Einfluss und Aufbau des Flagellenmotors auf die Biofilmbildung in *Shewanella oneidensis* MR-1**. Bochum: Ruhr Universität Bochum; 2007, Diploma thesis.

151. Atsumi T, Maekawa Y, Tokuda H, Imae Y: **Amiloride at pH 7.0 inhibits the Na(+)-driven flagellar motors of *Vibrio alginolyticus* but allows cell growth**. *FEBS Lett* 1992, **314**:114-116.

152. Kojima S, Yamamoto K, Kawagishi I, Homma M: **The polar flagellar motor of *Vibrio cholerae* is driven by an Na+ motive force**. *J Bacteriol* 1999, **181**:1927-1930.

153. Koerdt A: **Lokalisation der Statorkomplexe MotAB und PomAB und der Proteine MotX und MotY in *Shewanella oneidensis* MR-1**. Marburg: Philipps University Marburg; 2008, M.Sc. thesis.

154. Okabe M, Yakushi T, Homma M: **Interactions of MotX with MotY and with the PomA/PomB sodium ion channel complex of the *Vibrio alginolyticus* polar flagellum**. *J Biol Chem* 2005, **280**:25659-25664.

155. Okabe M, Yakushi T, Kojima M, Homma M: **MotX and MotY, specific components of the sodium-driven flagellar motor, colocalize to the outer membrane in *Vibrio alginolyticus***. *Mol Microbiol* 2002, **46**:125-134.

156. Koerdt A, Paulick A, Mock M, Jost K, Thormann KM: **MotX and MotY are required for flagellar rotation in *Shewanella oneidensis* MR-1**. *J Bacteriol* 2009, **191**:5085-5093.

157. Grant B, Greenwald I: **The *Caenorhabditis elegans sel-1* gene, a negative regulator of *lin-12* and *glp-1*, encodes a predicted extracellular protein**. *Genetics* 1996, **143**:237-247.

158. Mittl PR, Schneider-Brachert W: **Sel1-like repeat proteins in signal transduction**. *Cell Signal* 2007, **19**:20-31.

159. Wu L, Wang J, Tang P, Chen H, Gao H: **Genetic and molecular characterization of flagellar assembly in *Shewanella oneidensis***. *PLoS One* 2011, **6**:e21479.

160. Dohlich K: **Flagellare Untereinheiten des Filaments aus *Shewanella oneidensis* MR-1**. Marburg: Ruhr-Universität Bochum; 2009, M.Sc. thesis

161. Thompson JD, Gibson TJ, Plewniak F, Jeanmougin F, Higgins DG: **The CLUSTAL_X windows interface: flexible strategies for multiple sequence alignment aided by quality analysis tools**. *Nucleic Acids Res* 1997, **25**:4876-4882.

162. Arnold K, Bordoli L, Kopp J, Schwede T: **The SWISS-MODEL workspace: a web-based environment for protein structure homology modelling**. *Bioinformatics* 2006, **22**:195-201.

163. Guex N, Peitsch MC: **SWISS-MODEL and the Swiss-PdbViewer: an environment for comparative protein modeling**. *Electrophoresis* 1997, **18**:2714-2723.

164. Schwede T, Kopp J, Guex N, Peitsch MC: **SWISS-MODEL: An automated protein homology-modeling server**. *Nucleic Acids Res* 2003, **31**:3381-3385.

165. Kuwajima G: **Construction of a minimum-size functional flagellin of *Escherichia coli***. *J Bacteriol* 1988, **170**:3305-3309.

166. Correa NE, Peng F, Klose KE: **Roles of the regulatory proteins FlhF and FlhG in the *Vibrio cholerae* flagellar transcription hierarchy**. *J Bacteriol* 2005, **187**:6324-6332.

167. Kojima M, Nishioka N, Kusumoto A, Yagasaki J, Fukuda T, Homma M: **Conversion of mono-polar to peritrichous flagellation in *Vibrio alginolyticus***. *Microbiol Immunol* 2011, **55**:76-83.

168. Kusumoto A, Kamisaka K, Yakushi T, Terashima H, Shinohara A, Homma M: **Regulation of polar flagellar number by the *flhF* and *flhG* genes in *Vibrio alginolyticus***. *J Biochem* 2006, **139**:113-121.

169. Kusumoto A, Nishioka N, Kojima S, Homma M: **Mutational analysis of the GTP-binding motif of FlhF which regulates the number and placement of the polar flagellum in *Vibrio alginolyticus***. *J Biochem* 2009, **146**:643-650.

170. Kusumoto A, Shinohara A, Terashima H, Kojima S, Yakushi T, Homma M: **Collaboration of FlhF and FlhG to regulate polar-flagella number and localization in *Vibrio alginolyticus***. *Microbiology* 2008, **154**:1390-1399.

171. Murray TS, Kazmierczak BI: **FlhF is required for swimming and swarming in *Pseudomonas aeruginosa***. *J Bacteriol* 2006, **188**:6995-7004.

172. Pandza S, Baetens M, Park CH, Au T, Keyhan M, Matin A: **The G-protein FlhF has a role in polar flagellar placement and general stress response induction in *Pseudomonas putida***. *Mol Microbiol* 2000, **36**:414-423.

173. Breakwell DP, Moyes RB, Reynolds J: **Differential staining of bacteria: flagella stain**. *Curr Protoc Microbiol* 2009, **Appendix 3**:Appendix 3G.

174. Heß N: **Einfluss von FlhF und FlhG auf die Motilität von *S. oneidensis* MR-1**. Marburg: Philipps University Marburg; 2010, B.Sc. thesis

175. Scharf BE, Fahrner KA, Turner L, Berg HC: **Control of direction of flagellar rotation in bacterial chemotaxis**. *Proc Natl Acad Sci U S A* 1998, **95**:201-206.

176. Thormann KM, Duttler S, Saville RM, Hyodo M, Shukla S, Hayakawa Y, Spormann AM: **Control of formation and cellular detachment from *Shewanella oneidensis* MR-1 biofilms by cyclic di-GMP**. *J Bacteriol* 2006, **188**:2681-2691.

177. Toft C, Fares MA: **The evolution of the flagellar assembly pathway in endosymbiotic bacterial genomes**. *Mol Biol Evol* 2008, **25**:2069-2076.

178. McCarter LL: **Dual flagellar systems enable motility under different circumstances**. *J Mol Microbiol Biotechnol* 2004, **7**:18-29.

179. Doyle TB, Hawkins AC, McCarter LL: **The complex flagellar torque generator of *Pseudomonas aeruginosa***. *J Bacteriol* 2004, **186**:6341-6350.

180. Toutain CM, Zegans ME, O'Toole GA: **Evidence for two flagellar stators and their role in the motility of *Pseudomonas aeruginosa***. *J Bacteriol* 2005, **187**:771-777.

181. Wilhelms M, Vilches S, Molero R, Shaw JG, Tomas JM, Merino S: **Two redundant sodium-driven stator motor proteins are involved in *Aeromonas hydrophila* polar flagellum rotation**. *J Bacteriol* 2009, **191**:2206-2217.

182. Ito M, Hicks DB, Henkin TM, Guffanti AA, Powers BD, Zvi L, Uematsu K, Krulwich TA: **MotPS is the stator-force generator for motility of alkaliphilic *Bacillus,* and its homologue is a second functional Mot in *Bacillus subtilis***. *Mol Microbiol* 2004, **53**:1035-1049.

183. Allen RD, Baumann P: **Structure and arrangement of flagella in species of the genus *Beneckea* and *Photobacterium fischeri***. *J Bacteriol* 1971, **107**:295-302.

184. McCarter L, Silverman M: **Surface-induced swarmer cell differentiation of *Vibrio parahaemolyticus***. *Mol Microbiol* 1990, **4**:1057-1062.

185. Shinoda S, Okamoto K: **Formation and function of *Vibrio parahaemolyticus* lateral flagella**. *J Bacteriol* 1977, **129**:1266-1271.

186. Canals R, Altarriba M, Vilches S, Horsburgh G, Shaw JG, Tomas JM, Merino S: **Analysis of the lateral flagellar gene system of *Aeromonas hydrophila* AH-3**. *J Bacteriol* 2006, **188**:852-862.

187. Merino S, Shaw JG, Tomas JM: **Bacterial lateral flagella: an inducible flagella system**. *FEMS Microbiol Lett* 2006, **263**:127-135.

188. Shimada T, Sakazaki R, Suzuki K: **Peritrichous flagella in mesophilic strains of *Aeromonas***. *Jpn J Med Sci Biol* 1985, **38**:141-145.

189. Toutain CM, Caizza NC, Zegans ME, O'Toole GA: **Roles for flagellar stators in biofilm formation by *Pseudomonas aeruginosa***. *Res Microbiol* 2007, **158**:471-477.

190. Morehouse KA, Hobley L, Capeness M, Sockett RE: **Three *motAB* stator gene products in *Bdellovibrio bacteriovorus* contribute to motility of a single flagellum during predatory and prey-independent growth**. *J Bacteriol* 2011, **193**:932-943.

191. Venter JC, Remington K, Heidelberg JF, Halpern AL, Rusch D, Eisen JA, Wu D, Paulsen I, Nelson KE, Nelson W, et al.: **Environmental genome shotgun sequencing of the Sargasso Sea**. *Science* 2004, **304**:66-74.

192. Romine MF, Carlson TS, Norbeck AD, McCue LA, Lipton MS: **Identification of mobile elements and pseudogenes in the *Shewanella oneidensis* MR-1 genome**. *Appl Environ Microbiol* 2008, **74**:3257-3265.

193. Lassak J: **Evolution von Zwei-Komponenten-Systemen in *Shewanella oneidensis* MR-1: Die Histidinkinase ArcS und der Antwortregulator SO_4444, Zwei Komponenten, Zwei Modelle.** Marburg: Philipps University Marburg; 2010, PhD thesis vol Dr. rer. nat.

194. Hosking ER, Manson MD: **Clusters of charged residues at the C-terminus of MotA and N-terminus of MotB are important for function of the *Escherichia coli* flagellar motor**. *J Bacteriol* 2008, **190**:5517-5521.

195. Terahara N, Fujisawa M, Powers B, Henkin TM, Krulwich TA, Ito M: **An intergenic stem-loop mutation in the *Bacillus subtilis ccpA-motPS* operon increases *motPS* transcription and the MotPS contribution to motility**. *J Bacteriol* 2006, **188**:2701-2705.

196. Fujinami S, Terahara N, Lee S, Ito M: **Na(+) and flagella-dependent swimming of alkaliphilic *Bacillus pseudofirmus* OF4: a basis for poor motility at low pH and enhancement in viscous media in an "up-motile" variant**. *Arch Microbiol* 2007, **187**:239-247.

197. Chun SY, Parkinson JS: **Bacterial motility: membrane topology of the *Escherichia coli* MotB protein**. *Science* 1988, **239**:276-278.

198. Stader J, Matsumura P, Vacante D, Dean GE, Macnab RM: **Nucleotide sequence of the *Escherichia coli motB* gene and site-limited incorporation of its product into the cytoplasmic membrane**. *J Bacteriol* 1986, **166**:244-252.

199. Koebnik R: **Proposal for a peptidoglycan-associating alpha-helical motif in the C-terminal regions of some bacterial cell-surface proteins**. *Mol Microbiol* 1995, **16**:1269-1270.

200. Stolz B, Berg HC: **Evidence for interactions between MotA and MotB, torque-generating elements of the flagellar motor of *Escherichia coli***. *J Bacteriol* 1991, **173**:7033-7037.

201. Li N, Kojima S, Homma M: **Characterization of the periplasmic region of PomB, a Na+-driven flagellar stator protein in *Vibrio alginolyticus***. *J Bacteriol* 2011, **193**:3773-3784.

202. Jones DT: **Protein secondary structure prediction based on position-specific scoring matrices**. *J Mol Biol* 1999, **292**:195-202.

203. Hizukuri Y, Kojima S, Homma M: **Disulphide cross-linking between the stator and the bearing components in the bacterial flagellar motor**. *J Biochem* 2010, **148**:309-318.

204. Kojima S, Imada K, Sakuma M, Sudo Y, Kojima C, Minamino T, Homma M, Namba K: **Stator assembly and activation mechanism of the flagellar motor by the periplasmic region of MotB**. *Mol Microbiol* 2009, **73**:710-718.

205. O'Neill J, Xie M, Hijnen M, Roujeinikova A: **Role of the MotB linker in the assembly and activation of the bacterial flagellar motor**. *Acta Crystallogr D Biol Crystallogr* 2011, **67**:1009-1016.

206. Inoue Y, Lo CJ, Fukuoka H, Takahashi H, Sowa Y, Pilizota T, Wadhams GH, Homma M, Berry RM, Ishijima A: **Torque-speed relationships of Na+-driven chimeric flagellar motors in *Escherichia coli***. *J Mol Biol* 2008, **376**:1251-1259.

207. Morimoto YV, Nakamura S, Kami-ike N, Namba K, Minamino T: **Charged residues in the cytoplasmic loop of MotA are required for stator assembly into the bacterial flagellar motor**. *Mol Microbiol* 2010, **78**:1117-1129.

208. Okunishi I, Kawagishi I, Homma M: **Cloning and characterization of *motY*, a gene coding for a component of the sodium-driven flagellar motor in *Vibrio alginolyticus***. *J Bacteriol* 1996, **178**:2409-2415.

209. Kojima S, Shinohara A, Terashima H, Yakushi T, Sakuma M, Homma M, Namba K, Imada K: **Insights into the stator assembly of the *Vibrio* flagellar motor from the crystal structure of MotY**. *Proc Natl Acad Sci U S A* 2008, **105**:7696-7701.

210. Paul K, Brunstetter D, Titen S, Blair DF: **A molecular mechanism of direction switching in the flagellar motor of *Escherichia coli***. *Proc Natl Acad Sci U S A* 2011, **108**:17171-17176.

211. Lee LK, Ginsburg MA, Crovace C, Donohoe M, Stock D: **Structure of the torque ring of the flagellar motor and the molecular basis for rotational switching**. *Nature* 2010, **466**:996-1000.

212. Sutherland I: **Biofilm exopolysaccharides: a strong and sticky framework**. *Microbiology* 2001, **147**:3-9.

213. Kearns DB, Chu F, Branda SS, Kolter R, Losick R: **A master regulator for biofilm formation by *Bacillus subtilis***. *Mol Microbiol* 2005, **55**:739-749.

214. Godeke J, Paul K, Lassak J, Thormann KM: **Phage-induced lysis enhances biofilm formation in *Shewanella oneidensis* MR-1**. *ISME J* 2011, **5**:613-626.

215. Wolfe AJ, Visick KL: **Get the message out: cyclic-Di-GMP regulates multiple levels of flagellum-based motility**. *J Bacteriol* 2008, **190**:463-475.

216. Blair KM, Turner L, Winkelman JT, Berg HC, Kearns DB: **A molecular clutch disables flagella in the *Bacillus subtilis* biofilm**. *Science* 2008, **320**:1636-1638.

217. Guttenplan SB, Blair KM, Kearns DB: **The EpsE flagellar clutch is bifunctional and synergizes with EPS biosynthesis to promote *Bacillus subtilis* biofilm formation**. *PLoS Genet* 2010, **6**:e1001243.

218. Sambrook J, Russell DW: **Molecular Cloning: A Laboratory Manual** edn third: Cold Spring Harbor Laboratory Press; 2001.

219. Bertani G: **Studies on lysogenesis. I. The mode of phage liberation by lysogenic *Escherichia coli***. *J Bacteriol* 1951, **62**:293-300.

220. Hanahan D: **Studies on transformation of *Escherichia coli* with plasmids**. *J Mol Biol* 1983, **166**:557-580.

221. Gescher JS, Cordova CD, Spormann AM: **Dissimilatory iron reduction in *Escherichia coli*: identification of CymA of *Shewanella oneidensis* and NapC of *E. coli* as ferric reductases**. *Mol Microbiol* 2008, **68**:706-719.

222. Kibbe WA: **OligoCalc: an online oligonucleotide properties calculator**. *Nucleic Acids Research* 2007, **35**:W43-W46.

223. Miller VL, Mekalanos JJ: **A novel suicide vector and its use in construction of insertion mutations: osmoregulation of outer membrane proteins and virulence determinants in *Vibrio cholerae* requires toxR**. *J Bacteriol* 1988, **170**:2575-2583.

224. Schirm M, Kalmokoff M, Aubry A, Thibault P, Sandoz M, Logan SM: **Flagellin from *Listeria monocytogenes* is glycosylated with beta-O-linked N-acetylglucosamine**. *J Bacteriol* 2004, **186**:6721-6727.

225. Heimbrook ME, Wang WL, Campbell G: **Staining bacterial flagella easily**. *J Clin Microbiol* 1989, **27**:2612-2615.

226. Prospiech N: **A versatile quick prep of chromosomal DNA from gram-positive bacteria**. *Trends in genetics* 1995, **11**:217-218.

227. Sanger F, Coulson AR: **A rapid method for determining sequences in DNA by primed synthesis with DNA polymerase**. *J Mol Biol* 1975, **94**:441-448.

228. Inoue H: **High efficiency transformation of *Escherichia coli* with plasmids**. *gene* 1990, **96**.

229. Thormann KM, Saville RM, Shukla S, Spormann AM: **Induction of rapid detachment in *Shewanella oneidensis* MR-1 biofilms**. *J Bacteriol* 2005, **187**:1014-1021.

230. Southern E: **Southern blotting**. *Nat Protoc* 2006, **1**:518-525.

231. Feustel L, Nakotte S, Durre P: **Characterization and development of two reporter gene systems for *Clostridium acetobutylicum***. *Appl Environ Microbiol* 2004, **70**:798-803.

232. Laemmli UK: **Cleavage of structural proteins during the assembly of the head of bacteriophage T4**. *Nature* 1970, **227**:680-685.

233. Pilizota T, Bilyard T, Bai F, Futai M, Hosokawa H, Berry RM: **A programmable optical angle clamp for rotary molecular motors**. *Biophys J* 2007, **93**:264-275.

234. Petersen TN, Brunak S, von Heijne G, Nielsen H: **SignalP 4.0: discriminating signal peptides from transmembrane regions**. *Nat Methods* 2011, **8**:785-786.

235. Pedelacq JD, Cabantous S, Tran T, Terwilliger TC, Waldo GS: **Engineering and characterization of a superfolder green fluorescent protein**. *Nat Biotechnol* 2006, **24**:79-88.

ABBREVIATIONS

aa	**a**mino **a**cid
BFM	**b**acterial **f**lagellar **m**otor
BFPI	**B**ack **F**ocal **P**lane **I**nterferometry
bp	**b**ase **p**airs
CCW	**c**ounter **c**lock**w**ise
CW	**c**lock**w**ise
EDAC	1-**E**thyl-3-(3-**d**imethyl**a**minopropyl)**c**arbodiimide hydrochloride
e.g.	for example
mCherry	monomeric Cherry (red fluorescent protein)
PG	**p**eptido**g**lycan
pmf	**p**roton-**m**otive **f**orce
sfGfp	**s**uper-**f**olding **G**reen **f**luorescent **p**rotein
smf	**s**odium ion-**m**otive **f**orce
TIRF	**T**otal **I**nternal **R**eflection **F**luorescence

ACKNOWLEDGEMENT

[redacted]